



UNIVERSITY  
OF  
JOHANNESBURG

## COPYRIGHT AND CITATION CONSIDERATIONS FOR THIS THESIS/ DISSERTATION



- Attribution — You must give appropriate credit, provide a link to the license, and indicate if changes were made. You may do so in any reasonable manner, but not in any way that suggests the licensor endorses you or your use.
- NonCommercial — You may not use the material for commercial purposes.
- ShareAlike — If you remix, transform, or build upon the material, you must distribute your contributions under the same license as the original.

### How to cite this thesis

Surname, Initial(s). (2012). Title of the thesis or dissertation (Doctoral Thesis / Master's Dissertation). Johannesburg: University of Johannesburg. Available from: <http://hdl.handle.net/102000/0002> (Accessed: 22 August 2017).



UNIVERSITY  
OF  
JOHANNESBURG

## Effects of Multi-Pass Friction Stir Processing on Aluminium

By

Kayode Oyindamola

A dissertation submitted in partial fulfilment of the requirements for the  
degree of Master of Engineering in Mechanical Engineering in the  
Department of Mechanical Engineering Science  
University of Johannesburg, South Africa

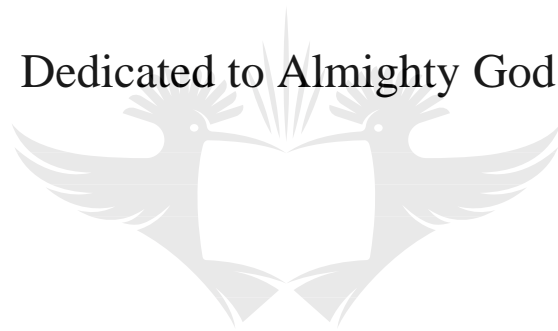
Supervisors

Prof. Esther Akinlabi

Dr. Oluwole Olufayo

December, 2016

Dedicated to Almighty God



UNIVERSITY  
OF  
JOHANNESBURG

## **Copyright Statement**

The copyright of this dissertation is owned by the University of Johannesburg, South Africa. No information derived from this publication may be published without the author's prior consent, unless correctly referenced.



# Author Declaration

I, Kayode Oyindamola hereby declare that the research work documented in this dissertation is my own, and no portion of the work has been submitted in support of an application for another degree or qualification at this or any other university or institute of learning. All sources used or cited are documented and recognised.

.....

Author's Signature

Date:



# Acknowledgment

I would like to express my sincere appreciation to my supervisor, Professor Esther Akinlabi for her invaluable support, inspiring guidance, and countless hours of involvement in the research. I am very proud and honoured to have had the intelligent guidance and help of one of the best in the field of friction stir welding and processing. Thank you so much Ma. I am also grateful to my co-supervisor, Dr. Oluwole Olufayo for his kind support, advice, and invaluable help with the molecular dynamics simulation aspect of this research. It is gratefully acknowledged.

I am most grateful to my parents, Professor and Mrs. Joshua Kayode, Mr. and Mrs. Oluwafemi Olonade, and my siblings, Doyinsola, Oyinlola, Oyindolapo, Olwaseunfunmi, and Ayomide for their endless support, advice, and encouragement, not only during this work but throughout my life. My parents have always lovingly supported me in achieving my goals and becoming someone in life; words are insufficient to show my sincere gratitude.

I would like to thank my mentor and his wife, Dr. and Mrs Abejide Ade-Ibijola for their support, and hospitality throughout this research. I would also like to thank all my colleagues and lecturers in the materials research group and the SMO Laboratory office. All of you have made the office and the research group a great place to work in.

Many thanks to Professor Kailas Satish of Indian Institute of Science, Bangalore, India for providing the friction stir welding platform used in conducting the experiments for this research. I am also grateful to Mr. Madhu, Ganesh, Sudheendra, Santosh, Mr. Azeez and everyone in the Surface Interaction and Manufacturing Laboratory (Indian Institute of Science) for their assistance with experiments and the preparation of my samples. I would also like to thank Mr. Micheal Bodunrin, and everyone who has helped me, at some point or another, throughout my study. I am very sorry I cannot mention everyone individually.

Finally, my deepest gratitude goes to my beloved Queen Asakemiowon Olayemisimi for her patience, inspiration and moral support throughout this work. This dissertation could not be done without her motivation, sacrifice and prayers.

# **Abstract**

## **Effects of Multi-Pass Friction Stir Processing on Aluminium**

Kayode O.

Friction stir processing (FSP) is a new solid-state processing technique for microstructural modification based on friction stir welding (FSW) developed by The Welding Institute (TWI) in 1991. Since its invention, the process has continually been improved, and its scope of application expanded leading to industrial applications and commercialisation in the microstructural modifications of materials to achieve desired mechanical properties.

The literature review investigates studies already conducted in the field of FSP on different aluminium materials. However, no published work on the correlation of microstructural homogeneity in multi-friction processed zone with mechanical properties seem to exist despite the fact that inhomogeneity in the friction processed zone might be a reason for the degradation in mechanical properties of single-pass FSP processed materials.

This dissertation focuses on the effect of multi-pass FSP on aluminium. FSP was conducted using constant rotational and transverse speeds of 1600 rpm and 40 mm/min respectively. A tool plunge depth of 5.3 mm and a 3° tilt angle was used. AA6061-T6 was the selected matrix alloy, and its microstructural homogeneity in correlation with the evolving mechanical properties after each successive FSP pass was studied in detail. Macrostructural and microstructural characterisation was carried out with an optical microscope (OM) and a scanning electron microscope (SEM), while tensile testing, and microhardness profiling was carried out to evaluate the mechanical properties of the processed materials using a tensile testing machine and a Vickers microhardness tester respectively. A study of the underlying thermodynamics occurring during the FSP process was also conducted using molecular dynamics (MD) simulation.

The macrostructural and microstructural evaluations of the processed samples revealed an increase in microstructural homogeneity as the number of FSP passes increases. The correlation of this homogeneity with the resulting mechanical properties indicates that a nearly 100% homogenous friction processed zone improved the mechanical properties in the processed aluminium materials. However, the BM was found to have better mechanical

properties with an ultimate tensile strength (UTS) of 338 MPa, a yield strength of 311 MPa, and an average Vickers microhardness of 99 HV, compared to the fully homogenous processed zone with a UTS of 177 MPa, yield strength of 172 MPa, and average Vickers microhardness of 67 HV. The resulting microstructural evolution and grain sizes after each FSP pass have also been observed to be strongly dependent on the processing parameters, thermal cycle, and presence of second-phase precipitates, rather than only on microstructural homogeneity. The results obtained from the MD simulation prove that it is possible to adequately represent MD simulations of FSP on aluminium alloys. The underlying thermodynamics was explained, and consistency between experimental FSP and the simulation process was achieved.



# Table of Contents

<b>Copyright Statement.....</b>	<b>i</b>
<b>Author Declaration .....</b>	<b>ii</b>
<b>Acknowledgment.....</b>	<b>iii</b>
<b>Abstract.....</b>	<b>iv</b>
<b>Table of Contents .....</b>	<b>vi</b>
<b>Abbreviations .....</b>	<b>ix</b>
<b>Nomenclature .....</b>	<b>xii</b>
<b>Units .....</b>	<b>xiii</b>
<b>List of Figures.....</b>	<b>xiv</b>
<b>List of Tables .....</b>	<b>xvii</b>
<b>Glossary of Terms .....</b>	<b>xviii</b>
<b>1 Introduction .....</b>	<b>1</b>
1.1 Background .....	1
1.2 Problem Statement .....	3
1.3 Aim.....	4
1.4 Objective .....	4
1.5 Hypothesis.....	4
1.6 Research Methods .....	4
1.7 Delimitations .....	5
1.8 Significance of Research.....	5
1.9 Project Layout .....	6
<b>2 Literature Review .....</b>	<b>7</b>
2.1 Introduction .....	7
2.2 Welding .....	7
2.2.1 Fusion Welding .....	7
2.2.2 Solid State Welding.....	8
2.3 Friction Stir Welding.....	9
2.4 Friction Stir Processing .....	9
2.5 Applications of FSW/FSP .....	11
2.6 Tool Design and Geometry .....	22

2.7	Tool Tilt and Plunge Depth.....	24
2.8	Transverse and Rotational Speeds.....	25
2.9	Tool Axial Force .....	28
2.10	Material Flow in Friction Stir Processing .....	29
2.11	Microstructural Studies on Friction Stir Processed Aluminium .....	32
2.12	Summary .....	43
<b>3</b>	<b>Experimental Procedures.....</b>	<b>45</b>
3.1	Introduction .....	45
3.2	Parent Material .....	45
3.3	FSW Platform.....	45
3.4	FSP Process Parameters .....	46
3.5	FSP Experimental Procedure .....	47
3.6	Sample Preparation .....	48
3.7	Microscopy.....	50
3.8	Vickers Hardness Testing.....	51
3.9	Tensile Testing .....	52
3.10	Summary .....	53
<b>4</b>	<b>Molecular Dynamics.....</b>	<b>54</b>
4.1	Introduction .....	54
4.2	Overview of Molecular Dynamics.....	55
4.3	Application of MD to Engineering Systems .....	56
4.4	Attributes of Molecular Dynamics Simulation .....	60
	4.4.1 Molecular Dynamics Procedure .....	60
	4.4.2 Advantages of Molecular Dynamics .....	62
	4.4.3 Limitations of Molecular Dynamics .....	62
4.5	Molecular Dynamics Basics.....	63
	4.5.1 Equation of Motion .....	63
	4.5.2 Computational Time Step.....	64
	4.5.3 Interatomic Potential .....	64
	4.5.4 Boundary Conditions .....	65
	4.5.5 Thermodynamic Ensemble.....	65
	4.5.5.1 Micro-Canonical or NVE.....	66
	4.5.5.2 Canonical or NVT .....	66

4.5.5.3 Isothermal-Isobaric or NPT.....	66
4.6 The MD Algorithm.....	66
4.6.1 The Velvet Algorithm .....	67
4.7 Process Methodology .....	68
4.7.1 MD Simulation Software .....	68
4.7.1.1 LAMMPS (Large-scale Atomic/Molecular Parallel Simulator) .....	68
4.7.1.2 OVITO (Open Visualisation Tool) .....	68
4.8 Simulation Configuration.....	69
4.8.1 The Face-Centred Cubic Structure.....	70
4.8.2 Model Atoms Number.....	71
4.8.3 Selection of Interatomic potentials and Thermodynamic Ensembles .....	71
4.8.4 Selection of Boundary Conditions .....	71
4.10 Summary .....	72
<b>5 Results and Discussion .....</b>	<b>73</b>
5.1 Introduction .....	73
5.2 Visual Appearance of FSPd Samples.....	73
5.3 Macrostructural Examination.....	74
5.4 Microstructural Examination .....	77
5.5 Tensile Properties.....	83
5.6 Hardness Properties.....	85
5.7 Molecular Dynamics Simulation Results.....	88
5.7.1 Temperature Variation .....	92
5.7.2 Pressure Variation and Force Analysis .....	93
5.7.3 Potential and Total Energy.....	95
5.8 Summary .....	96
<b>6 Coclusions and Future Work.....</b>	<b>97</b>
6.1 Introduction .....	97
6.2 Conclusions .....	98
6.3 Future Work .....	99
<b>References.....</b>	<b>101</b>
<b>Appendices.....</b>	<b>118</b>

# Abbreviations

AA	– Aluminium Alloy
AFM	– Atomic Force Geometry
AGG	– Abnormal Grain Growth
AL	– Aluminium
AS	– Advancing Side
ASTM	– American Society for Testing and Materials
BM	– Base Material
CFSWC	– China Friction Stir Welding Center
CPU	– Central Processing Unit
EAM	– Embedded-Atom Method
EDM	– Electric Discharge Machine
EMMS	– Energy Minimisation Multi-Scale
FCC	– Face-Centered Cubic
FSP	– Friction Stir Processing
FSPd	– Friction Stir Processed
FSSW	– Friction Stir Spot Welding
FSW	– Friction Stir Welding
FPZ	– Friction Processed Zone
GNU	– General Public License

HAZ	– Heat Affected Zone
HDS	– High-Density Steel
HV	– Vickers Hardness
IISC	– Indian Institute of Science
LAMMPS	– Large Scale Atomic/Molecular Massively Parallel Simulator
MD	– Molecular Dynamics
MIG	– Metal Inert Gas
MNM	– Micro/Nano Machining
NASA	– National Aeronautics and Space Administration
NGG	– Normal Grain Growth
NZ	– Nugget Zone
OM	– Optical Microscope
OVITO	– Open Visualisation Tool
PM	– Parent Material
RAM	– Random Access Memory
RS	– Retreating Side
SEM	– Scanning Electron Microscope
SZ	– Stir Zone
TMAZ	– Thermo-Mechanically Affected Zone

TWB – Tailored Welded Blanks

UTS – Ultimate Tensile Strength



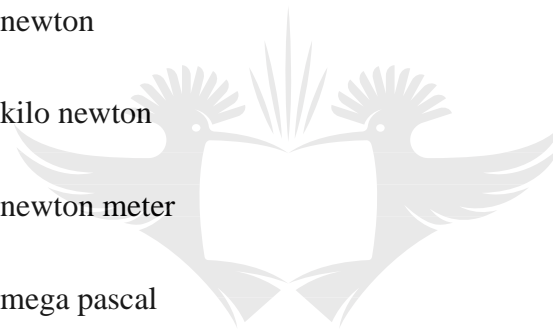
## Nomenclature

$F_x$	– Advancing force in the direction of welding (N, eV/Angs)
$F_y$	– Uniaxial force perpendicular to the $F_x$ during the welding process (N, eV/Angs)
$F_z$	– Vertical downward force on the tool (N, eV/Angs)
$T$	– Temperature (K).
$P$	– Pressure (Nm)
$N$	– Number of Particles
$\mu$	– External chemical potential
$t$	– Time (Secs)
$E$	– Energy (eV)



# Units

$\mu\text{m}$	– micrometer
mm	– millimeter
mm/min	– millimeter/minute
in/min	– inch/minute
g	– gram
secs	– seconds
N	– newton
kN	– kilo newton
Nm	– newton meter
MPa	– mega pascal
rpm	– revolutions per minute
kgf	– kilogram-force
eV	– electron Volt
Angs	– Angstrom



UNIVERSITY  
OF  
JOHANNESBURG

# List of Figures

## Chapter 1

Figure 1.1: Schematic of the (a) FSW process (b) FSP process .....	3
--	---

## Chapter 2

Figure 2.1: Fusion welding performances of aluminium to other metals .....	8
Figure 2.2: FSW applications in shipbuilding .....	11
Figure 2.3: Prefabricated FSW panels .....	12
Figure 2.4: A car featuring countless application areas of aluminium .....	13
Figure 2.5: Ford suspension link (a) in the middle of the manufacturing process and (b) the final product. ....	14
Figure 2.6: Riftec tailor welded blank for Audi.....	15
Figure 2.7: Honda Motor Company front subframe from FSW .....	16
Figure 2.8: Vertical welding machines at the Boeing Company .....	17
Figure 2.9: Manufacturing of Eclipse 500 using FSW .....	18
Figure 2.10: Prefabricated FSW panels used for suburban trains.....	19
Figure 2.11: Piston cast structure improvement with FSP.....	20
Figure 2.12: Ship door manufactured from superplastic forming.....	21
Figure 2.13: Formed FSP structural components for industrial applications .....	21
Figure 2.14: Schematics of the FSW/FSP tool .....	22
Figure 2.15: Basic FSW/FSP tool profiles.....	23
Figure 2.16: Advanced FSW/FSP tools developed at TWI.....	23
Figure 2.17: Typical FSW/FSP tool shoulder outer surfaces .....	23
Figure 2.18: Schematics of tilt angle and plunge depth of FSW/FSP tool .....	24
Figure 2.19: Schematics of tool movement showing metal flow.....	29
Figure 2.20: Copper marker shown in the joint line on the lower left of exit-hole damage in AA1100 alloy weld.....	31
Figure 2.21: Schematic drawing of marker configuration .....	32
Figure 2.22: Transverse section of FSW/FSP showing different regions.....	33
Figure 2.23: Schematic of the microstructural evolution in different zones of FSP/FSW material .....	34

Figure 2.24: (a) As-cast A356 illustrating casting porosity and dendritic structure, and (b) FSP A-356 showing a homogeneous microstructure in stir zone .....	36
Figure 2.25: Microstructure of A206 after FSP at 1000 rpm – 1 in/min: a) as-cast + T4; b) refined grains in the nugget. Microstructure of the transition zone between FSP zone and parent material of the A206 sample (1000 rpm – 1 in/min); c) retreating side boundary; d) advancing side boundary.....	37
Figure 2.26: Macrograph of FSPd Al-Ni particulate composite.....	39

### Chapter 3

Figure 3.1: FSW platform.....	46
Figure 3.2: High-density steel FSP tool.....	47
Figure 3.3: Concord wire electric discharge machine .....	48
Figure 3.4: Struers (a) hot mounting machine (b) polishing machine .....	49
Figure 3.5: Schematics of samples for microstructural and microhardness tests .....	49
Figure 3.6: Schematics of tensile samples (All dimensions in mm).....	49
Figure 3.7: Optical microscopy setup .....	50
Figure 3.8: TESCAN VEGA3 scanning electron microscope.....	51
Figure 3.9: TH713 Vickers microhardness tester .....	51
Figure 3.10: Instron tensile testing machine .....	52

### Chapter 4

Figure 4.1: Scales for simulation time and length .....	54
Figure 4.2: Overview of MD .....	55
Figure 4.3: Workflow integration of simulation to industrial applications .....	56
Figure 4.4: Evolution of machining accuracy-Taniguchi's predictions .....	59
Figure 4.5: MD simulation flow chart .....	61
Figure 4.6: Boundary conditions that can be used in molecular dynamics .....	65
Figure 4.7: MD simulation model.....	69
Figure 4.8: The face-centered cubic structure.....	70

## Chapter 5

Figure 5.1: Physical appearances of FSPd samples .....	73
Figure 5.2: OM macrographs of FSPd samples .....	75
Figure 5.3: AA6061-T6 base material microstructure .....	77
Figure 5.4: OM micrographs of multi-pass samples various zones.....	79
Figure 5.5: Graphic representation of the various FPZ zones grain sizes .....	80
Figure 5.6: Microstructural evolution of multi-pass FSP of AA6061-T6 .....	82
Figure 5.7: Graphic representation of tensile properties of the AA6061-T6 base material and FSPd samples .....	83
Figure 5.8: Average hardness values of the BM and FSPd samples .....	86
Figure 5.9: Microhardness profile of BM and FSPd samples.....	86
Figure 5.10: MD simulation snapshot of the FSP of AA6061-T6.....	89
Figure 5.11: Snapshots from the repeated MD simulation. ....	91
Figure 5.12: Shear strain distribution in FSP of AA6061-T6.....	92
Figure 5.13: Time step vs temperature plot of FSP of AA6061-T6 .....	92
Figure 5.14: Time step vs pressure plot of FSP of AA6061-T6 .....	93
Figure 5.15: Time step vs force plot of FSP of AA6061-T6 .....	94
Figure 5.16: Time step vs energy plot of FSP of AA6061-T6.....	95

## Appendices

Figure A1: AA6061-T6 chemical composition .....	119
Figure C1-1: 1 <sup>st</sup> FSP pass force feedback .....	121
Figure C1-2: 2 <sup>nd</sup> FSP pass force feedback .....	121
Figure C1-3: 3 <sup>rd</sup> FSP pass force feedback.....	122
Figure C1-4: 4 <sup>th</sup> FSP pass force feedback.....	122
Figure C1-5: 5 <sup>th</sup> FSP pass force feedback.....	123
Figure D2-1: Tensile behaviour – 1 <sup>st</sup> samples (T1) .....	125
Figure D2-2: Tensile behaviour – 2 <sup>nd</sup> samples (T2) .....	126
Figure D2-3: Tensile behaviour – 3 <sup>rd</sup> samples (T3).....	126

# List of Tables

## Chapter 2

Table 2.1: Evolving properties obtained by localised modification in FSP .....	10
--	----

## Chapter 3

Table 3.1: Chemical composition of AA6061-T6 .....	45
--	----

## Chapter 4

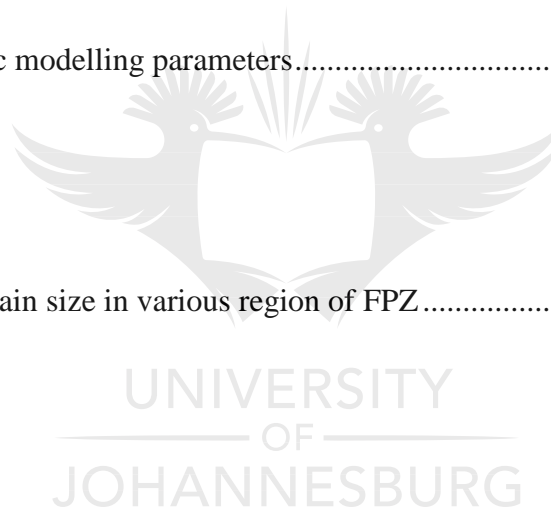
Table 4.1: Nanometric modelling parameters.....	70
---	----

## Chapter 5

Table 5.1: Average grain size in various region of FPZ .....	80
--	----

## Appendices

Table B1-1: Grinding procedure .....	120
Table B1-2: Polishing procedure .....	120
Table B1-3: Etchant procedure .....	120
Table D1-1: Ultimate tensile strength of the base material and processed samples .....	124
Table D1-2: Yield strength of the base material and processed samples .....	124
Table D1-3: Elongation percentage of the base material and processed samples .....	125
Table D3-1a: Hardness values; BM, single-pass, and two-pass .....	127
Table D3-1b: Hardness values; three-pass, four-pass and five-pass.....	128



## Glossary of Terms

**Advancing side** – The advancing side is the side of the weld where the local direction of the rotating tool is in the same direction of traverse.

**Alloy** – A substance having metallic properties and being composed of two or more chemical elements, of which at least one is a metal.

**Alloying element** – An element added to, and remaining in metal, that changes its structure and properties.

**Backing plate** – A layer of material that is placed below the materials to be processed. It provides a surface to oppose the vertical downward force on the material, and protects the machine bed.

**Clamping** – Holding and preventing the workpiece from moving during the large forces involved in the FSP process.

**Defect** – A discontinuity or discontinuities that accumulate to render a part unable to meet minimum acceptance standards or criteria of the design specifications.

**Deformation** – Change in the form of a body due to stress, thermal, or other causes.

**Ductility** – The ability of a material to deform plastically before fracture.

**Dwell time** – The period after the rotating tool has been plunged into the work and for which it remains stationary, generating frictional heat and plasticising the materials, before commencing the traverse along the joint (seconds).

**Elongation** – The increase in gauge length of a body subjected to a tension force, referenced to a gauge length of a body. Usually expressed as a percentage of the original gauge length.

**% Elongation** – The total percent increase in the gauge length of a specimen after a tensile test.

**Engineering strain** – This is a dimensionless value that is the change in length ( $\Delta L$ ) per unit length of the original linear dimension ( $L_0$ ) along the loading axis of the specimen; that is  $e = \Delta L/L_0$  the amount that a material deforms per unit length in a tensile test.

**Engineering stress** – The normal stress, expressed in units of applied force,  $F$ , per unit of original cross-sectional area,  $A_0$ ; that is,  $S = F/A_0$ .

**Equilibrium** – A state of dynamic balance between the opposing actions, reactions, or velocities of a reversible process.

**Etchant** – A chemical solution used to etch a metal to reveal structural details.

**Etching** – Subjecting the surface of a metal to preferential chemical or electrolytic attack to reveal structural details for metallographic examination.

**Extrusion** – The process where a material is shaped by force or squeezed through a die or nozzle.

**Exit hole** – A hole left at the end of the weld when the FSP tool is withdrawn, resulting from displacement of material during the plunge. Some special techniques are in-use to fill or prevent the occurrence of this hole.

**Face-centered cube** – This is a crystal system where atoms are arranged at the corners and center of each cube face of the cell.

**Filler Metal** – Metal added in making a welded, brazed, or soldered joint.

**Flash** – A build-up of weld material, normally on the retreating side of the rotating tool, which has a ‘peel-like’ effect; this is termed side flash in FSW/FSP.

**Force control** – A mode in the Friction Stir Process in which a known force from previous welds is added to other input process parameters to produce a weld.

**Fusion** – The melting together of filler metal and base metal, or of base metal only, which results in coalescence.

**Fusion welding** – Any welding process that uses fusion of the base metal to make the weld.

**Friction** – The force required to cause one body in contact with another to begin to move.

**Friction stir welding** – A process developed at The Welding Institute (TWI) that utilises local friction heating to produce continuous solid-state seams. It allows butt and lap joints to be made without the use of filler metals. The solid-state low distortion welds produced are achieved with relatively low costs, using simple and energy-efficient mechanical equipment.

**Friction stir processing** – Friction Stir Processing (FSP) is a new solid state processing technique for microstructural modification. It is a method of changing the properties of a metal through intense, localised plastic deformation resulting in a significant evolution in the local microstructure.

**Grain** – An individual crystallite in metals.

**Grain growth** – This is a phenomenon which occurs when the temperature of a metal is raised, the grains begin to grow and their size may eventually exceed the original grain size.

**Grain size** – A measure of the areas or volumes of grains in a polycrystalline metal or alloy, usually expressed as an average when the individual sizes are uniform. Grain size is reported in terms of number of grains per unit area or volume, average diameter, or as a number derived from area measurements.

**Grain boundary** – An interface separating two grains, where the orientation of the lattice changes from that of one grain to that of the other. When the orientation change is very small, the boundary is sometimes referred to as a sub-boundary structure.

**Grinding** – Removing material from the surface of a workpiece by using a grinding wheel or abrasive grinding papers.

**Hardness** – A term used for describing the resistance of a material to plastic deformation.

**Hardness test** – A test to measure the resistance of a material to penetration by a sharp object.

**Hardening** – Increasing hardness by suitable treatment.

**Heat affected zone** - The portion of the base metal which has not been melted, but whose mechanical properties have been altered by the heat of welding or cutting.

**Homogeneous** – A chemical composition and physical state of any physical small portion, and that is the same as that of any other portion.

**Indentation hardness** – This is the hardness, as evaluated from the measurements of an area of an indentation made by pressing a specified indenter into the surface of a material under specified static loading conditions.

**Joint** – A point or edge where two or more pieces of metal or plastic are joined together.

**Lap joint** – A welded joint in which two overlapping metal parts are joined by means of a fillet, plug or slot weld.

**Macrograph** – A graphic reproduction of a prepared surface of a specimen at a magnification not exceeding 25x.

**Macrostructure** – The structure of metals as revealed by macroscopic examination of the etched surface of a polished specimen.

**Mechanical properties** – The properties of a material that reveal its elastic or inelastic behaviour when force is applied, indicating the suitable mechanical applications.

**Mechanical testing** – The determination of mechanical properties.

**Metallurgy** – The science and technology of metals and their alloys including methods of extraction and use.

**Microstructure** – The structure of a prepared surface of a metal, as revealed by a microscope at a magnification.

**Onion-ring like structure** – A characteristic weld pattern featuring a cyclic ring or onion ring-like profile.

**Parameter** – The minimum and maximum parameters that will describe the operating range of a variable.

**Parent material** – This is the sheet-metal plate in its as manufactured form, as supplied.

**Plastic deformation** – This is the distortion of material continuously and permanently in any direction. The deformation that remains or will remain permanent after the release of the stress that caused it.

**Plasticity** – Capacity of a metal to deform non-elastically without rupturing.

**Polished surface** – A surface that reflects a large proportion of the incident light in a peculiar manner.

**Position control** – A mode in FSW in which the machine automatically adjusts the forces acting during the welding process.

**Plunge depth** – The plunge depth is the maximum depth that the tool shoulder penetrates the weld plates.

**Plunge force** – During the plunging stage of the tool pin in FSW, the vertical force in the direction of the Z-axis movement is normally referred to as the plunging force.

**Porosity** – A rounded or elongated cavity formed by gas entrapment during cooldown or solidification.

**Recrystallisation** – A change from one crystal structure to another, such as that occurring upon heating and / or cooling through a critical temperature.

**Residual stress** – Stress in a body which is at rest, in equilibrium, and at uniform temperature in the absence of any external force.

**Retreating side** – The retreating side of the tool is where the local direction of the weld surface due to tool rotation and the direction of the traverse are in the opposite direction.

**Rotational speed** – The tool rotation speed is the rate of angular rotation (usually specified in rpm) of the tool about its rotational axis.

**Spindle speed** – This is also referred to as the rotational speed. It is the speed of the work holding device (chuck), measured in revolutions per minute.

**Spindle torque** – The spindle torque required to rotate the FSW tool when plunging into and traversing through the workpiece along the joint (Nm).

**Stir zone** – The recrystallised central area of the joint interface.

**Tensile strength** – The maximum tensile stress which a material is capable of sustaining. Tensile strength is calculated from the maximum load during a tension test carried out to rupture, and the original cross-sectional area of the specimen.

**Tensile test** – This measures the response of a material to a slowly applied axial force. The yield strength, tensile strength, modulus of elasticity and ductility are obtained.

**Tool shoulder** – The part of the welding tool which rotates and is normally disk-shaped.

**Tool pin** – The part of the tool that rotates in contact with the surface of the workpiece.

**Tool plunge** – The process of forcing the tool into the material at the start of the weld.

**Tool tilt angle** – The angle at which the FSW tool is positioned relative to the workpiece surface; that is, zero tilt tools are positioned perpendicular to the workpiece surface (degrees).

**Traverse speed** – This is also referred to as feed rate; it is the speed at which the rotating FSW tool is translated along the joint line (mm/min).

**Unaffected material** – The bulk of material which is not affected by either heat or deformation during the welding process.

**Vickers hardness number** – A number related to the applied load and the surface area of the permanent impression made by a square-based pyramid diamond indenter.

**Void** – The space that exist between particles or grains. Normally in welding, voids are associated with defects.

**Welding** – The process of joining, in which materials are enabled to form metallurgical bonds under the combined action of heat and pressure.

**Workpiece** – The component to be welded.

**x-axis** – Relating to a specific axis (horizontal) or a fixed line determining the direction of movement or placement in a 2-Dimensional (2-D) or 3-Dimensional (3-D) co-ordinate system.

**y-axis** – Relating to a specific axis (perpendicular to x-axis) or a fixed line determining the direction of movement or placement in a 2-D or 3-D co-ordinate system.

**z-axis** – Relating to a specific axis (vertical) or a fixed line determining the direction of movement or placement in a 3-D co-ordinate system.



# 1. Introduction

## 1.1 Background

Aluminium and its alloys form part of some of the most widely used metals today with applications in the automotive, marine and aerospace industries because of their good castability, formability, and ability to be strengthened by artificial ageing [1-4]. These metals have widespread application, but their mechanical properties are highly affected by microstructural features which limit the mechanical properties of cast and wrought alloys, in particular hardness, toughness and fatigue resistance [5].

Friction stir processing (FSP) is a new solid-state processing technique for microstructural modification [6, 7]. It is most commonly used for processing aluminium and its alloys and in the homogenisation of powder metallurgy aluminium alloys, metal matrix composites, and cast aluminium alloys [8, 9]. It is a method that changes the properties of a metal through intense localised plastic deformation resulting in a significant evolution in local microstructure.

FSP is based on the same approach as friction stir welding (FSW) developed by The Welding Institute (TWI) in the United Kingdom in 1991 to develop local and surface properties at selected locations. Unlike the conventional welding processes where melting is involved, FSP eliminates porosity and creates a microstructure with fine, equiaxed grains without changing the phase by melting or otherwise. This homogeneous grain structure allows some aluminium alloys to take on superplastic properties.

FSW was invented as a solid-state joining technique, and initially applied to aluminium alloys [10, 11]. The basic idea is extremely simple. FSW consists of a non-consumable rotating tool with a specially designed pin and shoulder passed through a line of joint into two joined edges of sheets or plates to be joined. It can be divided into three phases which are plunge and dwell, transverse, and retract phase. Both the tool and the workpiece will be at an ambient temperature at the start of the plunge phase. This is the phase where the tool is forced into the material to be joined, while the dwell period is the period the tool rotates in contact with the plate, but with no transverse through the material. In the dwell phase, when the rotating friction stir tool is steadily inserted into the workpiece, the material is too cold to flow and the rubbing action creates chipping as in any machining procedure. The rate at

which the tool is inserted determines the rate of temperature rise and extent of plasticity. The process of tool insertion continues until the tool shoulder is in intimate contact with the workpiece surface. At this stage, the entire tool shoulder and pin surface contribute to frictional heating [12, 13].

Once the tool and workpiece interface are sufficiently heated up, the tool is moved along the desired direction to bring about the joining. The tool heats up the workpiece, and the movement of material as the tool stirs while passing along the lines produce the joint. The heating is accomplished by friction between the tool and the workpiece and the plastic deformation of the workpiece. The friction generated between the tool and workpiece in addition to the adiabatic heat from the metal deformation leads to localised heating which softens and plasticises the workpiece. The localised heating softens the materials around the pin, and combination of tool rotation and translation leads to movement of the material from the front of the pin to the back of the pin. Because of this process, a joint is produced in a 'solid state' [14]. The tool is finally retracted from the workpiece on the completion of the joining process. During FSW, the material undergoes intense plastic deformation due to the traverse of rotating pin along the butting surfaces and after welding, recrystallisation results in significant grain refinement in the welded joints. The fine microstructure obtained in friction stir welds produces good mechanical properties [15].

Compared to conventional welding methods, FSW consumes considerably less energy. No cover gas or flux is used, and there is no use of filler metal in joining which means that any aluminium alloy can be joined without concern for compatibility of composition, which is an issue in fusion welding [14]. Akinlabi et al [16] also classify the numerous advantages of FSW over previous conventional welding methods into two main categories, namely metallurgical and environmental benefits. The metallurgical benefits include low distortion, good dimensional repeatability, stability, greater weld strength, excellent metallurgical properties in the joint area, no loss of alloying elements, fine microstructure, good corrosion resistant and absence of cracks. The environmental benefits include surface cleaning, degreasing solvents, no negative harmful welding fumes and gases, no waste materials, and lower energy consumption compared to conventional welding.

The new process, FSP was later developed as a generic tool for microstructural modification based on the principles of FSW [12]. Figure 1.1 below gives a schematic of the FSW and FSP process.

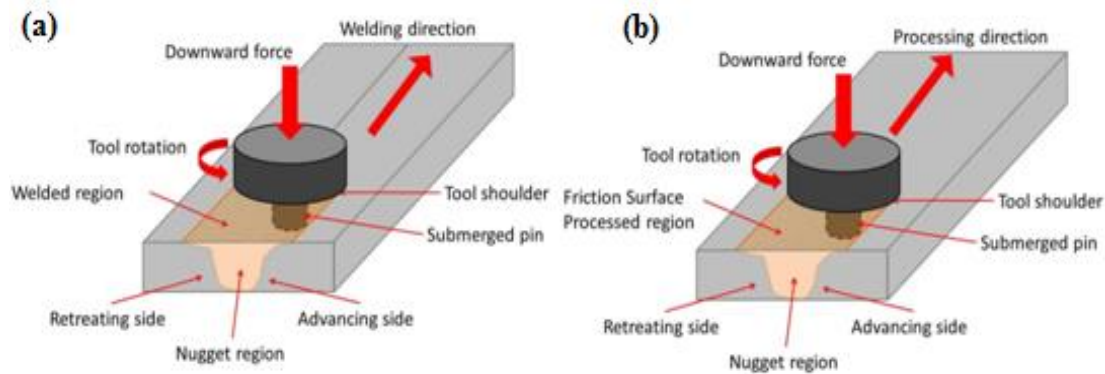


**Figure 1.1: Schematic of the (a) FSW process (b) FSP process**

FSW is concerned with joining two metals which may be either similar or dissimilar metals while FSP is used to strengthen some areas of a material [16]. FSP has been successfully applied to a variety of wrought and cast aluminium, magnesium and copper alloys to eliminate casting defects thereby improving their mechanical properties [17,18]. The process can be applied as a single-pass for processing a small area. For large engineering components in which the contact areas are relatively large, single-pass FSP may not be adequate. Multi-pass FSP with a certain level of overlap between the successive passes is required for large contact areas [19]. For both single and multi-pass processes, it is important to assess the microstructural evolution and its influence on the mechanical properties.

Although FSP is new and recently adopted, it has generated massive interest because of its eradication of defects such as porosity, cracks and changes in physical state which are associated with fusion welding processes. Research shows that FSP can be employed to homogenise the structure of a material.

## 1.2 Problem Statement

There have been some challenges associated with FSP which is a recently developed process not yet fully understood. Although, it has many advantages over various other materials processing technologies, the microstructural inhomogeneity in the transition of the base material in the friction processed zone (FPZ) observed in single-pass FSP is considered to be one of the major reasons for degradation in mechanical properties. It is envisaged that an increment in the number of FSP passes could give more homogenous material transition in the FPZ and improve the mechanical properties as a material begins to evolve after each pass, hence this study.

### **1.3 Aim**

The aim of this research is to characterise the effects of multi-pass friction stir processing on an aluminium alloy, and to conduct a molecular dynamics simulation of FSP interaction with the alloy.

### **1.4 Objectives**

The objectives of this research study are to:

- Derive the microstructures of the as-received and as-processed aluminium alloy
- Determine the effects of multi-pass FSP on the mechanical properties of the as-received and as-processed aluminium alloy
- Correlate the degree of homogeneity of the alloy with the mechanical properties obtained
- Obtain a thermodynamic description for the structural changes in the alloy using MD simulation

### **1.5 Hypothesis**

FSP is expected to give improved mechanical properties of aluminium because of an increased number of FSP passes. It is expected that an increase in the number of FSP passes on the aluminium material will result in a better homogeneous friction processed zone. This is expected to improve the mechanical properties of the material because of the refinement of grain structure and more material flow. Numerous researchers have established that ultrafine microstructures in metallic materials are responsible for increased hardness, wear behaviour, and strength.

### **1.6 Research Methods**

After gaining information from a review of the literature, a quantitative approach was adopted in this research. Preliminary laboratory tests were conducted to characterise the evolving macrostructure, microstructure, and microhardness properties of the aluminium parent material. FSP experiments were then conducted to produce single and multiple FSP passes on the material. Characterised properties of the effects were analysed.

A summary of the research methodology is as follows:

- FSP on materials
- Material characterisations
  - Macrostructural evaluation
  - Microstructural evaluation
  - Mechanical tests for tensile strength and hardness
- Statistical analysis
- Molecular dynamics (MD) simulation

Macro and microstructural evaluations were conducted to determine the homogeneity and grain refinement in the friction stir processed (FSPd) samples. The microhardness and tensile tests were carried out for physical-mechanical characteristics of the samples. This evaluation was used to characterise the hardness of the different zones in the FSP tracks, while tensile testing was conducted to determine the strength and ductility of the samples. These results were compared to the results from the preliminary characterisation of the parent material using statistical analysis. The molecular dynamics simulation was expected to give insight on the sub-surface thermodynamic phenomena going on during FSP at nanoscale.

### **1.7 Delimitations**

This research project only focuses on characterising the effects of multiple numbers of friction stir processing passes on aluminium, plus a molecular dynamics simulation study of friction stir processing pass on aluminium. The characterisation is limited to a study of the macrostructure, microstructure, microhardness, and tensile strength. The study was limited to a chosen fixed type FSP tool with a concave shoulder and probe, and a chosen FSP penetration depth and tilt angle for consistency. The study does not consider other types of FSP tools. Also, no heat studies were considered in order to concentrate on achieving the main aim and objectives of the research.

### **1.8 Significance of the Research**

This research provides a comprehensive characterisation and statistical analysis of the effect of multiple passes of FSP on aluminium. Experimental and statistical determination of the integrity of friction stir processed aluminium plates were used to determine the

characterisation. The research is expected to contribute and widen research studies on friction stir processing in academia and industrial applications. This will further contribute to solving part of the problems currently experienced in the engineering sector in South Africa in material selection, cost of production, and production time. The results of the molecular dynamics simulation will form the basis for new knowledge in the thermodynamic study of FSP on aluminium. This is a pioneer study of FSP with molecular dynamics; no such work has been done on the study of the thermodynamic microscopic details of FSP on aluminium. New insights and discoveries from this study will be of importance for industrial applications, where requirements on property profiles of materials are ever more demanding.

## **1.9 Project Layout**

This dissertation is divided into six chapters. The first chapter gives a brief introduction and offers the aim and objectives, the research hypothesis, the research methods, the delimitations and the significance of the research. The second chapter gives a literature review on the concept of FSP focusing on the significance of the process, its essential parameters, material flow, and a study of the few available literature sources on the effects of FSP on the microstructure and mechanical properties of aluminium and its alloys. The third chapter explains the experimental methodology used for achieving the set objectives. It entails description of the overall experimental set-up and preliminary investigation which includes the design of parameters, positions of workpieces during the FSP process, and the resulting processed material. The fourth chapter gives a literature review on the concept of molecular dynamics, its applications in engineering, and the methodology employed in this research. The fifth chapter presents and discusses the results. Finally, conclusions are drawn in chapter six with suggestions for possible future work.

## **2. Literature Review**

### **2.1 Introduction**

FSP is a new and emerging technique, and less research is available in the literature compared to FSW. Several studies have been conducted using the FSP technique on aluminium, but very few have been carried out on the effects of multiple numbers of FSP passes on aluminium plates. There is a slight difference between FSP and FSW insofar as FSW is used for joining two dissimilar metals and FSP for grain refinement and uniform microstructural distribution in metal. Most of the fundamental concepts are similar; only certain aspects are changed in FSP to achieve desired processing goals. A review of FSW in this study will therefore focus on contexts which are applicable to both FSW and FSP.

### **2.2 Welding**

Welding is a commonly used process for joining materials. Two metal pieces are joined as a result of significant atom diffusion of the welded pieces in the joint/weld region. The process is carried out by heating the pieces to be joined to melting point and fusing them together with or without filler material, or by applying pressure to the pieces in their cold or heated state. Different types of welding processes range from conventional, for example arc welding to advanced welding processes like laser welding with a variety of applications in buildings and bridges structures, pipelines, tanks and vessels, railroads, machinery elements, automotive industry, ships and aircraft constructions. Akinlabi [13] classifies welding types into two general categories, namely fusion welding and solid state welding.

#### **2.2.1 Fusion Welding**

Fusion welding is a type of welding process used in metalworking to join or fuse two pieces of metal by causing the metal to reach its melting point by means of heat. The process often requires the use of a filler metal which facilitates the process and provides bulk and strength to the joint. Different types of fusion welding are used for different applications. Common examples of are arc welding, electric resistance welding, oxy-fuel welding, thermite welding, electron beam welding, and laser beam welding.

The need for two metals to be heated to their melting temperatures is the main disadvantage of the fusion welding process. Akinlabi [13] explains that the melting and resultant solidification processes cause a decline in the mechanical properties of the joint such as low tensile strength, fatigue strength, and ductility. With increase in the application of aluminium alloys in the automotive, marine, and aerospace industries, the joining of aluminium to itself, but in particular to other materials becomes increasingly important. However, while joining of aluminium to itself is easily achieved with fusion welding, joining aluminium to other materials is difficult. Figure 2.1 illustrates the fusion welding performances of aluminium to other metals.

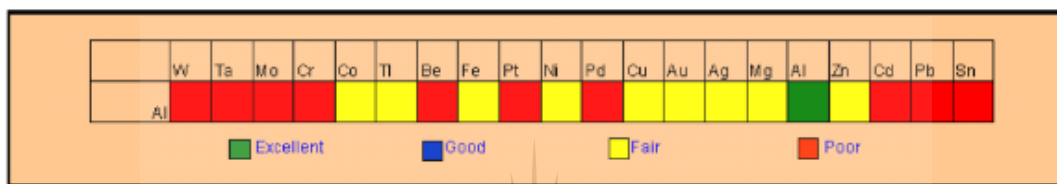


**Figure 2.1: Fusion welding performances of aluminium to other metals [20]**

As a result of this limitation, further research has led to the development of advanced welding techniques where metals are not required to reach melting temperatures to create a joint/weld of dissimilar metals. These improved techniques are known as solid-state welding.

### 2.2.2 Solid-state Welding

Solid-state welding, on the other hand, is a welding process in which metals are joined by the application of either pressure alone or a combination of heat and pressure. No filler metal is used, and when heat is used in the process, the temperature is below the melting point unlike in the case of fusion welding where the metals must reach melting point. Akinlabi [13] reported that there are fewer defects in solid-state welding because metals do not reach melting temperatures. This is an advantage because the parent metals retain their original properties. The main advantage of solid-state welding is its ability to weld dissimilar metals excellently, thereby overcoming the limitations of the difficulty of welding dissimilar metals experienced in fusion welding.

The commonly used solid-state welding processes are diffusion welding, explosion welding, electromagnetic pulse welding, cold pressure welding, friction stir welding and ultrasonic welding. However, this report focuses on friction stir welding.

### **2.3 Friction Stir Welding**

FSW, an innovative solid-state material welding method developed by TWI has been one of the most significant welding/joining technological developments in the last two decades. The fundamental design and advantages of FSW over conventional joining processes were explained in Chapter 1.

FSW allows for solid-state welding on many different types of joint geometries. It is advisable to use a backing plate in the case of butt and lap joints. This is required to resist the normal forces associated with FSW and the workpiece and to ensure that the plates in the butt configuration do not separate as a result of the large lateral forces acting during the initial tool plunge [13]. The backing plate also provides support and prevents the plasticised metal from extruding from the underside of the weld [21].

FSW has become a mature joining technology in aluminum alloys and is increasingly applied in different industries such as aerospace, automotive, and marine industries. Apart from the capacity to successfully join incompatible alloys, the stirring and forging action produces a fine-grain structure with better properties than can be achieved in a fusion weld [21]. This attribute of FSW has led to the development of a generic tool for microstructural modification and manufacturing known as friction stir processing.

### **2.4 Friction Stir Processing**

Material selection is very important in the marine, automotive and aircraft industries; materials are selected for specific properties in different applications. These industries experience limitations in getting materials processed to achieve specific properties like high strength and high ductility. The limitations impact on production cost and time. Most specific mechanical properties are obtainable when the materials have homogenous and highly refined grain structures. Thus, there is a need for a processing technique which refines grain structures and optimises the material properties to meet the requirements of strength,

ductility, and reductions in cost and time of production. Friction stir processing is one of the new techniques developed to serve this purpose.

FSP offers many advantages over conventional modification methods and the newer techniques in material processing such as: a single step process, the use of a simple and inexpensive tool, no expensive time-consuming finishing process, less processing time, use of existing and readily available machine tool technology, suitability to automation, adaptability to robot use, energy efficiency and environmental friendliness.

The above-mentioned FSP features and benefits make it a potential processing technique not only for aluminium sheets and alloys for various industrial applications, but also in the field of surface engineering. Table 2.1 illustrates the various properties which can be obtained by localised surface modification in FSP. Though the limitations of FSP are being reduced by intensive research and development, it still has a few limitations, for example rigid clamping of the workpiece, a backing plate requirement, different microstructural homogeneity in the transition from the base to the FSP zone, and defects such as a tunnel, cracks, and a keyhole at the end of each pass.

**Table 2.1: Evolving properties obtained by localised modification in FSP [12]**

<b>Property</b>	<b>Approach</b>
Elastic modulus	Addition of ceramic particles or intermetallic particles
Wear resistance	Addition of second-phase particles and microstructural refinement can enhance wear properties
Fatigue	Addition of shape memory particles can alter the residual stresses, thereby influencing the fatigue properties
Magnetic	Magnetic particles can be added in local regions to obtain magnetic properties in otherwise non-magnetic materials
Electrical conductivity	Second-phase additions can be used to enhance or lower electrical conductivity
Thermal conductivity	Second-phase particles can be used to enhance or lower thermal conductivity based on the thermal conductivity of matrix and reinforcement

## 2.5 Applications of FSW/FSP

Since the invention of FSW and FSP, these technologies have been widely adopted in many branches of manufacturing and engineering. Because of numerous advantages and benefits which FSW and FSP have over conventional joining and materials processing techniques, outlined earlier in this dissertation, these processes have generated aggressive study by aerospace, automobile, and shipbuilding industries as well as other areas of manufacturing and engineering. The processes have however been used predominantly in the fabrication and manufacturing of aluminium components and panels.

The first commercial application of FSW was the manufacturing of hollow aluminium deep freezer panels for freezing fish on fishing boats in November 1996 at Sapa in Finspång (Sweden), as shown in Figure 2.2a [22]. Since then, FSW has been increasingly applied in industries across the globe. The first vessel in world history made from FSW panels shown in Figure 2.2b was built by Fjellstrand AS in 1996. The panels were made by Marine Aluminium [23]. Figure 2.2c shows ESAB SuperStir™ FSW equipment installed at Marine Aluminium for welding panels. An over-hull structure made from FSW panels is shown in Figure 2.2d.

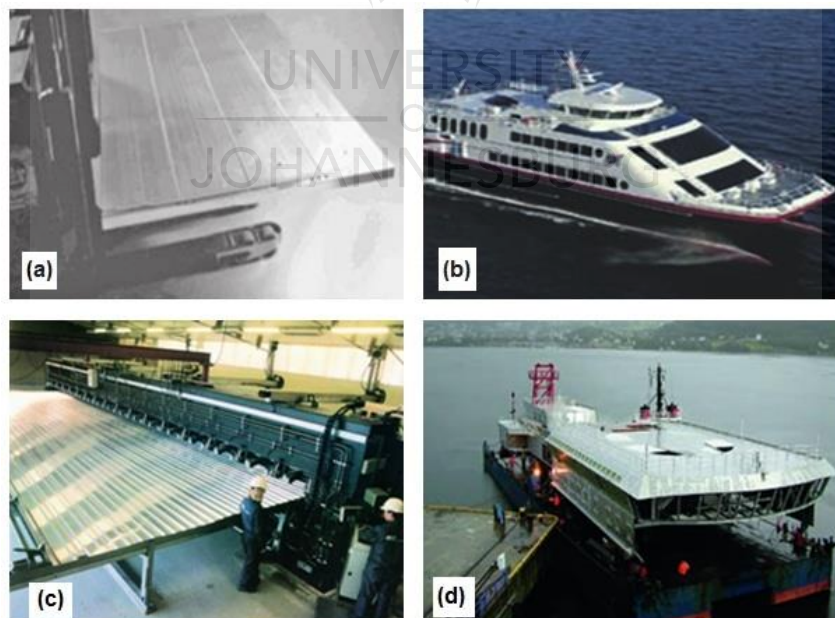


**Figure 2.2: FSW applications in shipbuilding [22,23]**

Areas of FSW applications in shipbuilding and marine industries include panels for decks, sides, bulkheads and floors, aluminium extrusions, hulls and superstructures, helicopter landing platforms, offshore accommodation, marine and transport structures, masts and booms in sailing boats, and refrigeration plants [24]. Other applications across the globe are the production of aluminium honeycomb panels and sea water-resistant panels used in ship cabin walls because of the good flatness of the weld underside used in Japan [25], as well as by the Nicholas Brothers Boat Builders in Freeland, Washington, USA for a 55 knots military ship of X-Craft class which was named ‘Sea Fighter’ [22].

The China Friction Stir Welding Centre (CFSWC) designed and fabricated its first FSW industrial product line for a small company in Chang Zhou in 2003 to produce FSW panels from aluminium extrusions for use in various sectors of the transport industry. They later designed and produced the first large FSW machine for wide ship panels in China in 2006. This machine is used for high-speed aluminium alloy ships. In mid-2005, the Donovan Group in Whangarei, New Zealand implemented FSW for the manufacturing of FSW panels used by Tenix Shipbuilding in Whangarei, New Zealand for assembling the superstructures of a number of 55-metre inshore patrol vessels for the Royal Australian Navy and Royal New Zealand Navy [22].

Pre-fabricated wide aluminium panels for high-speed ferry boats are made by joining extrusions and transported after welding. Figure 2.3a and Figure 2.3b show a prefabricated FSW panel for half the width of the superstructure of a cruise liner and a prefabricated FSW panel for a catamaran sidewall ready for transportation at Marine Aluminium. This company in Haugesund, Norway produce and deliver more than 70km of defect free FSW panels annually [24].

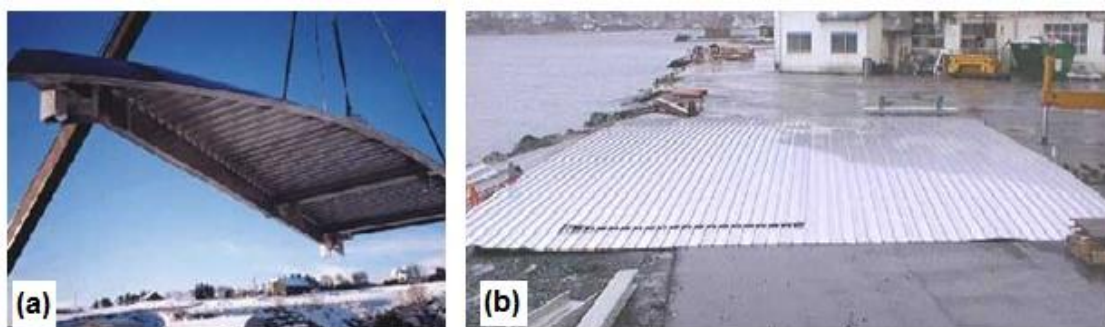


**Figure 2.3: Prefabricated FSW panels [26]**

Prefabricated FSW panels for shipbuilding is also a popular product in Chinese shipyards in Wuhan, Dalian, Guangxi, Shanghai, and Guangzhou where these wide panels are successfully used in many shipbuilding projects, including ships designed and fabricated for export to Vietnam and Micronesia [22]. Compared to fusion welding, the heat input is very low which results in low distortion and reduced thermal stresses.

These panels are also commonly used for making leak-tight helicopter platforms on oil-rigs, to avoid burning aircraft fuel dropping after a helicopter crash landing. SLP Engineering in Lowestoft (UK) ordered a batch of FSW floor panels from Marine Aluminium in 2008 for the living quarters of the Valhall redevelopment project in the Norwegian sector of the North Sea under contract by BP Norge AS [22]. The use of FSW panels in shipbuilding continues to grow.

The automotive industry has created a perfect field for FSW application in that all aluminium components in cars can be friction stir welded. These components ranging from bumper beams, rear spoilers, crash boxes, alloy wheels, air suspension systems, rear axles, drive shafts, and intake manifolds to stiffening frames, can be seen in Figure 2.4, a photograph taken at the Sapa stand at Aluminium 2002 Fair in Germany. The scope for application is wider and easily adaptable in the components of large road transport vehicles with long, straight or curved welds, such as trailer beams, cabins, spoilers, front walls, closed body or curtains, drop side walls, frames, rear doors and tail lifts, floors, sides, front and rear bumpers, chassis, fuel and air containers, tool boxes, wheels, and engine parts [23].



**Figure 2.4: A car featuring countless application areas of aluminium [23]**

Automobile manufacturers have found the use of aluminum very important in making vehicles lighter. This reduction in weight leads to enhanced fuel efficiency and improvements in dynamic and safety performance. The use of aluminium has also helped manufacturers to reduce rivet costs in riveted joints, and the large equipment in mechanical clinging. A study of aluminium tailored welded blanks (TWB) for door panels which demonstrated new concepts in FSW drive shafts and space frames, started by TWI in 1998 in a confidential group sponsored project involving BMW, Chrysler, EWI, Ford, General Motors, Rover, Tower Automotive and Volvo, produced encouraging results which led to the use of FSW and its variant namely friction stir spot welding (FSSW) in a series of aluminium automotive components at several locations worldwide [22]. A TWB consists of various sections of flat sheet, sometimes with different thicknesses, abutted and joined together. These joined flat sheets then enter a forming operation to shape the final geometry.

In 2000, Tower Automotive got the delivery of the SuperStir™ unit designed by ESAB for making a large profile from two or more extrusions. A lightweight suspension link is obtained by cutting the welded profile into a small width. The successful production of aluminium suspension links for the Ford Motor Company by Tower Automotive using a FSW process is the first time in the United States of America that FSW has been used in the manufacturing of an automotive component [23]. Figure 2.5 shows the production of this suspension link. Ford also applied friction stir welding to the center tunnel of their 2005 GT model.

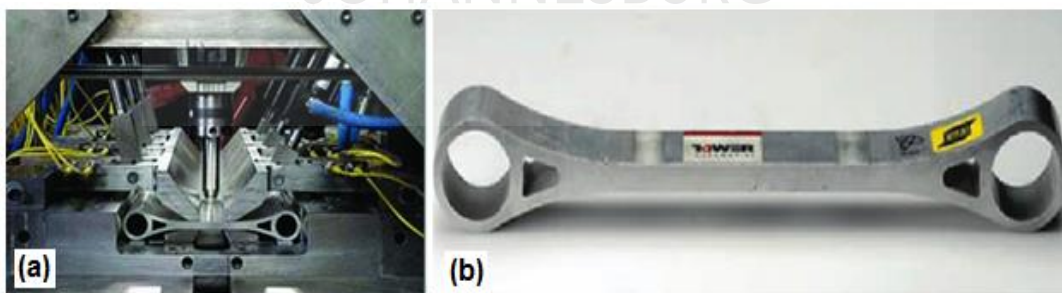


**Figure 2.5: Ford suspension link (a) in the middle of the manufacturing process and (b) the final product. [23]**

The purpose of using a TWB is to optimise material usage, not only for improved consumption but also for the weight reduction in the final formed component [24]. Riftec in Geesthacht (Germany) has been supplying friction stir welded tailored blanks, which are

subsequently deep-formed for making the center closing panel of the Audi R8 since 2006. They supply approximately 7000 units of these tailor welded blanks (Figure 2.6) per year. The blanks with a dissimilar thickness of 1.7 and 2.4mm have a 240mm long friction stir weld and are used to produce the Audi R8 series. This leads to more than 20% in material savings which translates into approximately 1kg weight saving per car. FSW has not given Audi the ability to reduce vehicle weight, but has also increased efficiency because of the reduction in material and forming costs.

Other automobile manufacturers have also adopted FSW technology in their production process. Mazda in Hiroshima, Japan developed and uses friction stir spot welding for the rear doors and bonnet of the Mazda RX-8. The technology has helped them eliminate the need for large currents and coolant/compressed air that conventional resistance welding requires. There is a nearly 99% and 80% drop in energy consumption for aluminum and steel respectively, with equipment costs also dropping by 40% since there is no longer a need for large-scale sources of electricity and specialised joining equipment [22].



**Figure 2.6: Riftec tailor welded blank for Audi R8 [22]**

In late 2012 the Honda Motor Company announced their development of a new technology for the continuous welding of dissimilar metals of steel and aluminium. They first applied it to the North American version of the all-new 2013 Accord as shown in Figure 2.7, and then expanded it to other models.

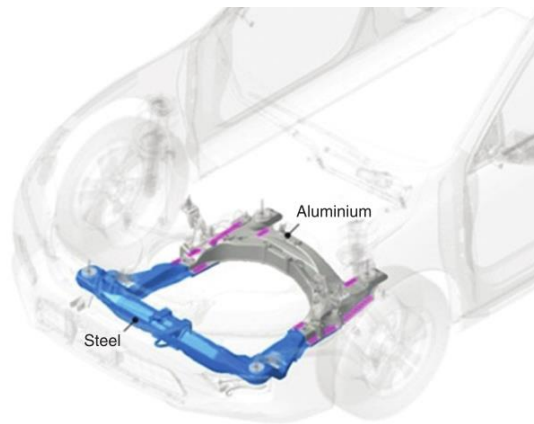


**Figure 2.7: Honda Motor Company front subframe from FSW [24]**

It was reported that the technology contributes to improved fuel economy by reducing weight by 25% compared to a conventional steel subframe, reduces electricity consumption during welding process by approximately 58%, increases the rigidity of the mounting point of suspension and contributes to the vehicle's overall dynamic performance [24].

Various other applications of FSW in the automotive industry include but are not limited to welding hollow aluminium extrusions from both sides simultaneously, to produce foldable rear seats of the Volvo V70 station wagon, assembling small hollow pistons used in the compressor stage of automotive air conditioning systems from aluminium castings, the production of a wheel rim from rolled aluminium 6061-O sheets, and joining two parts of a car wheel [22].

The significant cost, time and weight savings derived from FSW is the main rationale for employing FSW in the manufacture of aerospace components for the space industry and civil aviation. The reduction in weight enables higher speeds and/or reduced fuel consumption which translates directly into cost savings [23]. FSW, can be used in wings, fuselages, empennages and cryogenic fuel tanks for space vehicles, aircraft fuel tanks, external throw-away tanks for military aircraft, military and scientific rockets, and the repair of faulty MIG welds [24].

The first commercially successful experiment of FSW in the aerospace industry was in the non-reusable and largest element of the spacecraft, namely the space shuttle's gigantic external tank, by Lockheed Martin Laboratories in Baltimore who was challenged by NASA in 1993 to develop a high-strength, low-density, lighter-weight replacement for the

aluminium alloy Al-2219 used in the original space shuttle external tank. Lockheed Martin, Reynolds Aluminium and the laboratories at Marshall Space Flight Center in Huntsville, successfully developed a new alloy known as aluminium-lithium, Al-Li-2195, which reduced the weight of the external tank by 3402kg. FSW was applied on the longitudinal barrel welds of both tanks, the liquid oxygen, and liquid hydrogen barrels. External tank 134, launched in January 2005, was the first tank to incorporate the process [24].

Boeing has applied FSW in the manufacturing of the Delta II and Delta IV rockets. Figure 2.8 shows one of two identical vertical welding machines at the Boeing Company in Decatur, USA. The welding length (height) is 12 metres and the diameter 5 metres. FSW has been adopted and used for manufacturing rocket-fuel tanks achieving a great reduction in production time and several cost savings. The FSW specific design of Delta IV achieved a 60% cost saving, reduced manufacturing time from 23 to 6 days, and increased the weld strength of the common booster core tanks by between 30% to 50% [22,24].

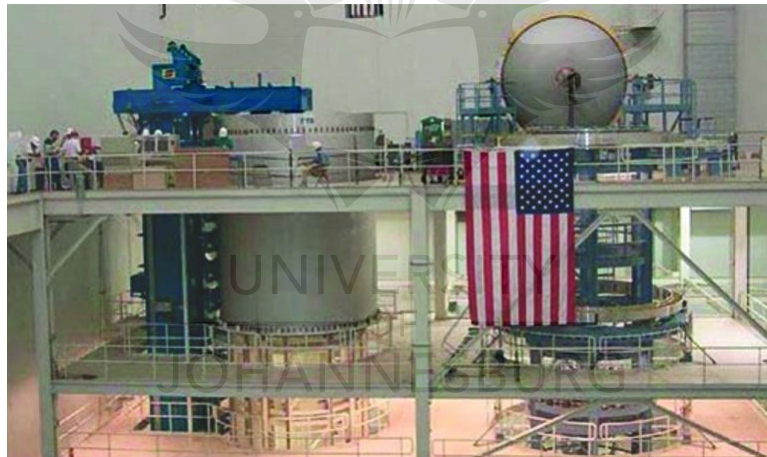


**Figure 2.8: Vertical welding machines at the Boeing Company [24]**

Phantom Works of the Boeing Company has also been using FSW on thin butt, lap and T-joints, and thick butt joints for various aircraft missile and space applications. They have successfully demonstrated FSW in sandwich assemblies by welding T-joints for a fighter aircraft fairing which was flight tested. They have also demonstrated curvilinear FSW in complex landing gear using a patented force actuator [22].

The first application of FSW in commercial aircraft production was in the manufacture of the Eclipse 500 by the Eclipse Aviation Corporation of Albuquerque, New Mexico, USA. The Eclipse Aviation Corporation announced in June 2002 that the FAA (USA Federal Aviation

Administration) had approved the FSW specification created for use in the assembly of the Eclipse 500 jet (Figure 2.9a). They decided to use FSW to replace traditional riveting and bonding processes with the benefit of lower cost and assembly time. Figure 2.9b shows the FSW gantry for welding stringers and spars to aluminium cabin panels at the Eclipse Aviation Corporation. The use of FSW for the Eclipse 500 eliminated 7000 rivets and fasteners, replaced associated hole drilling and has resulted in joining speeds: four times faster than manual riveting and twenty times faster than manual riveting. FSW also increased the joint strength by up to three times at comparable or better fatigue data [22].

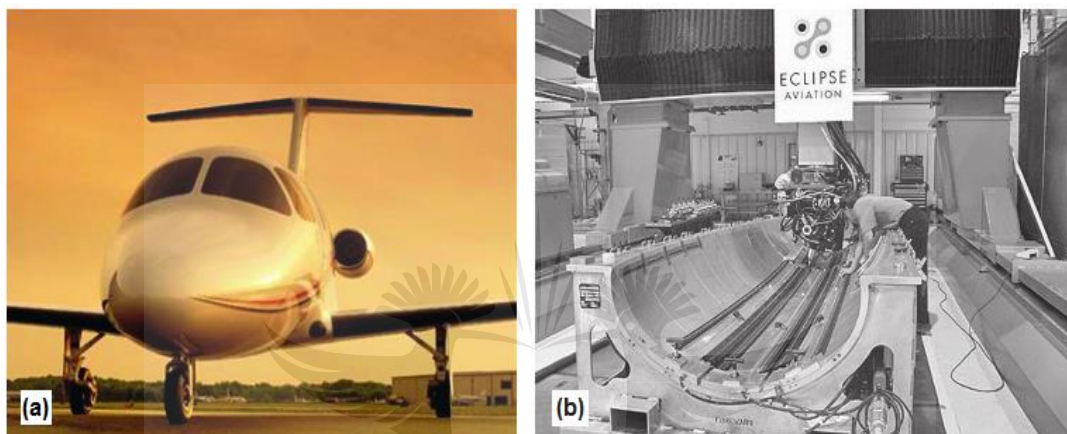


**Figure 2.9: Manufacturing of Eclipse 500 using FSW [22,24]**

Eriksson and Larsson [27] reported that a number of different applications in the commercial and military aircraft industry including carrier beams, floors and complete fuselages and wings were under evaluation. Further applications of FSW in the aerospace industry include the manufacturing of the toenails for the Boeing's C-17 cargo ramp, and friction stir welded floor panels in the Airbus A400M military transport aircraft [22].

Manufacturers of rolling stock (rail cars and train carriages) have also found extensive uses for FSW in manufacturing a range of components. Applications include high-speed trains, rolling stock in railways, underground carriages, trams, railway tankers, goods wagons, and container bodies [24]. It has been reported that complete trains are assembled from hollow extrusions using this innovative process. Recent investigations into the crashworthiness of aluminium railcars also demonstrate the benefits of using innovative joint and tool designs and optimised procedures for FSW.

Modern railway carriages are increasingly produced from longitudinal aluminium extrusions with integrated stiffeners. Using this concept, the whole-body shell can be made from either single-wall or hollow double-skin extrusions which enhance the crashworthiness of vehicles because of the absence of transverse welds and high buckling strength of panels under longitudinal compression. The cost effectiveness and good weld performance of FSW have been the main reasons for its adoption in the manufacture of rolling stock [22].

Sapa and Hydro Marine Aluminium were the first companies in Europe to commercially apply the FSW process in the manufacture of single-wall aluminium roof panels for rolling stock applications. Since 1997, Alstom LHB in Salzgitter, Germany, has purchased and used prefabricated friction stir welded aluminium floor and side panels (Figure 2.10a) in the construction of its suburban trains (Figure 2.10b) [28].



**Figure 2.10: Prefabricated FSW panels used for suburban trains [28]**

Another major train-industry pioneer, Hitachi of Japan, has used friction stir pre-fabricated floor elements in its Shinkansen trains. They use a double-skin design in the car which is constructed from FSW aluminium extrusions. To date, Hitachi has delivered a range of vehicles for both commuter and express use in Japan.

Kawasaki Heavy Industries in Japan use FSW to attach stringers to roof panels. They have developed a new aluminium car body shell using this method. It was reported that the main reason for using FSW is the fact that it improves the flatness and visual appearance of the skin panels because of the low heat input [22].

Other applications of FSW in engineering and manufacturing industries include joining steel with other high temperature materials; manufacturing of motor and loudspeaker housing by

PDC Technik in Helsingør, Denmark; producing heat sinks by several companies in Europe; producing heating, ventilating, and air conditioning units by Riftec, Germany; producing mass water cooled copper backing plates by Hitachi Cable Ltd and Hitachi Copper Product Ltd in Tsuchiura City, Japan; and producing aluminium freeze drying food trays and vacuum-tight X-ray equipment for Siemens Medical Solutions by Riftec, Germany [22]. It is clear that FSW offers many opportunities for future applications.

Although numerous applications of FSW in manufacturing and engineering have been outlined, FSW is not to be confused with the main focus of this research, namely the FSP process which originated from the observation that FSW locally modifies the material properties in and around the weld area [29]. While FSW has found wide applications in manufacturing and engineering, the same can be said for FSP.

The widest application of FSP has been the purpose of its development, namely the local improvement of material properties. FSP's ability to locally modify various material properties, includes but is not limited to ductility/elongation, fatigue, static, corrosion, and hardness [30]. Detailed microstructural studies on FSP on aluminium and modifications are discussed later in this chapter. Examples of practical applications include refining the microstructure of steel blades in hunting knives by DiamondBlade LLC in Denison, Texas, USA, and improving the quality of the metallographic cast structure in the cast aluminium component in a piston (Figure 2.11).



**Figure 2.11: Piston cast structure improvement with FSP [23]**

The ability of FSP to enhance the ductility of various alloys also enables formability in components against the welding of a number of detailed components. FSP has been demonstrated to impart superplastic behaviour (elongation greater than 200%) that enables superplastic forming (high temperature forming) in several aluminium alloy sheets with

thickness mostly below 6mm. This allows for replacement of a multi-component assembly with a formed sheet. This application is found in door structures in various industries (Figure 2.12).



**Figure 2.12: Ship door manufactured from superplastic forming [29]**

FSP of both thin and thick plates followed by room temperature bending have also been reported to have wide potential applications ranging from marine, truck trailer, rail cars etc. with significant cost reduction [29]. Roll forming or press brake forming of angle, C-channels, and other shapes can be done with FSP of thin plates usually between 6mm and 13mm and mostly single-pass FSP, followed by room temperature bending (Figure 2.13a). Fusion welding of multiple sections of thick plates could also be replaced by multiple FSP of thick plates (Figure 2.13b) which has been formed.

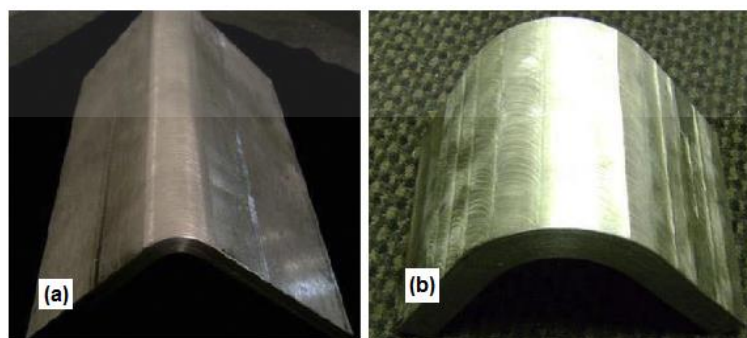


**Figure 2.13: Formed FSP structural components for industrial applications [29]**

## 2.6 Tool Design and Geometry

The FSP tool is very important since its geometry and parameters play a significant role in the material flow which dictates the transverse rate at which FSP can be conducted and in the processed material. FSP tools typically consist of a shoulder and pin as shown in Figure 2.14.

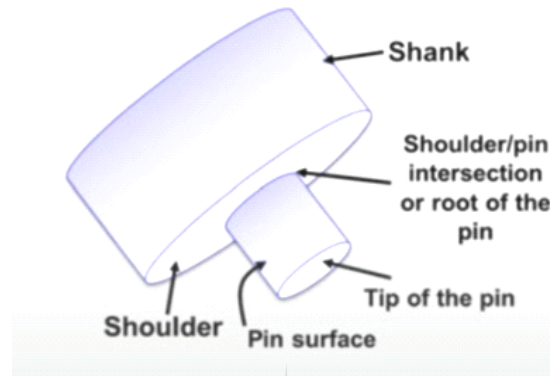


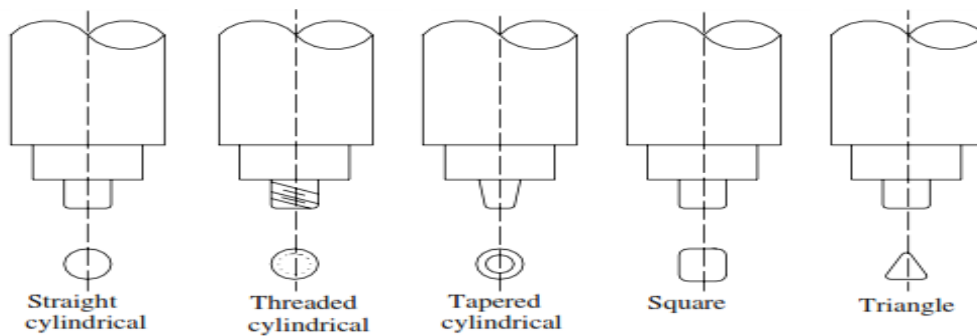
**Figure 2.14: Schematics of the FSW/FSP tool [12]**

Each of the tool parts (pin and shoulder) has a different function. The shoulder is responsible for generating most of the heat during FSP, applying a downward pressure on the workpiece surface, constraining the plasticised material around the pin and preventing the escape of the plasticised material while the rotating pin mainly plasticises, drags along and mixes the adjacent material in the stir zone. Thus, the best tool design may consist of the shoulder and pin constructed with different materials.

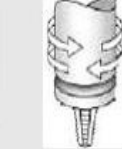
Surekha and Akinlabi [31] reported that the tool material selection is based on the material to be processed. Tool steels, Ni and Co based alloys, cermet, cubic boron nitride and tungsten, and Mo-based alloys are widely used as tool materials. They stated that tool steel can be used for lighter materials like Al and Mg. Thin copper plates of up to 6 mm thick can also be processed using tool steels. It has also been established that tool steel is the most commonly used tool material in FSP [30]. Surekha and Akinlabi [31] stated that having too big a shoulder diameter will affect the material flow and the pin length is determined by the thickness of the plate to be processed. It is usually little shorter than the thickness of the plate.

Improvements in tool design have been shown to cause substantial enhancements in productivity and quality. The tools mainly consist of a concave shoulder profile with a threaded pin; the shoulder-to-pin ratio ranging between 2.5:1 and 3.0:1 for thin sheets [32].

Figures 2.15 and 2.16 give an overview of the basic and advanced types of FSP tools, while Figure 2.17 shows typical FSW/FSP tool shoulder outer surfaces.



**Figure 2.15: Basic FSW/FSP tool profiles [33]**

Tool	Cylindrical	Whorl™	MX triflute™	Flared triflute™	A-skew™	Re-stir™
Schematics						
Tool pin shape	Cylindrical with threads	Tapered with threads	Threaded, tapered with three flutes	Tri-flute with flute ends flared out	Inclined cylindrical with threads	Tapered with threads

**Figure 2.16: Advanced FSW/FSP tools developed at TWI [33]**

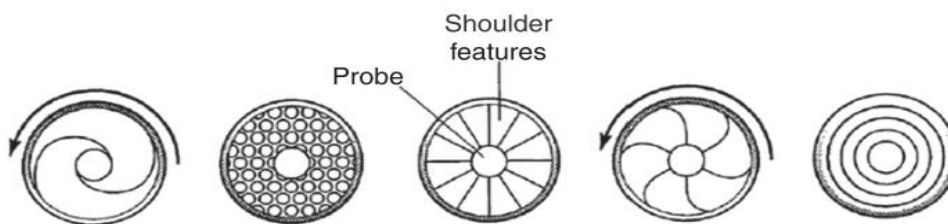


**Figure 2.17: Typical FSW/FSP tool shoulder outer surfaces [34]**

The workpiece and tool materials, tool process parameters (tool rotation and travel speeds), as well as the user's own experiences and preferences, are factors to consider when selecting the shoulder and pin design. In FSP, correct tool material selection entails knowing the

material characteristics that are important in a particular FSP application. Mishra and Mahoney give a summary of current FSW/FSP tool materials [30].

Even though the physical properties of a material are paramount in the selection of tool material, other properties that may dictate selection include ambient and elevated temperature strength, elevated temperature stability, wear resistance, tool reactivity, fracture toughness, thermal expansion coefficient, uniformity in microstructure and density, and availability of tool material [33, 34].

## 2.7 Tool Tilt and Plunge Depth

The depth of the shoulder below the surface of the workpiece during FSW/FSP is defined as the plunge depth. This depth determines the downward pressure required for the tool to penetrate the workpiece properly to obtain a defect-free surface. The proper and adequate setting of plunge depth is very important as high plunge depth damages the backing plate through the rubbing action of the pin on the plate, and low plunge depth causes defects [31].

Suitable spindle tilt towards the trailing direction ensures that the shoulder of the tool holds the stirred material by the threaded pin and moves the material efficiently from the front to the back of the pin. The tool is usually characterised by a small tilt angle ( $\theta$ ), and as it is inserted into the sheets, the blank material undergoes a local backward extrusion process up to the tool shoulder [35]. Figure 2.18 illustrates the tilt angle and the plunge depth of a conventional FSW/FSP tool.

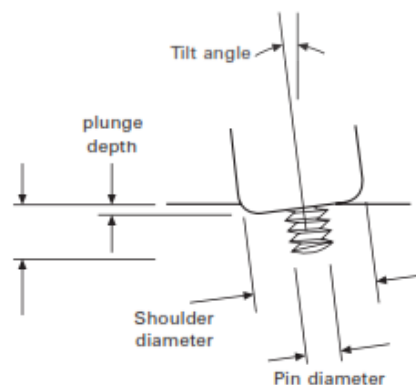


**Figure 2.18: Schematics of tilt angle and plunge depth of FSW/FSP tool [36]**

The tool parameters are very important to the processing quality of the material and need to be given a careful consideration. When the plunge depth is shallow, the shoulder of the tool does not contact the original workpiece surface making the rotating shoulder unable to move the stirred material efficiently from the back of the pin. This will result in the generation of processed material with an inner channel. An insufficient plunge depth in FSP could result in an inaccurate processing depth or the development of voids in the material while too high plunge depth can cause contact and sliding between the pin and the backing plate, which will damage the tool. Also, a large amount of flash may be generated if there is a high plunge depth which could result in a large mismatch in the thickness between the base material and the processed zone [14].

In a study of the effect of tilt angle on metal flow phenomena in the FSW of aluminium alloys and A1100 pure aluminium by Shinoda [37], it was found that the tilt angle affects the metal flow pattern in both the bottom and surface flow directions. Another study by Arici and Selale on the effect of tool tilt angle on the tensile strength and fracture locations of FSW of polyethylene [38], showed that the tensile strength of the material decreased with increasing tool angles.

In general, to improve the quality of the process, a slight tilt can thus be applied by angling the tool by 2-4°, so that its front is higher than the back. With the tool being at an angle, the surface contact between the material and the shoulder of the tool will be reduced, therefore reducing the heat input. As a result, the tilt angle is mostly set between 2-4°, but no greater than 4° [39].

## **2.8 Transverse and Rotational Speeds**

These are important parameters to be very carefully considered to achieve successful FSP. The transverse speed is the speed at which the substrate is moved while rotational speed is the speed at which the tool is moved. [31]. The rotation direction of the tool and the transverse sliding of the substrate or the processing direction is illustrated in Figure 1.1b. These parameters greatly affect the plastic deformation imposed on the material, and hence the generated heat, microstructure, and mechanical properties.

Studies on the effects of tool rotational and transverse speed have been found them to strongly affect the mechanical and microstructural properties of materials. As far as this study

is concerned, these properties include the hardness, tensile strength, grain size, and shape. It is expected that the hardness of the material increases with the generation of fine and equiaxed grains as a result of grain refinement after FSP, and that wear resistance would increase in a corresponding manner with an increase in hardness [13]. The yield and tensile strengths in the FSPd samples are also compared to assess the strength and ductility of the processed sample to the base material.

In a study of FSP on Al 1050 alloy by Kwon et.al [40], it was observed that the hardness and tensile strength of the processed alloy increased significantly with decreased tool rotation speed. It was noted that, at 560 rpm, these properties seemed to increase due to grain refinement by up to 37% and 46% respectively compared to the material at the start of the process. Also, in a study on the effect of welding parameters on mechanical and microstructural properties of AA6056 joints produced by FSW conducted by Cavaliere et al [41], it was found that when high rotating and welding speeds are used, the hardness of the material reaches higher values compared with the base metal, and the profiles become less uniform across the weld center. Tsai and Kao [42] in their research on improvement of mechanical properties of cast Al-Si base alloy using FSP, also stated that increasing the transverse speed and rotational speed results in increased hardness and tensile strength and a large improvement in ductility.

Sato et al. [43] in their study on the microstructure and hardness during FSW on Al 6063-T5 conclude that the maximum temperature of a welding thermal cycle increases with an increase in rotational speed. They observed that the recrystallised grain size increased exponentially with increased maximum temperature. This led them to the conclusion that there is an increase in grain size as the rotational speed increased. Asadi et al [44] in their fabrication of AZ91/SiC surface composite using FSP, also recorded an increase in grain size and a decrease in hardness when tool rotational speed is increased, while Mahmoud et al [45] reported the formation of defects at higher tool rotational speeds in their study of a synthesised AA1050/SiC surface composite by FSP.

Weglowski and Dymek [46] in their study on FSP of an AlSi6Cu4 cast aluminium alloy, stated that increase in the rotational speed causes a decrease in penetration depth, while an increase in travelling speed has a rather negligible effect on penetration depth compared to the influence of rotational speed. This decrease in penetration depth during FSP could result in voids and negatively affect the uniformity in the required processing area.

Furthermore, it has been established that the heat input to a workpiece during FSP increases with higher rotation speed or decreasing transverse speed. If the heat generated is too high, the surface layer can melt which can lead to voids and affect the microstructure of the workpiece as a result of re-solidification. However, if there is insufficient heat generation during FSP, voids and defects could also develop in the processed zone. This may also damage the FSP tool [47].

Wais et al [48] studied the effect of FSP on mechanical properties and the microstructure of pure aluminium and reported that the process temperature was found to increase with increasing rotation rate, and/or reducing transverse speed. At low rotational and high transverse speeds, the amount of heat input is reduced, thereby reducing the softening effect of the tool as it passes the material.

Aruri et al [49] studied the influence of rotational speed on wear, and the mechanical properties of a 6061-T6 aluminium alloy surface hybrid composite [(SiC + Gr) and (SiC + Al<sub>2</sub>O<sub>3</sub>)] fabricated by FSP. They reported that the microhardness and tensile properties decreased with an increase in rotational speed.

From the reviewed literatures, it is appropriate to assume that an increase in transverse speed and a decrease in the rotational speed help to achieve improvement in mechanical properties and reduced heat input. This agrees with the conclusion by Sato et al in their study of the effect of process parameters on microstructure in a FSW process, namely that the recrystallised grain size can be reduced by decreasing the tool rotation rate as well as the heat input [40]. This was reported to have resulted into a fine equiaxed homogeneous grain size which improves the mechanical and microstructural properties of a material. However, the conclusions drawn in other studies [5,49,50, and 51] that high tool rotation rate creates a more homogenous microstructure, nullify this assumption.

Ma et al [5] observe that no branded structure was detected in the nugget zone when the highest rotation rate of 900rpm out of the three used (namely 500 rpm, 700 rpm, and 900 rpm) was used with transverse speeds of 102 mm/min and 203 mm/min out of the three transverse speeds (51 mm/min, 102 mm/min and 203 mm/min). Also, there was no branded structure when a tool rotation rate of 500 rpm was used with 51 mm/min, except that a branded structure was detected for a transverse speed of 102 mm/min.

Elangovan and Balasubramanian [50] and Salman [51] also reported that increased tool rotation rates result in enhanced mechanical properties due to reduced porosity and grain size, which is as a result of frictional heating and stirring present at higher rotational rates creating a higher temperature in the process zone. It can thus be assumed that the rotational and transverse speed to be used in FSP to get good mechanical properties depend strongly on the material to be processed.

## **2.9 Tool Axial Force**

Axial forces act on a tool during FSW/FSP. Akinlabi [13], in a study of dissimilar friction stir welds between 5754 aluminium alloy and C11000 copper, describes these forces as the downward force ( $F_z$ ), transverse force ( $F_x$ ), lateral force ( $F_y$ ), and torque.

The torque is the force required to rotate the tool. This force depends on the downward force, the flow strength of the material and the friction coefficient. The positive force acting towards the advancing side of the weld/stirred zone as in FSW/FSP is known as the lateral force. The downward force is necessary to maintain the position of the tool at or below the material surface while the transverse force acts parallel to the tool motion and is positive in the transverse direction. The study further found that since this force arises as a result of the resistance of the material to the motion of the tool, it might be expected that the transverse force will decrease as the temperature of the material around the tool is increased [52].

Miranda et al [53] in their study on surface modification by friction based processes, emphasised that material consolidation is greatly generated and promoted by the axial forces which affect the friction between the shoulder and the substrate surface. The research stated that a high axial force causes excessive heat and forging pressure, obtaining grain growth and coarsening, and may also result in shear lips or flashes with excessive height of beads on both the advancing and retreating sides, causing metal thinning at the processed area and poor yield and tensile properties. Low axial forces on the other hand lead to poor material consolidation due to insufficient forging pressure and friction heating. Surface finishing is greatly controlled by axial force.

## 2.10 Material Flow in Friction Stir Processing

Material movement resulting from the rotation of the tool in FSP is a very important factor in determining the microstructure of the processed material. The formation of a defect-free zone strongly depends on material flow during FSP and the material flow determines the development of the microstructural features.

Numerous studies have been carried out to study material flow during FSW/FSP in recent years. The techniques used include steel ball tracing technology, stop-action technology, metallography, the marker material method, tracking of tracer particles post-welding by microscopy [54,55], microstructural analysis of dissimilar alloy joints [56,57], in-situ observation using x-ray transmission systems [58], simulation by numerical modeling, and practical flow visualisation techniques [31,54-62].

According to Mishra and Ma [14], material flow is very complex and depends on tool geometry, process parameters, and the material to be welded/ processed. It is very important to understand the material characteristics for optimal tool selection and parameters design as this significantly affects material flow. It was explained in the first chapter that during FSW/FSP, the rotating tool is plunged into the workpiece and advances through the material with a transverse motion. As a result of this rotation, the material on either side of the tool behaves differently [63,64]. This difference in behaviour is because, on one side, the general rotation path and the transverse direction of the tool is in the opposite direction while on the opposite side the rotation and the transverse direction will appear to be in the same direction. These two sides of the tool are known as the ‘retreating side’ (RS) and the ‘advancing side’ (AS), respectively. However, there is need to note that the position of the two sides depends on the transverse direction and whether the tool is spinning clockwise or anticlockwise. This is shown in Figure 2.19.

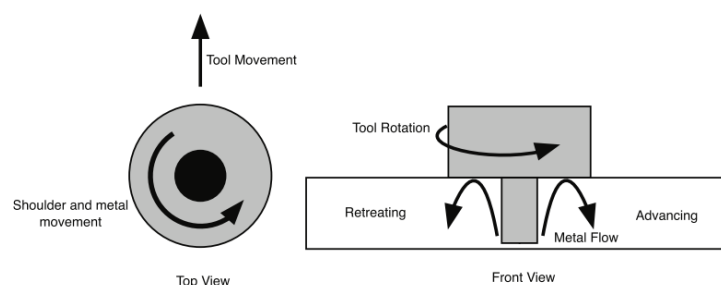


**Figure 2.19: Schematics of tool movement showing metal flow [65]**

As the rotating tool transverses along the region to be processed on the substrate clamped on a backing plate support, the tool shoulder makes firm contact with the top surface of the workpiece with an applied load. Severe plastic deformation is experienced around the tool and a flow of the plasticised metal from the front of the tool to the trailing edge occurs [66].

The tool shoulder facilitates bulk material flow while the pin helps in the layer by layer material flow. The shape of the pin and shoulder has significant influence on the flow of the plasticised material. It has been reported that square tool geometry results in a more homogeneous distribution of particles than other tools. However, circular tools seem to show much less wear than flat-faced tools [67].

Nandan et al [32] in their study on recent advances in FSW process, weldment structure and properties stated that in general, three types of flow transport the plasticised material during FSW/FSP. First, tool rotation and the friction between the tool and the substrate material heat and stir the softened material near the tool. Second, downward material flow in the region close to the tool created by using a threaded pin causes an upward motion at the outer edge of the mixing region of the stir zone and finally, material flows along the welding direction as a result of the movement of the tool. It is shown that most of the material flow caused by these three types, happens on the retreating side.

Mishra and Mahoney [30] reported that the definition of the flow paths of plasticised materials was first obtained in a study by Colligan [63]. In recent years, different marker materials such as aluminium alloys that etch differently from the parent material [64,68,69], copper foil [70], small steel shots [63,71] and other techniques [72,73] have been used to track material flow during FSW/FSP.

Colligan [63,71] studied the material flow behaviour during FSW on aluminium alloys by means of a steel shot tracer and “stop action” technique using a small steel ball of 0.38mm diameter embedded along the welding direction at different positions in the weld joint of two aluminium plates. The study revealed that the tracer steel shot distribution is divided in two categories; chaotic and continuous distribution. In the chaotic distribution, the elements were scattered in an irregular way within a relatively wide zone behind the welding tool pin in the region near the top surface of the weld, and the chaotically deposited tracer steel shots have moved to a greater depth from the original position. In the continuous distribution, the initial continuous line of the steel shots was reoriented and deposited as a roughly continuous line

behind the pin in the other region of the weld. It was concluded that not all the materials were stirred, and rather a large amount of material was simply extruded around the retreating side of the tool and deposited behind.

Guerra et al [70] studied the material flow of FSW on AA6061 using a faying Copper foil surface tracer and a pin removed at the end of the welding process, and concluded that the movement of materials around the pin in FSW can be divided into two processes. First, the materials on the AS front of the weld entered a zone that rotates and advances at the same time as the pin, with the materials getting highly deformed and the zone showing a high Vickers microhardness. Second, the materials on the RS front side of the pin extruded between the rotational zone and the parent material with the zone exhibiting a lower Vickers microhardness. Figure 2.20, shows the copper of 0.5mm thick sheet which is used as a marker to visualise the material flow in FSW.

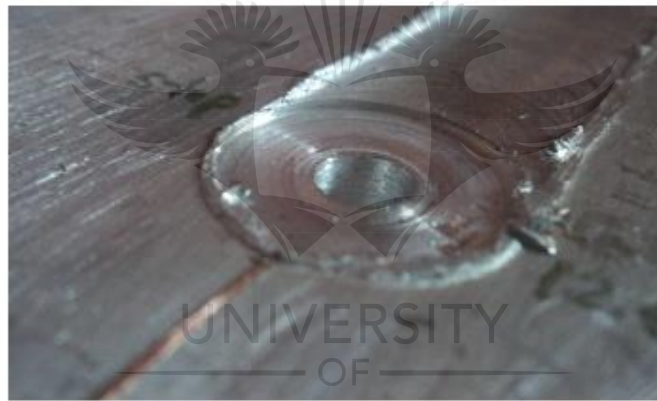


**Figure 2.20: Copper marker shown in the joint line on the lower left of exit-hole damage in AA1100 alloy weld [63].**

Reynold et al [64, 68] in their investigation of the material flow behaviour in FSW on 2195 Al-T8 embedded markers made of 5454Al-H32 as shown in Figure 2.21 reported that all welds exhibit some common flow patterns and that the flow is not symmetrical about the weld centre line.

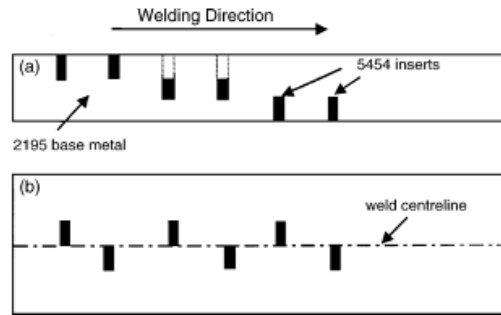


**Figure 2.21: Schematic drawing of marker configuration [64]**

It was also revealed that the bulk of the marker material moved to a final position behind the original position, and this backward movement was limited to one pin diameter behind its original position. Also, there was a well-defined interface between the advancing side and the retreating side. The materials were not really stirred across the interface during the FSW process but was reported to have been pushed downward on the advancing side, and moved towards the top at the retreating side in the pin diameter, indicating that a stirring of material occurred only at the top of the weld where the rotating tool shoulder that moves the plasticised materials from the retreating side around the pin to the advancing side has significant influence.

The flow of material during FSW/FSP is a very complex process not yet fully understood despite numerous investigations [63-78]. Material flow is largely uncharacterised because it is difficult to measure and trace the markers. In lieu of this, a mathematical model is required to analyse the material flow. Models that have been employed so far include a Thermo-Mechanical Flow Model (STIR-3D) by Smith et al [75] and Bendzsak and Smith [76], a Slipping Interface and Frictional Contact Model for simulation of FSW process by Xu et al [77], a two-dimensional finite element method code DEFORM [78], a Nunes Kinematic Model, and Arbogast Metal-Working Model [31].

## **2.11 Microstructural Studies on Friction Stir Processed Aluminium**

A basic understanding of the evolution of the microstructure in the recrystallised region of friction stirred material after FSW/FSP, is essential. Generally, FSW/FSP divides the microstructure of joints/processed zones into distinct zones which are the unaffected or parent material (PM) also known as the base material (BM), heat affected zone (HAZ), nugget zone (NZ) or stir zone (SZ), thermo-mechanically affected zone (TMAZ) shown in Figure 2.22.

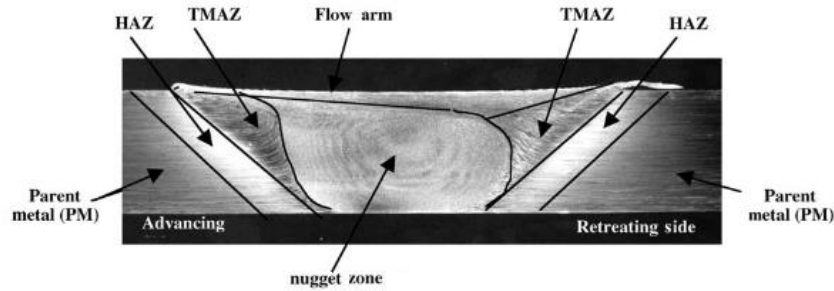


**Figure 2.22: Transverse section of FSW/FSP showing different regions [30]**

The nugget or stir zone (the location of the pin during stirring) is composed of equiaxed grains. During FSW/FSP, the coincidence of heat and heavy plastic deformation results in the occurrence of dynamic recrystallisation at the centre of the weld/processed zone. The grains in the nugget zone are often smaller than the grains in the BM. TMAZ has the common feature of elongated or rotated grains, and recrystallisation does not happen in this area because of inadequate heat and plastic deformation. In this region, the FSP tool has plastically deformed the material, and the generated heat has had some influence on the material. In the HAZ region, lies closer to the TMAZ, the material has experienced a thermal cycle, which modifies the microstructure or the mechanical properties. However, the plastic deformation has not occurred in this area. The most common metallurgical phenomena usually occurring in this area are grain growth, and coarsening of strengthening precipitates. The BM is the material far from the stir zone without deformation; and although it may experience a thermal cycle from the stir, it is not affected by the heat in terms of the microstructure or mechanical properties [14]. Figure 2.23 below shows the microstructural evolution in different zones of FSP/FSW material.

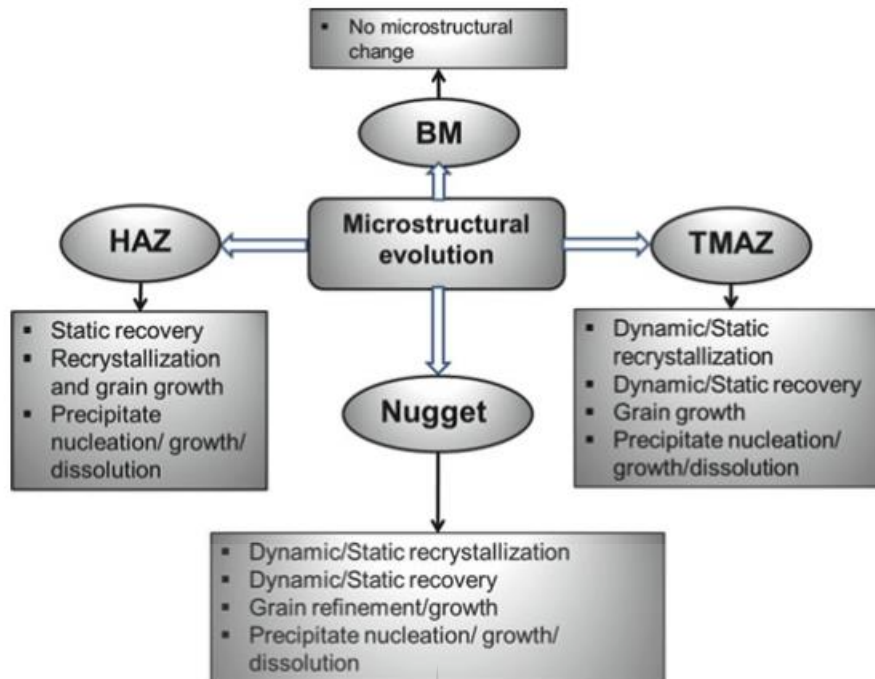


**Figure 2.23: Schematic of the microstructural evolution in different zones of FSP/FSW material [12]**

Yadav and Bauri [79] studied the FSP of commercially pure aluminium to understand the developed microstructure and its effect on the metal's mechanical properties. A single-pass FSP was performed on a 12 mm thick plate with an M2 steel tool with a shoulder diameter of 12 mm and a pin with 3 mm diameter and 2.1 mm length. The FSP performed at a tool rotational speed of 640 rpm and a transverse speed of 150 mm/min, and recorded a significant decrease in the grain size from 84  $\mu\text{m}$  to 3  $\mu\text{m}$  through dynamic recrystallisation process. The yield and tensile strengths improved significantly from 35 MPa to 82 MPa and 72 MPa to 90 MPa respectively. The hardness also showed a significant improvement of 34% when compared to the base material of 29 HV. These major improvements in the yield strength, tensile strength, and hardness are recorded to have resulted from the finer grain size from FSP. However, there is also a 10% reduction in the ductility of the material after FSP.

Gan et al [80] also reported fine, equiaxed and fully recrystallised grains in their study of the evolution of the microstructure and hardness of rolled pure aluminium after FSP. They carried out a single-pass FSP on a 2 mm thick plate with a 10 mm shoulder diameter and a cylindrical probe of 5 mm diameter and 1.65 mm length. The tool was operated at a tilt angle of 2.5° with a rotational speed of 800 rpm, and transverse speed of 200 mm/min along the

rolling direction of the plate. They recorded different average grain sizes 2.97, 2.61 and 3.11  $\mu\text{m}$  across three different locations defined by  $5^\circ$  misorientation in the stir zone, with the smallest grain size recorded towards the RS. However, contrary to the report by Yadav and Bauri [79], there was a reduction in material hardness from 31 HV to  $\sim 24$  HV with the lowest hardness in the stir zone, making the hardness curve a U-shaped as against a W-shaped usually recorded in aluminium alloys. They observed a local material softening in the FSPd zone, and recorded that the decrease in hardness is resulted from the dissolution of precipitates during FSP being pure aluminium.

Chainarong et al [81] studied the FSP of SSM3356 aluminium alloy at a rotating speed of 1750 rpm and a tool transverse speed of 160 mm/min. They recorded a refinement in material grain size which consisted of uniformly distributed silicon particles throughout the stir region. A significant increase of 59.07% to 64.55 HV in the hardness was recorded, and an increase of 11.8% in the tensile strength to 188.57 MPa was observed compared to the base material.

Kapoor et al [82] studied the effect of FSP on the tensile and fatigue behaviour of cast A206 alloy. A single-pass FSP was carried out on the material in the cast +T4 condition using a conical tool with a shoulder diameter of 25.4 mm, a conical pin with 8.1 mm base diameter and length of 6.8 mm at a tool rotation of 1000 rpm and a transverse speed of 2.5 mm/s, using a plunge depth of 6.8 mm and a tilt angle of 2.5 mm/s. The A206 alloy in cast condition consists of large grains with pores and intermetallic particles which are mostly located at grain boundaries. The average grain size and intermetallic particles of 210 and 6  $\mu\text{m}$  in size respectively in the base material was refined to 3.5 and 3  $\mu\text{m}$  after FSP. The tensile strength and ductility improved after FSP while the yield strength showed no improvement. Pore elimination and a reduction in the intermetallic particle size were reported to have contributed significantly to the increased fatigue life of the material.

Mahoney and Lynch [83] reported on the elimination of casting porosity in a single-pass FSP of cast A356 aluminium. There was a formation of a relatively homogenous fully recrystallised fine grain microstructure as illustrated in Figure 2.24, which showed an 18% increase in tensile strength to 34 MPa and an increase from 3% to 17% in strain to failure.

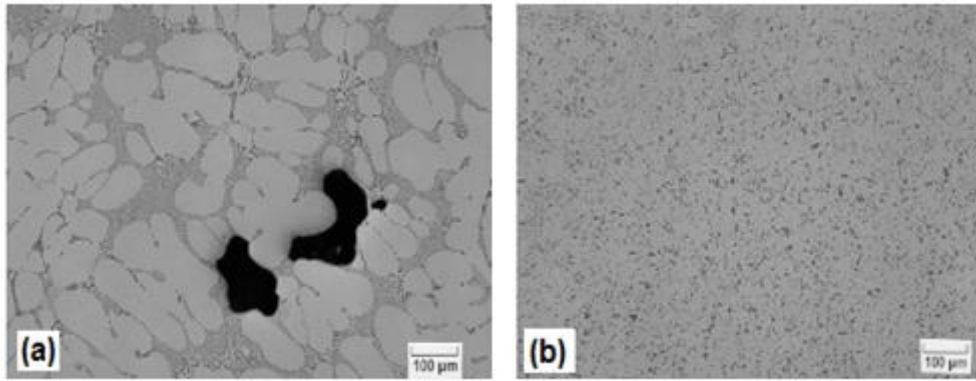


**Figure 2.24: (a) As-cast A356 Al illustrating casting porosity and dendritic structure, and (b) FSP A-356 showing a homogeneous microstructure in stir zone [86]**

Sun and Apelian [84] studied the microstructural evolution during single-pass FSP of aluminium cast alloys. They carried out FSP on a one inch thick sand casting A206 aluminium workpiece with a processing parameter of 1000 rpm – 1 in/min and recorded high grain refinement in the stirred zones to micrometer levels with a significant reduction in porosity, which was almost eliminated. Microstructural, tensile and microhardness tests were carried out on the FSPd A206 specimen to investigate the effect of FSP on the microstructure and mechanical properties of the alloy. It was revealed that FSP resulted in higher ductility in the as-cast-T4 A206 because of the elimination of porosity. There was high grain refinement in the nugget zone which leads to a great improvement in the microhardness profile in most nuggets as shown in Figure 2.25. However, a relatively lower microhardness was recorded in the TMAZ; this may have been the result of large grain size and dissolution of precipitates into the matrix during FSP.

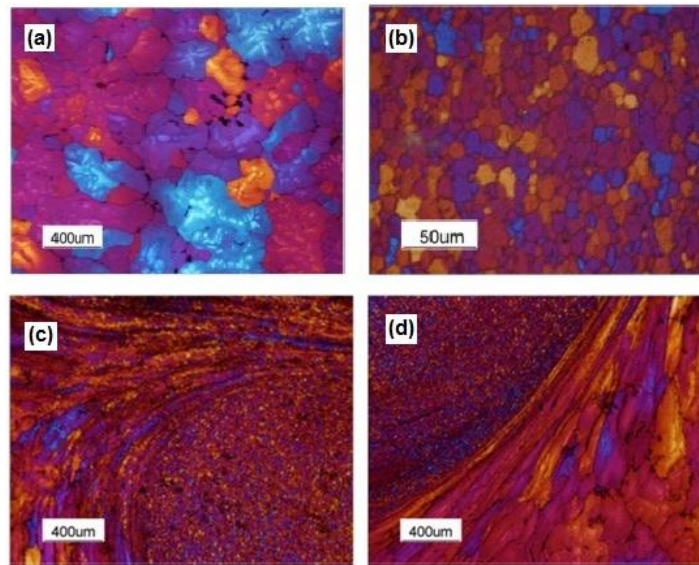


**Figure 2.25: Microstructure of A206 after FSP at 1000 rpm – 1 in/min: a) as-cast + T4; b) refined grains in the nugget. Microstructure of the transition zone between FSP zone and parent material of the A206 sample (1000 rpm – 1 in/min); c) retreating side boundary; d) advancing side boundary [84]**

Hashim et al [85] studied the effect of FSP on 2024-T3 aluminium alloy. The process was carried out on a 5mm thick plate with a tool steel tool which had a 10 mm pin diameter at a constant rotation and a transverse speed of 945 rpm and 85 mm/min respectively and a plunge depth of 0.25 mm. A refinement in the grain size from 192 µm in the as-received aluminium 2024-T3 alloy to 45 µm was recorded, and the second-phase particles were refined as a result of the mixing action of the tool. The microhardness of the material increased to 190 HV from 130 HV recorded in the base material. There was also an increase of 15% and 9% in the yield and tensile strengths respectively. The yield strength increased to 372 MPa from 323 MPa while the tensile strength increased from 446 MPa to 487 MPa. The FSP had no effect on the ductility of the material.

Karthikeyan [86] studied the effect of single-pass FSP on the microstructure and mechanical properties of extruded cast 2285 aluminium alloy using a tool with a 4 mm long tool pin and a flat shoulder of 16 mm, with the tool angle set at 2° at a low feed rates of 10 mm/min, 12 mm/min, and 15 mm/min. FSP improved the microstructure of the extruded cast Al alloy as expected and the defects in the metal were eliminated. However, the tensile and yield strengths showed a slight decrease with an increase in feed rate from the lowest to the highest feed rate used. A negligible reduction in the hardness was also noticed, decreasing from 110

HV at a feed rate of 10 mm/min to 109 HV at a feed rate of 12 mm/min, and finally to 108 HV at a feed rate of 15 mm/min. The ductility also showed a slight decrease with increasing feed rate. However, there is an improvement in the hardness, ductility, tensile and yield strengths compared to the base metal.

Weglowski [87] studied the microstructural characterisation of a single-pass FSPd cast 6 mm AlSi9Mg aluminium alloy performed with 500 rpm rotational speed, 560 mm/min transverse speed, at a tilt angle of 1.5°, and reported that the uniform concentration distribution of Fe, Si, and Mg in the FSP area was significantly improved compared to that in the as-cast sample; the porosity was also eliminated thereby refining the microstructure of the material. The hardness distribution was non-uniform in the modified area, and lower than the base material in the stir zone, and higher in the TMAZ.

Salman [51] also studied the effect of single-pass FSP on mechanical properties and the microstructure of Al-Zn-Mg-Cu alloy and reported that FSP resulted in significant grain refinement, elimination of casting defects, and that there was an improvement in the tensile strength and ductility of the aluminium alloy. The hardness also increased and relatively uniformly distributed in the processed zone.

A recent study of the effect of FSP on Al-Zn-Mg alloy was conducted by Mandal [88]. Single-pass FSP was conducted with a tool with a 3 mm pin diameter and 5 mm pin height at 1025 rpm rotation speed and a workpiece transverse speed of 75 mm/min. The tilt angle was set at 2.5°. It was recorded that there was significant grain refinement after FSP, which was achieved through large plastic deformation with intensifying heat which induces the generation of severe crystal lattice rotations and simultaneously an extremely high number of dislocations rearranging themselves into new long and high-angle grain boundaries. The yield and tensile strengths increased from 53.7 MPa to 162 MPa and 83.9 MPa to 278 MPa respectively after FSP. However, an evaluation of the hardness of the material was not conducted in the study.

The effect of single-pass FSP on mechanical properties and microstructure of sand casting eutectic Al-12wt%Si alloy was studied by Wais et al [89]. They reported that the grain structures of the hypoeutectic Al-12wt%Si alloy were found to be very coarse after casting with grains closer to the surface of the plate finer than those developed at the centre of the material. The microstructure of the Al-Si was found to be greatly refined by FSP. After FSP

all the Si was greatly refined. However, microstructural homogeneity was not necessarily achieved throughout the processed zone; the refined particles were found to be finer and more homogeneous on the AS than the RS of the processed zone.

The mechanical properties of the as-cast were very poor due to the presence of large pores and brittle Si particles which existed in the material after casting acting as crack nucleation. The alloys demonstrated significant improvement in tensile properties with an increment in the tensile strength from the initial 123 MPa to more than 159 MPa, and ductility higher than 14% due to the elimination of porosities and refinement of the microstructure. However, it was reported that the latter had little influence on the hardness of the material; only small changes in hardness were observed. This does not happen often in non-heat-treatable alloys which generally tend to show a great improvement in hardness because of the refinement in the microstructure.

Ma et al [5] in their study of the effect of a single-pass FSP on the microstructure of cast A356 aluminium reported that FSP resulted in a breakup of both the fibrous Si particles and the aluminium dendritic structure with quite a uniform redistribution of Si particles in the aluminium matrix. FSP resulted in the generation of a fine and recrystallised microstructure with a grain size of  $\sim 3\text{-}4\ \mu\text{m}$  in the FSPd A356 sample. It was concluded that the distribution pattern, size, and volume fractions of Si particles at various locations in the processed zone indicate inhomogeneous material flow. No test was done on the mechanical properties in the research.

A clear illustration of the microstructural inhomogeneity in the transition from the base to the processed zone in a single-pass was shown by Sampath et al [90] in their fabrication of FSPd Al-Ni particulate composite (Figure 2.26). Single-pass FSP was carried out at a tool rotation speed of 800 rpm and 0.3 mm/s transverse speed on a 5 mm thick plate with a tool of shoulder diameter 10 mm, pin diameter of 6 mm, and pin depth of 3 mm.

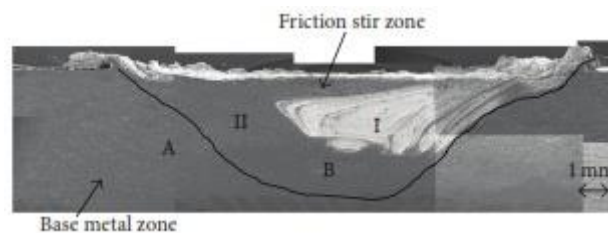


**Figure 2.26: Macrograph of FSPd Al-Ni particulate composite [90]**

The friction stir/processed zone (FPZ) has two clearly distinguished zones; one with an onion-ring-like structure (region I), and the remaining unmixed region (region II) showing that the stirring action is more severe in region I compared to region II. It was suggested that these microstructural differences result from the difference in the metal flow between the tool AS and RS which results in a fluctuation in hardness values across the FPZ.

A similar observation in microstructural inhomogeneity was reported by Salehi et al [91] in their optimisation of process parameters for producing AA6061/SiC nanocomposites using FSP. While there were no voids and cracks in their samples, they observed some unmixed SiC powder in the FPZ which they attributed to the application of a single FSP pass. They also recorded that the part of the FPZ with better microstructure characteristics could be attributed to more vigorous stirring during FSP. They concluded that single-pass FSP is not sufficient, which is in accordance with conclusions in other studies [18, 92].

Chen et al [93] carried out a three-pass FSP with 100% overlap on a 3.5 mm thick cold rolled Al-5083 aluminium alloy sheet at a rotational speed of 1200 rpm and a tool transverse speed of 360 mm/min with an H13 steel tool with a concave shoulder of 12.5 mm and a tapered pin of 5-8 mm. They observed a defect free SZ in the FPZ. While the base material grain size and mechanical properties were not reported, it was observed that the grains were elongated due to cold rolling and that there was a refinement in grain size due to recrystallisation to 3.12  $\mu\text{m}$  in the first pass. There was no substantial change in grain size after subsequent overlapping passes. Grain sizes of 2.98  $\mu\text{m}$  and 3.02  $\mu\text{m}$  were recorded after the second and third FSP passes respectively. All the FSP passes exhibited reduced hardness, yield strength and tensile strength in the SZ compared to the base material while the elongation improved to double that obtained in the base material. However, there was no significant effect on all these properties with subsequent multiple passes. Nascimento et al [94] reported a similar result for AA7022- T6 alloy which showed a reduction in grain size from 160  $\mu\text{m}$  to an average grain size of 7.1  $\mu\text{m}$  after single-pass FSP; this remained relatively constant independent of the number of passes and overlap ratios.

The influence of multi-pass friction stir processing on the microstructural and mechanical properties of 6 mm thick commercial 6082-T651 AA plates was studied by El-Rayes and El-Danaf [95]. Samples with one through three passes with 100% overlap were created using FSP to locally modify the microstructural and mechanical properties of AA6082-T6. A tool steel with a flat shoulder of 15 mm diameter, 5 mm pin length and 6 mm edge length at a

constant rotational speed of 850 rpm and three different traverse speeds, was used for processing. It was reported that FSP caused dynamic recrystallisation of the stir zone leading to equiaxed grains with high angle grain boundaries which increased with increased number of passes.

The accumulated heat accompanying multiple passes resulted in an increase in the grain size, dissolution of precipitates and fragmentation of second-phase particles in all three transverse speeds used. There was a decrease in the hardness and tensile strength across the three transverse speeds after subsequent multiple passes. The hardness reduction was reported to be caused by the SZ softening which accompanied the increase in the number of passes. This softening was attributed to larger grain size after subsequent FSP passes. It was also suggested that the reduction in the tensile strength was due to the over aging effect which the subsequent passes caused to the previous one.

Rao et al [96] similarly reported that the average hardness values in both single-pass FSP and two-pass FSP were lower than that of the base metal. However, two-pass FSP with 100% overlapping on the top of the first pass itself had a significant effect on size, shape, and distribution of the Si particles in Al-30Si. The reduction in the average size of the Si particles after single-pass FSP is 98%., which further refined to 99% after the second pass.

Shafiei-Zarghani et al [97] in their recent attempt to incorporate nano-sized Al<sub>2</sub>O<sub>3</sub> into the surface layer of 6082 Al alloy observed that after a single-pass FSP, the Al grains were refined down to ~4.8 μm. However, although the nanoparticles were integrated into the Al matrix, they tended to be distributed in clusters. After multiple-pass processing, the dispersion of the nano-sized Al<sub>2</sub>O<sub>3</sub> particles was improved. The grain size was further reduced to ~0.7 μm after four-pass FSP because the homogeneously distributed particles were effective in pinning and suppressing grain boundary migration. As a result, the hardness and wear resistance of the surface composite layer was increased by three times, compared to the base material.

Yang et al [98] carried out four-pass FSP with 100% overlap on a 6 mm thick plates Al<sub>3</sub>Ti/A356 composites to study the effect of multi-pass FSP on the microstructure and mechanical properties. No defects were observed on any of the FSPd samples, and a completely homogenous zone was reported after the fourth pass. The SZ homogenous contrast significantly widened towards the RS, eliminating the porosity completely after the

third FSP pass. The Al<sub>3</sub>Ti particles were completely homogenous after the fourth pass FSP. There was a significant decrease in the grain size from 80µm in the base material to 5.4, 1.8, 1.5 and 0.8 µm in the first, second, third, and fourth passes respectively. The yield strength, tensile strength, and ductility also improved after every subsequent pass from the first to the fourth. These were reported to be a result of the grain refinement. No study on the hardness was conducted; however, it was concluded that microstructural homogeneity can be greatly achieved by multi-pass FSP.

A contrary report to that of Yang et al [98] regarding the microstructure and mechanical properties followed on the study of the effect of multi-pass FSP on aluminium metal matrix by Krishna and Satyanarayana [99]. They carried out three-pass FSP with 100% overlap with an HSS steel tool with a 16mm shoulder diameter and 2.3 mm tapered pin diameter and pin length of 2 mm on a 4 mm Al6331+SiC composite. While the grain sizes and silicon flakes were reported to be reduced after subsequent FSP passes, there was also a reduction in yield strength, tensile strength, hardness, and elongation with an increase in the number of passes. This reduction was attributed to the precipitate dissolution and the limited re-precipitation by the thermal cycles of FSP.

Several reviewed studies also describe the microstructural observations and mechanical characteristics at different overlapping percentages. Ma et al [100] applied five multi-pass FSP (with 50% overlap) on a cast Al–Si–Mg A356 alloy and it was established that overlapping FSP did not exert a significant effect on the size and distribution of the Si particles; the particles which were broken by FSP were uniformly distributed in the entire processed zones. It was found that in the as-processed condition, the strength and ductility of the transitional zones between two FSP passes were slightly lower than those of the nugget zones. In addition, the strength of the previously processed zones was higher than that of the subsequently processed zones due to over aging from the FSP thermal cycles.

Nakata et al [101] improved the mechanical properties of an aluminum die casting alloy by multi-pass friction stir processing due to microstructural modification. They conducted the experiment on 4 mm thick plates of ADC12 aluminum die casting alloys. FSP was continuously applied fourteen times by moving in 4 mm increments towards the AS. The hardness of the multi-pass FSP part is a uniform 110 HV, which is about 20 HV higher than that of the base metal. The hardness of the base metal is variable; the hardness increase is caused by deleting the casting defect, a fine dispersion of Si particles, and grain refinement.

The tensile properties of the ADC12 base metal and the FSPd specimens were also compared, and it was found that the tensile strengths of the processed specimens were much higher than that of the base metal. The average tensile strength of 330 MPa in the parallel direction increased by about 1.7 times over that of the base metal of 190 MPa. The elongation of the multi-pass samples was reported to be higher than the base metal; the average of 7.8% increased by about 3.5 times over that of the base metal of 2.2%.

A study similar to Nakata et al above was conducted on AA7029 alloy by Sinhmar et al [102]. They carried out multi-pass FSP with 50% overlap on a 5 mm thick AA7039 alloy plate with a die steel tool which had a concave shoulder of 20 mm diameter, a conical pin of 5 mm diameter and 2 mm length at a tilt angle of 2°. The rotational and transverse speed was 1025 rpm and 75 mm/min respectively. A single-pass FSP refined the grain size from 44.3 µm in the BM to 4.5 µm, while multi-pass FSP was reported to have led to a slight coarsening of the grain zone which was processed by previous FSP passes. This was attributed to the application of additional heat during subsequent passes in the overlapped region of SZ and to the retention of high temperature for a longer period in the already processed zone.

The yield strength, tensile strength, and hardness of the processed samples decreased compared to the base material. The reduction in tensile strength was attributed to recrystallisation and reversion (dissolution of strengthening MgZn<sub>2</sub> caused by friction heat generated during FSP). The hardness in the stir zone was 92.1 HV, which was lower than the hardness in the BM of 139 HV. The reduction in the hardness in the first pass was attributed to reversion. An increase in the hardness to 101.1 HV was observed after the second FSP pass. This increase was reported to be as a result of the increase in work hardening effect of the already processed material, and the re-precipitation of few strengthening precipitates (MgZn<sub>2</sub>) which occurred due to the thermal cycle experienced. The ductility showed higher elongation after FSP which was attributed to grain refinement.

## **2.12 Summary**

This literature review examined the applications and significance of FSP, and gives basic insights into FSP parameters, material flow in FSP, and microstructural studies on FSP aluminium materials. Wide research has been undertaken on the FSW process which is the

origin of FSP, but there is very limited literature available about FSP on aluminium materials compared to the former, most especially on the study of multi-pass FSP.

It was observed that most researchers use FSW and FSP interchangeably in research. The difference in these processes was outlined in the first chapter of this dissertation. It is very important to note that reviews on microstructural studies conducted in this research on aluminium materials were strictly based on FSP and not FSW and only studies related to the research objectives were studied. The FSP processing parameters were explained to fully understand the dependency of microstructural evolution on processing parameters in pure aluminium, alloys and composites. Most of the reviewed reports show clearly that FSP completely depends on FSP processing parameters and the material of the workpiece, for both single and multiple passes. It was observed in the literature on FSP that a random set of parameters was used for processing. The most important aspect in FSW/FSP is the selection of optimum processed parameters to achieve a defect-free material. The processing parameters were observed to greatly influence the material flow in a workpiece during FSP.

Material flow was observed to be the prime factor in determining the homogeneity of the processed zone in the material but a correlation between this homogeneity and mechanical properties has not been ascertained. However, a number of researchers have suggested that multi-pass FSP could increase homogeneity in processed zones if more research on this is carried out. In this study, the effect of 100% overlapping multi-pass FSP on AA6061-T6 is evaluated.

Aluminium 6061 is one of the most extensively used aluminium alloys because it has most of the good qualities of other aluminium alloys. It offers good mechanical properties and corrosion resistance, and it's easy to join/weld [103]. However, the aluminium alloy 6061 in its T6 condition is of great interest because it usually tends to lose some strength in the weld region after joining/welding because its solution heat-treated and artificially aged. It is noteworthy that the multi-pass samples are identified with their respective number of passes. The homogeneity of the processed zone, the mechanical properties, the microstructural evolution, as well as their correlation was investigated. The experimental procedures employed in this research study are detailed in the next chapter.

## 3. Experimental Procedures

### 3.1 Introduction

This chapter outlines the experimental techniques used in evaluating the effect of multi-pass FSP on aluminium. It describes in detail the materials and methods employed in the research ranging from laboratory analysis of the tests conducted on parent metals to the characterisation procedures followed for the FSP materials. The chapter discusses the material composition, experimental set-up employed to produce multiple numbers of FSP passes on the materials, and the measurements of the material properties before and after FSP.

### 3.2 Parent Material

The parent materials used in this research was AA6061-T6. The dimension of the test coupon for each plate was 250 x 210x 6 mm and the length of the welds produced was 200 mm. The chemical composition of the parent material was confirmed, using a spectrometer (Appendix A), and was found to conform to the standard AA6061-T6 specifications [103]. Table 3.1 shows the chemical composition of the parent material.

**Table 3.1: Chemical composition of AA6061-T6**

Element	Si	Fe	Cu	Mn	Mg	Cr	Ni	Zn	Ti	Al	Ag
Wt. %	0.68	0.49	0.21	0.08	0.84	0.06	0.01	0.07	0.07	97.40	Balance

### 3.3 FSW Platform

An FSW machine at the Indian Institute of Science (IISc), Bangalore, India was used to produce the welds. It is a custom designed computer controlled 2-Axis FSW machine with the tool in a horizontal position and the specimen held in a vertical position. This machine was developed with the help of ETA technologies in Bangalore and has the capability to vary tool rotational speed, traverse speed and plunge depth during a process. This platform is shown in Figure 3.1.

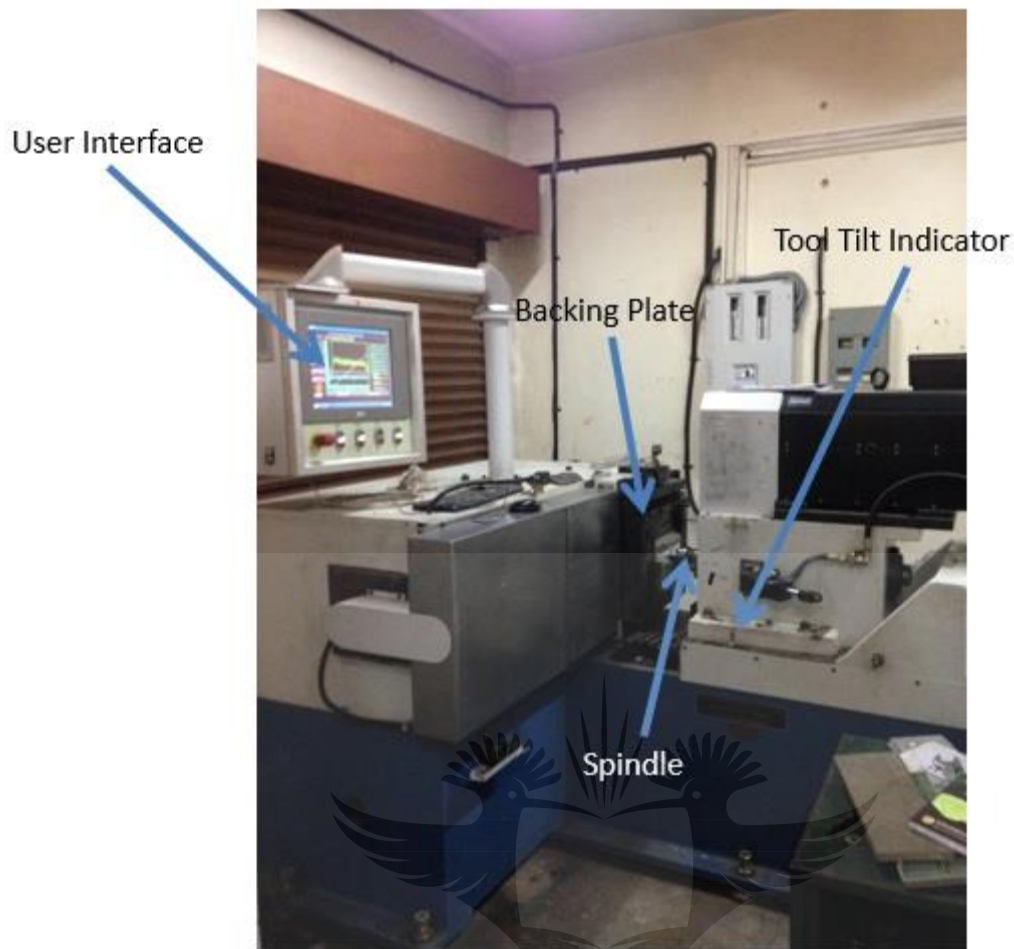


**Figure 3.1: FSW platform**

### **3.4 FSP Process Parameters**

The FSP tool used for this research was a high-density steel (HDS) tool with a concave shoulder diameter of 25 mm and a cylindrical pin with a tapered diameter of 6-7 mm, and length of 5 mm (Figure. 3.2). The HDS tool was chosen because of its high strength, hardness, availability and low cost. The geometry and parameters of the tool were also based on literature reviews. A constant 3° tilting angle was applied to the tool, and all FSP was performed in a position control mode, with a plunge depth of 5.3 mm. The plunge depth ensured that the necessary downward pressure was achieved and the tool fully penetrated the weld, while the tool tilt angle ensured that the rear of the tool was lower than the front. A constant rotational and transverse speed of 1600 rpm and 40 mm/min respectively was maintained throughout the FSP. These were optimum parameters earlier obtained for FSP on AA6061 [91].

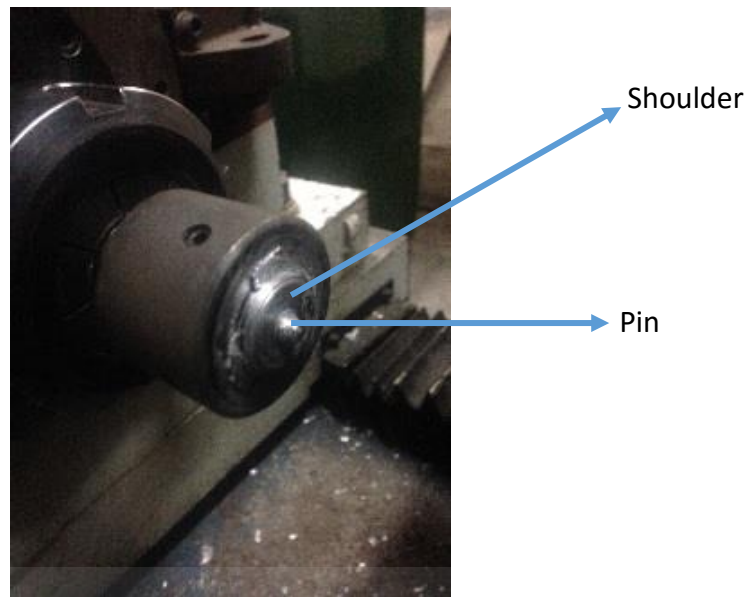


**Figure 3.2: High-density steel FSP tool**

### **3.5 FSP Experimental Procedure**

The FSW machine has an installed customised programme to control the FSW/FSP process which provides the interface to input the process parameters required to execute the process. The motions of the tool assembly in the x and z directions, as well as the other parameters are defined with this customised programme. The FSP process began with a clean workpiece firmly clamped to the backing plate already provided on the FSW platform. The FSP programme was computed by inputting parameters, after which the tool assembly was moved to the process start position. After the spindle rotation started, the tool was plunged into the workpiece dwelling for five seconds to achieve a sufficiently plasticised state. The tool was then moved along the desired direction with specified combination of rotational and translation speeds. The tool was retracted from the workpiece after reaching the weld length as defined in the welding programme. Since this is a position controlled process, the forces generated during the entire process are recorded using the data acquisition system provided on the customised welding programme. The processed sheets are then unclamped from the backing plate and prepared for microstructural and mechanical testing. In this research, five FSP passes with 100% overlap were conducted with increasing passes on different workpieces. The processed samples were cooled down to room temperature before successive passes were conducted.

### 3.6 Sample Preparation

Samples were sectioned using a Concord wire electric discharge machine (EDM) (Figure 3.3) employing a 0.2 mm diameter molybdenum cutting wire. For optical microscopy (OM), samples of 25 x 6 x 6 mm were sectioned at the processed zone, and mounted in polyfast thermoplastic resin as shown in Figure 3.5, with a Struers hot mounting machine (Figure 3.4a), and identified according to the number of FSP passes with an engraving tool. The samples were then ground and polished using a Struers polishing machine (Figure 3.4b), and cleaned with distilled water. The samples were mounted, ground and polished with the AS of the weld always to the right following the standard metallographic procedures shown in Appendix B [104]. After this, samples were chemically etched to reveal their microstructures. At the initial stage of the research, the samples were etched with Keller's reagent (190 ml distilled H<sub>2</sub>O, 5 ml HNO<sub>3</sub>, 3 ml HCL, and 2 ml HF) but the grains were not visible, hence Weck's reagent (100 ml distilled H<sub>2</sub>O, 4 g KMnO<sub>4</sub>, 1 g NaOH) was subsequently used. The samples were observed under a microscope for microstructural characterisation and tested for microhardness. The tensile samples were sectioned from the processed aluminium material using the EDM according to ASTM E8M-13 standard [105] (Figure 3.6) and tested for tensile strength.



**Figure 3.3: Concord wire electric discharge machine**

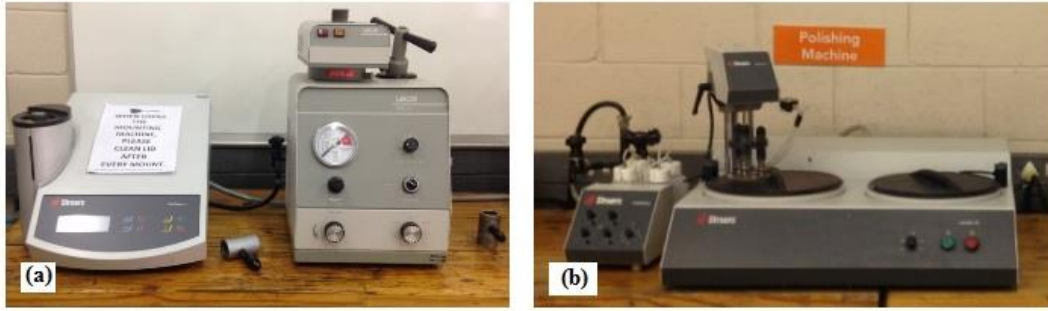


**Figure 3.4: Struers (a) hot mounting machine (b) polishing machine**

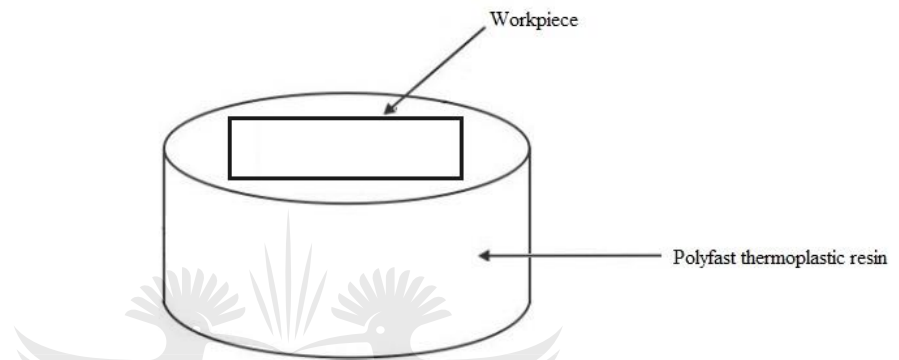


**Figure 3.5: Schematics of samples for microstructural and microhardness tests**

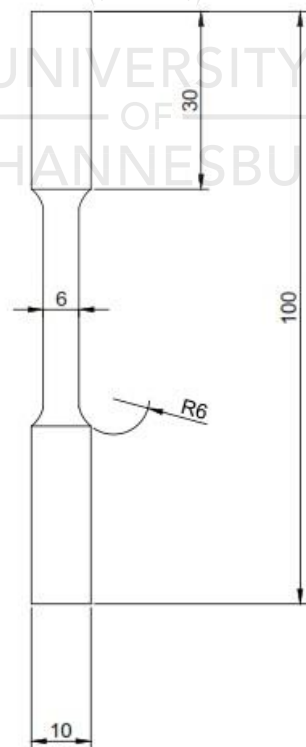


**Figure 3.6: Schematics of tensile samples (All dimensions in mm)**

### 3.7 Microscopy

Optical microscopy was conducted using Olympus BX51M and Olympus SZX16 optical microscopes as shown in the workstation (Figure 3.7). The Olympus BX51M was used to observe the microstructures, while the Olympus SZX16 was employed to observe the sample macrographs. Digital output was captured and processed using Olympus Stream Essential software. Microstructures of the FSP samples were obtained for the BM, SZ, TMAZ, and HAZ zones for comparison. The grain sizes of the different zones were determined according to the standard test method for determining average grain size: ASTM E112 – 12[106]. A TESCAN VEGA3 scanning electron microscope (SEM) set-up (Figure 3.8) was used to study and compare the microstructures observed in the base material. Vega TC software was used to acquire the image on the SEM.



**Figure 3.7: Optical microscopy setup**



**Figure 3.8: TESCAN VEGA3 scanning electron microscope**

### **3.8 Vickers Hardness Testing**

Vickers microhardness values were measured using a TH713 Vickers microhardness tester, by Beijing Cap High Technology Co. Ltd (Figure 3.9) according to ASTM 384-16 [107]. Hardness profiles were obtained across the process zones in the FSPd samples. The measurements were taken in as-polished conditions across the cross-sections of the process zones with a load of 200 g and a dwell time of 15 secs. The indentations were taken at 1.5 mm intervals on the sample, the indentations were manually focused, and the hardness measurements digitally displayed.



**Figure 3.9: TH713 Vickers microhardness tester**

### 3.9 Tensile Testing

Transverse tensile tests were performed using a servohydraulic Instron tensile testing machine model 1195 (Figure 3.10) to obtain tensile strength and elongation.



**Figure 3.10: Instron tensile testing machine**

The tensile samples were tested according to the ASTM E8M-13 standard [105]. Before starting the test, the computer system connected to the machine was set up by inputting the necessary information of each sample's gauge length and width. The computer system was then prepared to record the data and to output the necessary load-deflection graphs. The test was conducted at room temperature by gripping the ends of the samples in the tensile test machine and then loading at a constant cross head speed until failure. An extensometer was used to measure the strain of the samples during the experiment at an extension rate of 5 mm/min and a gauge length of 25 mm with a maximum load of 100 kN. The load-deflection curve was shown on the computer screen as a visual representation, and the data collected using a customised Instron Bluehill2 software. The tests were repeated three times to check for consistency and accuracy. After testing, the final length of the failed samples was measured to determine the ductility of the samples.

### 3.10 Summary

The experimental techniques used in this research namely the parameters, equipment, and procedures employed were discussed in this chapter. The parameters were carefully selected based on preliminary investigations, and ensured to be optimal. The next chapter gives details about the molecular dynamics simulation, its procedures, applications, and configurations.



# 4. Molecular Dynamics

## 4.1 Introduction

Molecular dynamics (MD) is a computer simulation method for studying the physical movements of atoms and molecules at nanoscale. It allows interaction between the atoms and molecules for a fixed period, giving an understanding of the system as they dynamically begin to evolve. Figure 4.1 shows where MD falls in the simulation time and length scales. The paths of the atoms and molecules are determined by numerically solving Newton's equations of motion for a system of interacting atoms, where interatomic potentials or molecular mechanics force fields are used to calculate forces and potential energies between the atoms [108]. In this chapter, the basic parameters used in MD simulations are briefly discussed. An MD simulation of the FSP of AA6061-T6 is carried out to explain the invisible thermodynamic microscopic details which occur during FSP. However, the aim of the MD simulation is not to predict precisely the process, but to predict the average thermodynamic behaviour of the process that was conducted in a practical state. This is to further enhance the understanding of the FSP process.

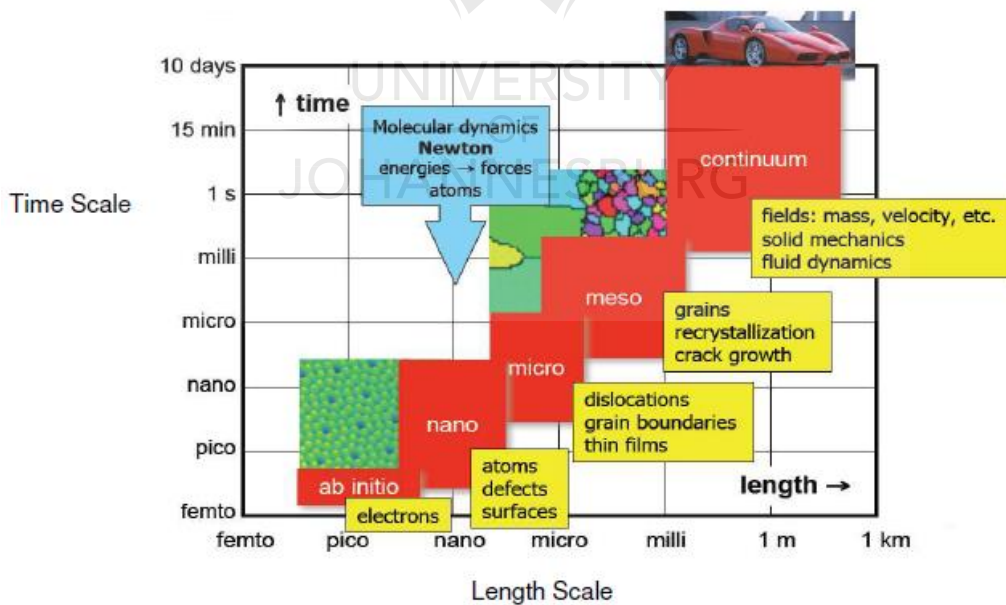
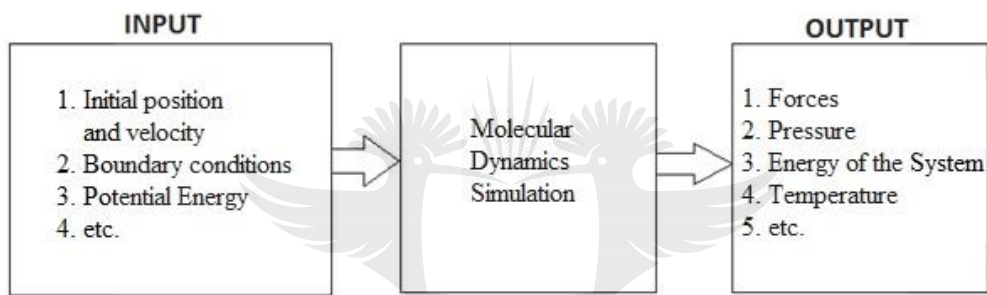


Figure 4.1: Scales for simulation time and length [109]

## 4.2 Overview of Molecular Dynamics

MD was originally developed in 1957 by Alder and Wainwright at the Lawrence Radiation Laboratory for the study of statistical mechanics, and first used in the perfect simulation of an elastic collision between hard spheres [110]. Many important insights concerning the behaviour of simple liquids emerged from these studies. The next major advance was in 1964 when Rahman carried out the first simulation using a realistic potential for liquid argon [108]. In 1974, Rahman and Stillinger performed the first molecular dynamics simulation of a realistic system, namely the simulation of liquid water [111]. Raymond and Giovanni [112] give a full documentation of the evolution of MD. An overview of MD is shown in Figure 4.2.



**Figure 4.2: Overview of MD [113]**

Beginning in theoretical physics in the 1970s, MD has now been applied in various fields. It is frequently used to refine three-dimensional structures of proteins and other macromolecules in biochemistry. In physics, MD has been used to examine the dynamics of atomic-level phenomena that cannot be directly observed, such as thin film growth and ion-subplantation. It has also been used to examine the physical properties of nanotechnology devices that have not been or cannot yet be created. In biophysics and structural biology, this simulation method is frequently applied to study the motions of biological macromolecules such as proteins and nucleic acids, which can be useful for interpreting the results of certain biophysical experiments as well as modelling interactions with other molecules. An example of such a biophysical experiment with MD application is ligand docking [108]. Other applications of MD found in engineering are discussed below.

### 4.3 Application of MD to Engineering Systems

Researchers have begun to realize the potential advantages of molecular dynamics and have made significant advances in quantifying engineering systems in higher accuracy and spatiotemporal resolutions, for which experimental methods alone are insufficient in many cases. MD has become one of the important tools used to tackle many of the complex problems faced by engineers. The early development of software packages has really helped the growth of molecular dynamics simulation. This has led to industrial applications of molecular dynamics in a well-established range of engineering fields from electrical engineering to oil and gas, and particularly materials science [108].

Meuner [114] outlines various industrial applications of molecular simulations focusing on ascertaining material selection at a molecular scale that can be routinely determined, is efficient, has sufficient accuracy, and preferably has known error margins. This has led to the concept of workflow integration shown in Figure 4.3.

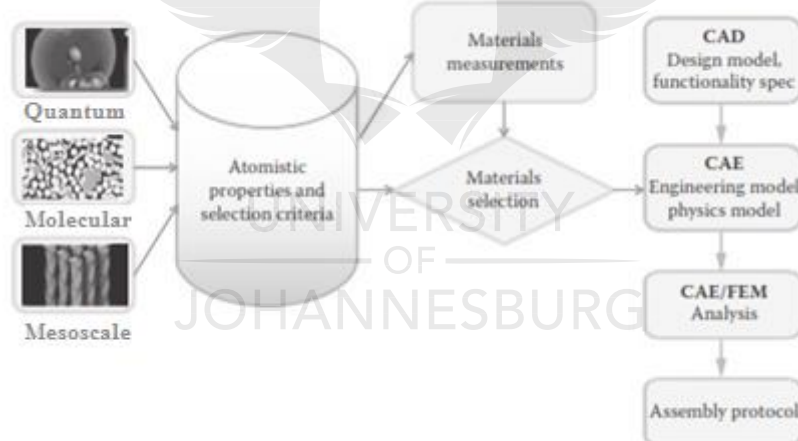


**Figure 4.3: Workflow integration of simulation to industrial applications [114]**

The figure shows that simulations at different scales play a role depending on the intended engineering application. However, the simulation does not provide the integration pathway itself; defining the criteria which are both specific and selective to a problem at hand remains the task of the engineer to adapt to the modelling approach. MD has been applied across engineering systems over the years. In this report, only a few recent studies will be reviewed to elaborate on these applications.

Molecular dynamics has been used to study the mechanical behaviour and properties of materials, since the selection of a material in any industrial application mostly depends on whether its properties are suitable for the intended application. Ansari et al [115] investigated the buckling behaviour of a novel three-dimensional metallic carbon nanostructure known as T6 with MD simulations. Kurban and Erkoc [116] examined the mechanical properties of CdZnTe nanowires under uniaxial stretching and compression with MD and obtained results valuable for future research on CdZnTe nanowires applications.

Tavakoli and Tarighat [117] conducted an MD study on the mechanical properties of Portland cement clinker phases. The research aimed to meet the need for accurate knowledge about the nanostructure and mechanical properties of cement. It was reported that using nano-scale calculation methods lead to better understanding of material functionality, and that using a molecular dynamics method was suitable for estimating the mechanical properties of cement phases. Their findings are proposed to be applied in larger and multi-scale simulations.

Another important application of MD in civil engineering by Bhasin et al [118] is investigating self-healing mechanisms in asphalt binders. Self-healing is a process that reverses the growth of fatigue cracks during rest periods between load applications. The findings reported in their research expand on the understanding of the relationship between molecular architecture, self-diffusivity, and self-healing properties of asphalt binders.

Xu et al [119] analysed the role of MD simulations in chemical engineering. MD has been very effective in chemical engineering systems because it typically involves multi-scales, from the material level of atoms, molecules, and assemblies to the reactor level of particles and clusters, and then to the system level of reactors and processes. They discussed engineering MD simulation in the EMMS paradigm as well as by extending its element model, and concluded that it is a very powerful tool for understanding the microscale behaviour of materials and processes in chemical engineering.

Ungerer et al [120] reported on the application of molecular simulation in oil and gas production and processing. They investigated how MD has been applied to reservoir engineering, oil and gas production, processing and transport. It has been used to predict the properties of natural gases at high pressure (such as the Joule-Thomson coefficient, which is particularly difficult to measure by experimental means) or the behaviour of hydrogen

sulphide-hydrocarbon systems (for which the amount of available data available is not sufficient for a reliable design of acid gas reinjection in deep reservoirs). In oil and gas transport and processing, molecular simulation has been used to predict the behaviour of hydrocarbon mixtures with water and polar solvents like methanol or amines. It is a useful tool to model the solubility of gases in pipe-coating polymers. Molecular simulation is also very useful in hydrocarbon processing to predict phase equilibria in process conditions (e.g. around 400°C), where experiments would be impossible due to the fast degradation of hydrocarbons.

Nyden et al [121] studied the applications of reactive MD to the thermal decomposition of polymers and nanoscale structures. They performed molecular simulations with reactive force fields on the homologous series of vinyl polymers: polyethylene, polypropylene, and polyisobutylene with specially built MD simulation software called MD\_REACT. Based on the results they were able to formulate a general mechanism for the thermal decomposition of vinyl polymers.

Jabbarzadeh and Tanner [122] investigated the application of MD to nano-rheology. They reported that MD simulations among other molecular simulation methods have been a valuable tool in studying the relationship of the molecular structures and rheological properties of materials. It has helped to understand the behaviour of polymers qualitatively and facilitated important progress in predicting quantitative rheological properties such as the viscosity of simple liquids such as alkanes. Their research focused on the application of MD in the nano-rheology of ultra-thin confined films. The application of MD to the behaviour of confined fluids and lubricants at nano-scales revealed important properties. It also explains the underlying physics of observed molecular occurrences which include enhanced viscosity, relaxation time and the role of normal stress differences in supporting large loads. They concluded that these methods are appropriate for investigating phenomena where channel sizes and/or surface roughness approach molecular size, and postulate that MD will be an increasingly useful tool in the resolution of nanotechnology problems in the future.

Yan et al [123] used a three-dimensional MD model to investigate the effect of atomic force microscope (AFM) tool geometry on the deformation process of a workpiece and the nature of deformation process at the atomic-scale. Zhu et al [124] also conducted a study of a AFM-based nanometric cutting process on copper using molecular dynamics, with significant

results. Molecular dynamics has wide applications in the field of nanometric cutting/machining.

A rapid emergence of a variety of non-conventional micro-/nano-machining (MNM) processes applicable to a wide range of engineering materials, including metals, ceramics, plastics, and composites has emerged in the 21<sup>st</sup> century. This is in accordance with the prediction in the 1980s by Taniguchi, who proposed a predictive map of the developments in ultra-precision manufacturing (Figure 4.4).

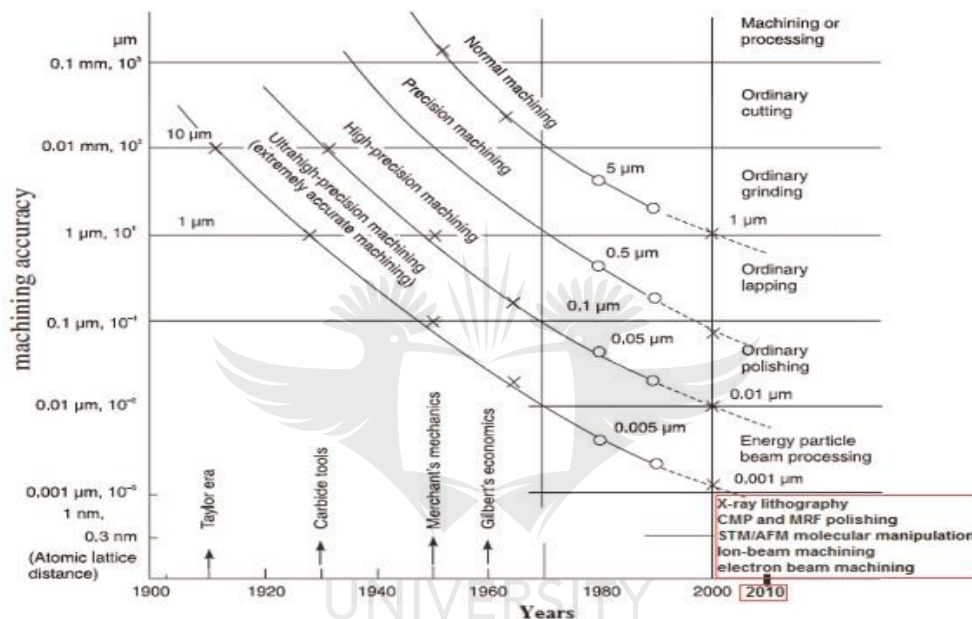


**Figure 4.4: Evolution of machining accuracy-Taniguchi's predictions [125]**

The concept of MD in the framework of nanometric cutting was pioneered in 1990 by Belak and Stowers. [126]. Ever since then, various researchers have contributed significantly to the study of nanometric cutting processes using MD simulation. Goel et al [127] in a review of advances in molecular dynamics simulation in diamond machining of silicon, show how MD has enhanced understanding of ductile regime machining of brittle materials such as silicon. This agrees with the conclusion by Olufayo and Abou-El-Hossein [128] in their study of MD modelling of nanoscale silicon machining in which they used MD simulations to study plastic material flow at the tool/workpiece interface during orthogonal cutting. Both studies yielded similar reservations about the shortfall of MD in observing real-world scale simulation models instead of nano-portions.

Other MD studies conducted on nano-machining include but are not limited to nanometric cutting processes of brittle materials [129-131], simulation of nano-machining of copper [132, 133], molecular dynamics simulation for nanometric cutting of single crystal face-centered cubic metals [134], simulation of machining of composite materials [135], and investigation of tool geometry in nanometric cutting [136].

A similar approach to the application of MD simulations to nanometric cutting is its application to the FSW process. Being a relatively new process, very few MD simulation studies have been conducted on FSW. Dmitriev et al [137] studied the patterns of microstructure formation during friction stir welding with MD simulation and concluded that simulation results are in good qualitative agreement with those of experimental studies.

In recent times, Konovalenko et al [138] studied the mass transfer of FSW at atomic scale. The study has helped to show the effects of increasing velocity movement and decreasing angle velocity of the tool, as well as increasing the amplitude of vibrations applied to the friction stir welding tool. It is thus the aim of this research to use MD simulation to study the sub-surface thermodynamic phenomena of FSP of aluminium. The examples of MD simulations discussed above are just a few of the wide range of studies on their application in engineering systems.

#### **4.4 Attributes of Molecular Dynamics Simulation**

MD simulations are characterised by pre-defined procedures and a variety of advantages. However, it also has certain limitations. This section describes the procedures employed in MD and discusses the advantages and limitations.

##### **4.4.1 Molecular Dynamics Procedure**

A flow chart of molecular dynamics is shown in Figure 4.5.

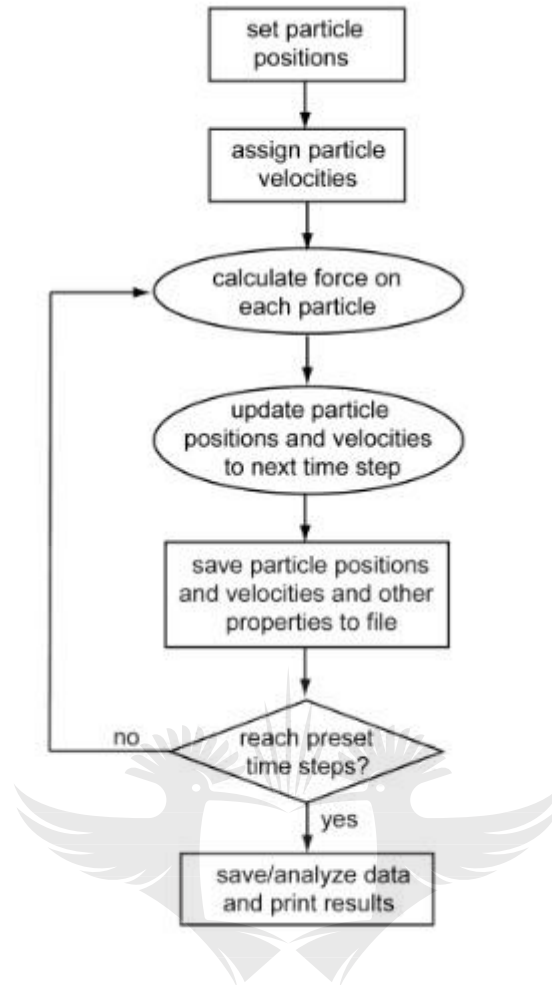


**Figure 4.5: MD simulation flow chart**

The MD procedure can be described as follows:

1. Ambient conditions (initial temperature (T) and pressure (P), number of particles (N), volume (V), and external chemical potential ( $\mu$ )) are determined.
2. To begin the simulation, initial positions and velocities must be assigned for all particles of the system.
3. Periodic boundary conditions and interatomic potentials are defined.
4. Newton's equation of motions is used to determine the forces acting between atoms.
5. Integration breakdown to many small stages:  $\Delta t$ . The total force on each particle in the configuration at a time t is the vector sum of its interactions with other particles. From the force, the acceleration of the particles is determined and combined with positions and

velocities at time  $t$  to be calculated at the current time. The force is constant during the time step  $t + \Delta t$ .

6. New positions and velocities are determined with molecular dynamic algorithms.
7. Post processing (evaluation or visualisation of desired parameters at the end of current simulations).

#### **4.4.2 Advantages of Molecular Dynamics**

1. MD algorithm enables the consideration of a more fundamental unit of matter (i.e. the atom) which means that material properties are described by their interaction potential. Thermodynamics and basic mechanisms underlying FSP process can thus be suitably studied through MD.
2. MD permits online monitoring of the machining processes with good quality temporal and spatial resolution in a reversible manner. Any time step can simply be reversed through a computer programme for analysis it at any given time.
3. MD simulation avoids the use of expensive equipment and apparatus which are key requirements to perform nanometric cutting and FSP experiments. Moreover, in experimental trials, material once consumed must be reordered, whereas MD can perform any number of trials with many varying parameters.
4. MD simulation offers repeatability. The type of work material, cutting tool material, and environmental conditions can all be kept intact and maintained at pre-determined values.
5. MD simulation provides flexibility to perform the simulation at any place. A computer system is mobile whereas a friction stir welding machine (exhibiting high stiffness) requires a conventional location for experimentation.

#### **4.4.3 Limitations of Molecular Dynamics**

1. MD cannot predict the attainable experimental measures of material mechanical properties which is a prime requirement that governs the choice of materials in industrial applications. Even if a theoretical value is estimated, it will always remain an ideal limit which can only be attained under an ideal set of machining conditions.

2. Time to finish a simulation is a major challenge associated with a realistic processing conditions and specimen size.
3. The atomic size of a simulation and its scale are limited to the current processing limitations of the computing device.
4. A prerequisite for a real FSP experiment is the clamping of the workpiece, and use of a backing plate which often cannot be achieved during MD simulations.
5. Only an advanced researcher can perform an appropriate MD simulation, as it requires an accurate understanding of various disciplines. An FSP trial can be performed using less trained technicians.

#### **4.5 Molecular Dynamics Basics**

The MD basics are fundamental elements in MD simulation. These elements govern the arrangement and interaction of the particles in the simulation. They also specify the thermodynamic, boundary and operating conditions, and are discussed in the subsections below.

##### **4.5.1 Equation of Motion**

Newton's second equation of motion is used to describe the movement of atoms in MD. It is assumed that all the atoms or molecules present in the system, their locations, and velocities integrate the Newton's equation. MD works on the systematic solution of the Newton's second equation of motion for a set of N atoms;

$$F_i = m_i a_i \quad (4.1)$$

where  $m_i$  is the mass of atom i,  $a_i = \frac{d^2 r_i}{dt^2}$  is the acceleration of the atom i and  $F_i$  is the resultant force acting on atom i. These forces need to be balanced by the potential energy between atoms [139].

### 4.5.2 Computational Time Step

The computational time step is a very important factor, which influences the total CPU time required by a simulation. This is the length of time between the evaluations of the potential. The time step indicates the amount of time between each calculation interval in which force and velocities applied to each atom are calculated. These are repeated ( $t_i + 1 - t_i = \Delta t$ ) until the chosen number of iterations is completed. The time step must be small enough to avoid discretisation errors (i.e. smaller than the fastest vibrational frequency in the system). Typical time step values for classical MD are in the order of 1 femto second ( $10^{-15}$  s) [108]. The time step and total duration of the simulation must be adjusted to control the calculation period. However, simulations should be made appropriate to match the time scales of the natural processes being studied to make the simulation results statistically valid. As a parameter of importance, time steps have made MD simulations very computationally intensive in some cases. However, ongoing research is being done on hardware, parallel computing, and algorithm improvements to enable longer time-scale MD simulations.

### 4.5.3 Interatomic Potential

Atomic interaction amidst molecular atoms in MD is characterised by the action of interatomic forces. The effect of these forces is responsible for atomic movement. As the atoms move, their relative positions and the forces acting on them change. Interatomic potential energy binds atoms in any system and can be defined by the interatomic potential function. MD simulation uses this definition to determine how the atoms will interact with each other. The selection of the potential function in an MD simulation is a critical task; right potential must be ensured to avoid erroneous results. Various researchers explain in detail the types of potentials used in MD which include empirical, semi-empirical, pairwise and many-body, and polarisable potentials [139-141]. The pairwise and many-body potential is considered the simplest interatomic potential to use in the interactions of a set of atoms. The most commonly used of this type of function includes Lennard-Jones, Morse, Born-Mayer, Tersoff, and embedded-atom method (EAM) potentials.

#### 4.5.4 Boundary Conditions

One of the most important elements to be considered in molecular dynamics are the boundary conditions. Molecular dynamics is typically applied to small systems containing thousands of particles. Boundary conditions, as the name implies, are used to specify the behaviour of the movement of the atoms. There are four possible boundary conditions, namely periodic, free surface, rigid and flexible boundary [142]. Periodic boundary conditions are used in the simulation of bulk materials; the simulation box is periodic, the particles interact across the boundary, and can exit one end of the box and re-enter the other end [143]. The free surface boundary condition allows atoms to leave the surface, while the rigid condition allows atoms to be fixed, and the flexible boundary allows small displacements of atoms in response to forces exerted on the cell at the perimeter of the computational cell [144]. Periodic, free surface, rigid, and flexible boundary conditions are illustrated as a, b, c, d respectively in Figure 4.6.

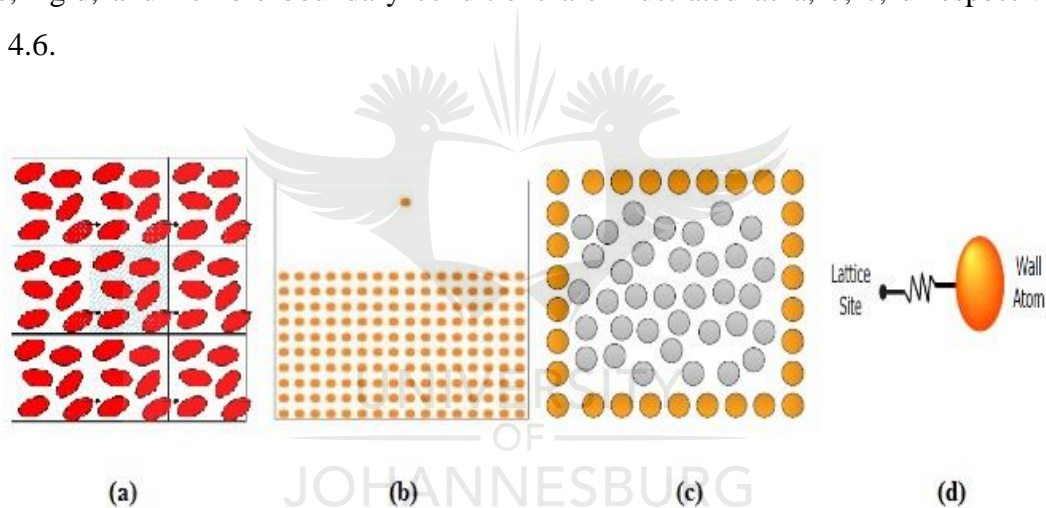


**Figure 4.6: Boundary conditions that can be used in molecular dynamics**

#### 4.5.5 Thermodynamic Ensemble

MD simulations facilitate the study of the microscopic dynamics in a system (atomic position, velocities, and acceleration). In MD simulations, a system could be modelled on definite temperature, pressure, density, total energy, or number of atoms. These parameters describe the thermodynamic state of the system and are controlled by statistical ensembles. An ensemble is a large group of atoms or systems which are in different microscopic states but have the same macroscopic or thermodynamic states [139]. It is defined as an all possible quantum state of  $N$  identical atoms system. It is an idealisation of a large number of atoms in

a system considered all at once. The statistical ensembles act as a link that integrates the microscopic state of the system with observable macroscopic data. In this way, the macroscopic conditions of an atomic system can be examined from a molecular viewpoint. Common thermodynamic ensembles used in MD are briefly discussed below.

#### **4.5.5.1 Micro-canonical or NVE**

In an NVE ensemble, the system is restricted from changes in atoms (N), volume (V) and energy (E). It corresponds to an adiabatic process i.e. no heat change. An NVE integrator updates position and velocity for atoms in the group for each time step. It corresponds to an adiabatic process with no heat exchange. Total energy is conserved, and there is an exchange of potential and kinetic energy as the trajectory of atoms in the system is generated.

#### **4.5.5.2 Canonical or NVT**

In an NVT ensemble, the number of atoms (N), the volume of the system (V) and the system temperature (T) are the independent variables and are kept constant. The energy of endothermic and exothermic processes is exchanged with a thermostat to add and remove energy from the boundaries of the MD system in a way that is similar to a real-life system. A variety of thermostats is used to control the temperature. However, a Noose-Hover thermostat is commonly used.

#### **4.5.5.3 Isothermal–Isobaric or NPT**

NPT is the isothermal-isobaric ensemble in which a number of atoms (N), pressure (P) and temperature (T) are conserved. The volume of the system can change over time. A barostat is needed in addition to a thermostat; to control the pressure to approximate a real situation. Temperature and pressure are mostly controlled by a Nose-Hoover thermostat and a Nose-Hoover barostat.

### **4.6 The MD Algorithm**

Many methods exist to perform a systematic numerical integration of a Newton's second equation of motion (eq. 3.1). These equations are known as MD algorithms and include Verlet and predictor-corrector algorithms. Characteristics of these equations typically include the following:

1. They are stiff, in other words there may be short and long timescales, and the algorithm must cope with both.
2. The algorithms can perform the calculation of the forces as frequently as possible.
3. Simulation algorithms are of a low order (i.e. they do not involve storing high derivatives of positions and velocities) to make the time step as large as possible and allow it to be increased as much as possible without jeopardising energy conservation. All these observations tend to favour the Verlet algorithm in one form or another and make it the algorithm of choice for a wide range of MD application [141].

#### 4.6.1 The Verlet Algorithm

Given N number of atoms in a system, the three-dimensional vectorial representation of position, velocity, and acceleration of the atoms at time t are given by  $r_i(t)$ ,  $v_i(t)$ , and  $a_i(t)$  respectively, where i (1, 2, ..., N) is the atom index, and is omitted in formulas which apply to all atom independently. Vector components are represented by subscripts x, y, z. The equation of this algorithm can be written as:

$$r(t + \Delta t) = r(t) + \Delta t v(t) + \frac{1}{2} (\Delta t)^2 a(t) + O((\Delta t)^3) \quad (4.2)$$

$$a(t + \Delta t) = a(r_1(t + \Delta t), \dots, r_N(t + \Delta t); v_1(t + \Delta t) \dots, v_N(t + \Delta t); t + \Delta t) \quad (4.3)$$

$$v(t + \Delta t) = v(t) + \frac{1}{2} \Delta t [a(t) + a(t + \Delta t)] + O((\Delta t)^3) \quad (4.4)$$

In many simple MD simulation problems without external magnetic fields, the atoms acceleration do not depend on their velocity, so equation (4.3) can be replaced by

$$a(t + \Delta t) = a(r_1(t + \Delta t), \dots, r_N(t + \Delta t); t + \Delta t) \quad (4.5)$$

With the help of equation (4.2) we can calculate  $r(t + \Delta t)$  at the time t and using equation (4.5) we can find  $a(t + \Delta t)$ . Finally, to find the  $v(t + \Delta t)$ , use the equation (4.4). The implicit character of equation (4.4) thus disappears when applying the equation (4.5) for the acceleration [141].

## **4.7 Process Methodology**

### **4.7.1 MD Simulation Software**

A wide range of software has been developed for MD simulations over the years. While some are free, others are commercially available. In this research, computational resources available in the Department of Mechanical Engineering Science at the University of Johannesburg were used. The computer system provides 3 terabytes of data storage, a 32 gigabytes RAM, with an Intel® Core™ i7-5960X processor. The MD simulation software programmes LAMMPS and OVITO were used for MD processing and pre-processing respectively. These were chosen based on ease of access and suitability for the intended application.

#### **4.7.1.1 LAMMPS (Large-scale Atomic/Molecular Massively Parallel Simulator)**

LAMMPS is a classical molecular dynamics simulation programme from Sandia National Laboratories designed to run efficiently on parallel computers. It is free, open-source software, distributed under the terms of the General Public License (GNU), and has the capacity to model an ensemble of particles in a liquid, solid, or gaseous state. It can model atomic, polymeric, metallic, granular, and coarse-grained systems using a variety of force fields and boundary conditions. LAMMPS integrates Newton's equations of motion for collections of molecules, atoms, or macroscopic particles which interact by short- or long-range forces with a variety of initial and/or boundary conditions. It uses a neighbour list to keep track of nearby particles. A typical LAMMPS input script has four parts namely initialisation, atom definition, settings, and 'run a simulation'. It executes commands from an input script by reading one line at a time and exits when the input script ends.

#### **4.7.1.2 OVITO (Open Visualisation Tool)**

OVITO is a scientific visualisation and analysis software programme for atomistic simulation data developed at the Darmstadt University of Technology, Germany. The programme is open source and freely available on all major platforms. It has been widely used in MD simulation studies as a useful tool to analyse, understand, and illustrate simulation results.

## 4.8 Simulation Configuration

The MD simulation model was created using LAMMPS code with the parameters stated in Table 4.1. It consists of a tool and workpiece as shown in Figure 4.7. The tool was modelled as a rigid body. The initial displacement of the workpiece and the tool was created from a crystal structure of the material (face-centered cubic (FCC) structure). The workpiece was divided into boundary, Newtonian and thermostat atoms. The thermostat atoms are applied to the MD simulation model to ensure that the heat generated during the process can conduct out of the processed region properly while the Newtonian zone is determined solely by the forces derived from the potential energy function and Newton's equation of motion.

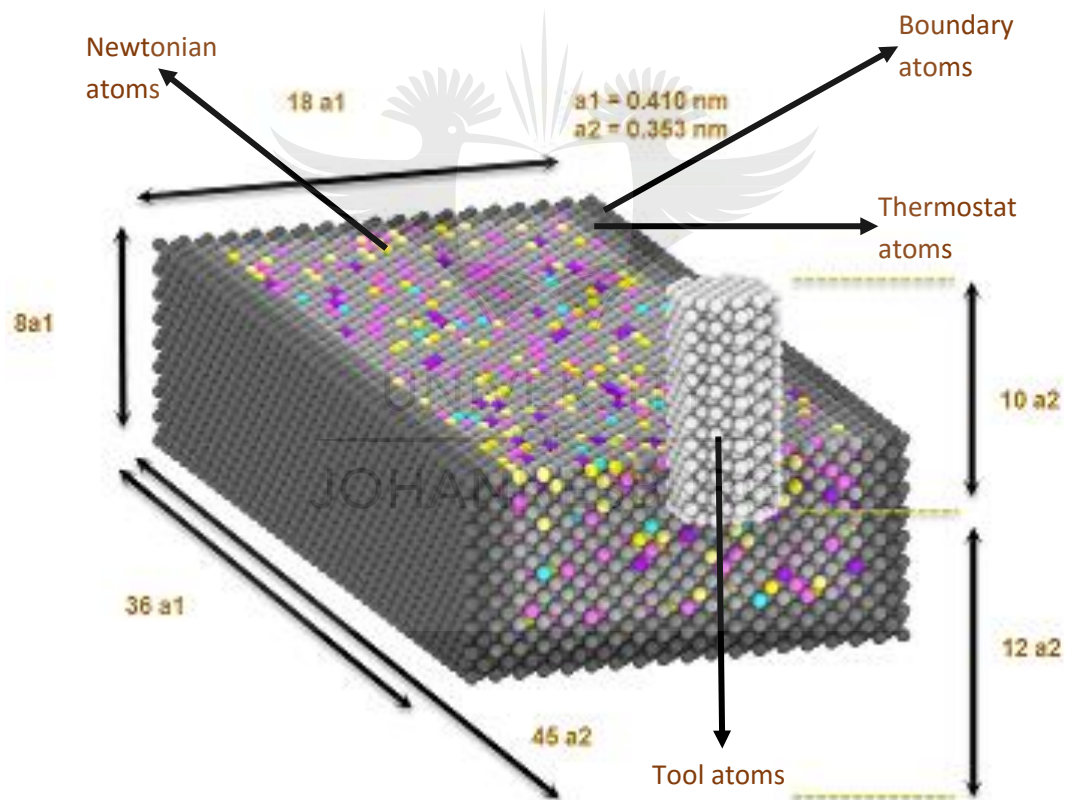


Figure 4.7: MD simulation model

**Table 4.1: Nanometric modelling parameters**

---

Workpiece material	Aluminium 6061-T6
Workpiece dimension	36a1 x 8a1 x 18a1
Lattice constant of workpiece	a1 = 0.4.10 nm
Crystal orientation	(001)
Tool material	Carbide tool
Tool dimension (cylinder)	z-axis, y= 12 a2, x =45 a2 Radius= 2.5, y = 10a2
Lattice constant of tool	a2 = 0.353 nm
Tool shape	Rotational tool
Tool angular velocity	0.1 ps <sup>-1</sup>
Tool radius	5nm
Depth of cut	2.05 nm
Cutting speed	5 and 500 m/s
Bulk temperature	293 K
Time steps	2 fs (2 x 10 <sup>15</sup> s)

---

#### 4.8.1 The Face-Centered Cubic Structure

The face-centered-cubic structure has atoms located at each of the corners and in the centres of all the cubic faces (Figure 4.8). Each of the corner atoms is the corner of another cube so the corner atoms are shared among eight unit cells. It has a coordination number of 12 and each cell has a net total of 4 atoms.

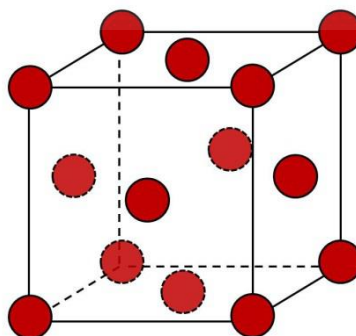


**Figure 4.8: The face-centered cubic structure**

#### **4.8.2 Model Atoms Number**

The total number of atoms present in the assembly is 23756 as determined from the model configuration. The tool consists of 797 atoms while the workpiece has a total of 22957 atoms. The workpiece atoms are further divided into 13007 Newtonian atoms, 4566 thermostat atoms, and 5386 boundary atoms.

#### **4.8.3 Selection of Interatomic Potentials and Thermodynamic Ensembles**

The potentials used for the simulation are the Tersoff potential, Morse potential, and EAM/alloy potential. The Tersoff potential was used between tool-to-tool atoms based on the concept of bond order. The Morse potential was used between the tool and the individual elements of the workpiece due to its suitability to cubic metals and its ability to adequately model the interactions between an atom and a surface [139]. The EAM/alloy potential is present between the elements of the workpiece which are aluminium, iron, magnesium, copper, titanium, silicon etc. as represented in Table 3.1. The EAM/alloy potential was selected based on conclusion by Oluwajobi and Chen [133] that the EAM should be used rather than LJ and Morse potentials for the modelling of FCC metals because it provides the best description of metallic bonding in the workpiece. An NVE ensemble was used for the simulation to maintain the number of particles, volume, and energy in the system. The particles are first equilibrated, i.e. given a time to find equilibrium at 293K before the actual simulated FSP process was conducted on the assembly. A Velocity-Verlet integrator was used for minimisation.

#### **4.8.4 Selection of Boundary Conditions**

The boundary for the simulation assembly in each direction was set. Fixed and periodic boundary conditions were used. Fixed boundary conditions are applied to the boundary atoms to maintain symmetry in the lattice and to reduce the edge effects. Applying fixed boundary conditions to boundary atoms means that particles do not move across the boundary in the simulation in the x and y-axis. If they exit the created lattice box, they are lost from the simulation. The periodic boundary conditions are maintained along the z direction. In the z-axis, the atoms are shrink wrapped which means that the simulation box lattice can adjust in that axis according to the movements of the atoms.

## 4.9 Summary

This chapter highlights the concepts of MD, its basic elements, advantages and limitations. The parameters and applications of MD to engineering systems were also discussed. The procedures employed in the use of MD to study FSP on aluminium have been detailed. The results from the MD simulation study and the experimental study are discussed in the next chapter.



## 5. Results and Discussion

### 5.1 Introduction

This chapter discusses the effect of multi-pass FSP on the microstructure and mechanical properties of friction stir processed AA6061-T6. One to five FSP passes with 100% overlapping on previous passes were performed. The results of the molecular dynamics simulation are also presented in this chapter.

### 5.2 Visual Appearance of FSPd Samples

The visual appearance of surfaces of AA6061-T6 alloy plates after multiple FSP passes are shown Figure 5.1. No defects such as tunnel, void, cracks, or incomplete root penetration, were visually observed in any of the FSPd samples. The surfaces of all the samples were characterised by the presence of smooth semi-circular streaks at the contact surface between the shoulder and the plate without any irregularities or discontinuity. These smooth streaks and the absence of defects show that the tool rotational and transverse speed used for the welds are good processing parameters for the material.



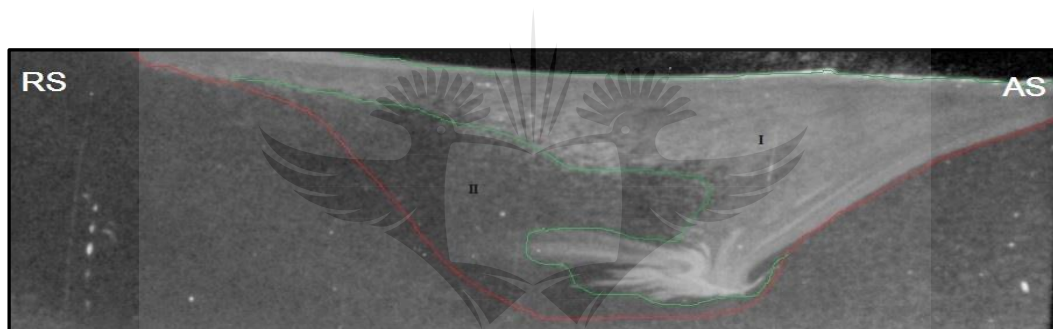
**Figure 5.1: Physical appearances of FSPd samples**

Flashes can be observed on the RS in all the FSPd samples, which increases with an increase in the number of FSP passes; flashes curl over the ones from the previous pass. The material was mostly transported below the shoulder and around the tool probe from the AS to the RS which, combined with the local severe shearing action, results in flash flow and curling giving

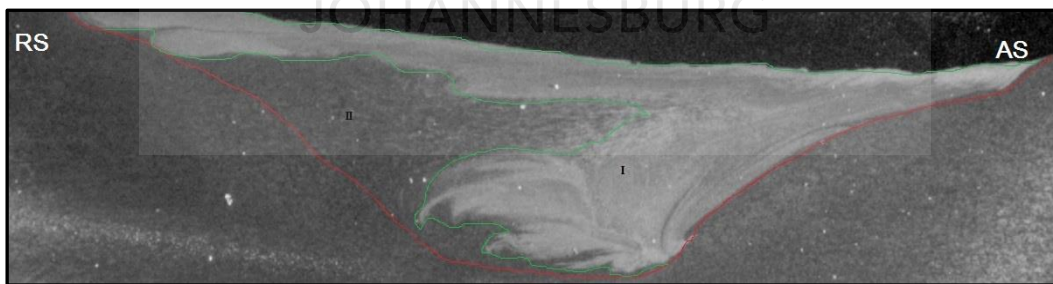
a wavelike finish to the RS edges of the samples as seen in Figure 5.1. This shows that some metal was displaced by the pin and not contained by the shoulder. The processing parameters selected for this experiment appear to have heated the metal to high temperatures, providing ease of metal flow, and making it difficult for the tooling to constrain the displaced metal. Keyholes were present in all the FSPd samples as a result of the exit of the tool from the workpiece. A macroscopic study of the plates is examined in the next section to reveal more information about possible defects in the material, and flow in the material during each pass.

### 5.3 Macrostructural Examination

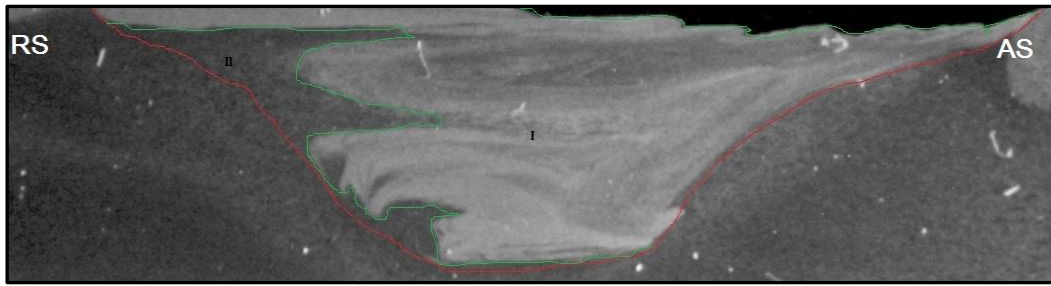
Macrographs of FSPd samples are shown in Figures 5.2 in increasing order from the first pass to the fifth pass. It can be clearly seen that no internal defect is present in any of the FSPd samples.



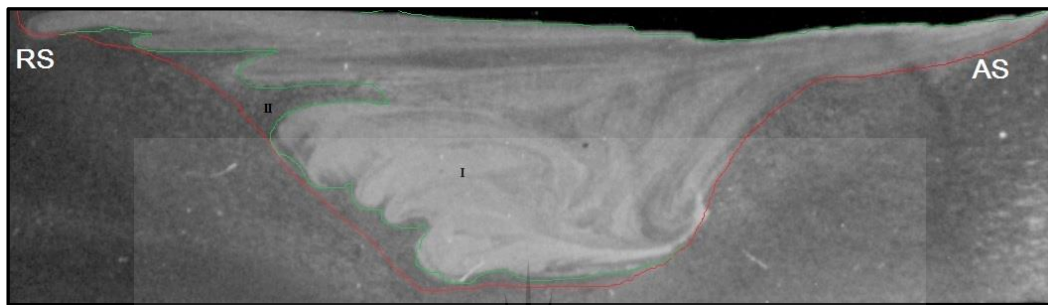
Single-pass



Two-pass



### Three-pass



### Four-pass



### Five-pass

**Figure 5.2: OM macrographs of FSPd samples**

The absence of internal defects can be correlated to the process parameters and relatively stable axial force obtained in the force feedback presented in Appendix C. Shahl and Bahmouz [145] reported that the forces and torque in FSW can be considered online indicators of weld quality. Their values during processing should be in a safe and stable range to obtain defect-free welds. It was reported in section 2.9 of this dissertation that high axial forces may result in shear lips or flashes causing metal thinning at the processed area, while low axial forces lead to poor material consolidation due to insufficient forging pressure and friction heating. This is confirmed in a report by Akinlabi [13] that a high degree of variation

in the Fz observed in a weld produced with a 25 mm shoulder diameter tool (1200 rpm; 150 mm/min), produced a poor-quality weld. In all the force feedbacks from the FSP of the samples from the first to the fifth pass, the processing forces were observed to be very high during penetration of the tool as expected due to shearing, but tended to decrease as there was sufficient frictional heat generated. The forces then remain almost constant throughout the process. These are similar to forces obtained in studies by Perumalla et al [146] and Krishna et al [147] which are reported to have produced defect-free welds.

The micrographs show two clearly distinguished zones; one with onion-ring-like structure and the remaining unmixed region which has been labelled region I and region II respectively, similar to the result by Sampath et al [90] reported earlier in this dissertation. The shoulder driven flow can be observed on the top portion of the macrographs while the probe driven flow is seen towards the bottom part. Several researchers [54, 63, and 64] have described the material flow as a combined process of pin-driven extrusion and shoulder-driven material stirring and mixing. The differences in the volume of microstructural homogeneity is a result of the differences in metal flow in the various number of FSP passes in the samples. Region I depicts the area of the FPZ where the stirring action is severe while region II shows the unmixed area of the FPZ. A sharp boundary was only visible on the AS until the fifth pass where the FPZ is completely homogenous. It was clear that region I increases in volume with an increase in the number of FSP passes towards the RS of the samples, significantly widening the basin-like shaped FPZ towards the upper surface due to the forging effect of the tool shoulder on material flow during FSP. This shows that multi-pass FSP increases the microstructural homogeneity of materials, confirming the suggestion by Salehi et al [91] and other studies [18, 92] that a single-pass FSP is not sufficient to attain microstructural homogeneity in the FSP of most materials.

The inhomogeneity from the single-pass FSP (Figure 5.2) could be attributed to different levels of strain on both sides of the AS and RS. The material in the AS is exposed to more shear stress than that in the RS. The material close to the non-consumable tool has a high plastic deformation and temperature gradients, which cause a higher deformation rate on the AS than on the RS. The increase in the volume of region I as the number of FSP passes increases could be attributed to the ability of the tooling to penetrate the material and improve material flow due to less stress and strain localisation as a result of the significant SZ softening. This softening is caused by dynamic recovery that has occurred from the intense

plastic deformation and high temperature from frictional heating during FSP. El-Rayes and El-Danaf [95], and Woo et al [148] reported that increasing the number of passes at a constant traverse speed is accompanied by SZ softening. This explains the widening of SZ in the basin-like shaped FPZ towards the upper surface.

#### 5.4 Microstructural Examination

An optical microscopy examination was carried out to study the influence of the multiple numbers of passes on the microstructure of FPZ. Figure 5.3 illustrates typical micrographs of the base material before FSP. The base material has a honeycomb-like microstructure with spherical shaped grains, and relatively equiaxed grain size. Clearly visible in-homogeneously distributed second-phase precipitates were seen within the entire base material microstructure matrix. Numerous studies have reported that the main second-phase strengthening precipitate found in AA6061 is mostly  $Mg_2Si$  [95, 149-157]. This precipitate is expected because AA6061 is a precipitate-hardening aluminium alloy, containing magnesium and silicon as major alloying elements. The average grain size was found to be  $6.69 \mu m$  using an intercept procedure [106], while the average size of the precipitates in the base material was found to be  $6.57 \mu m$ .

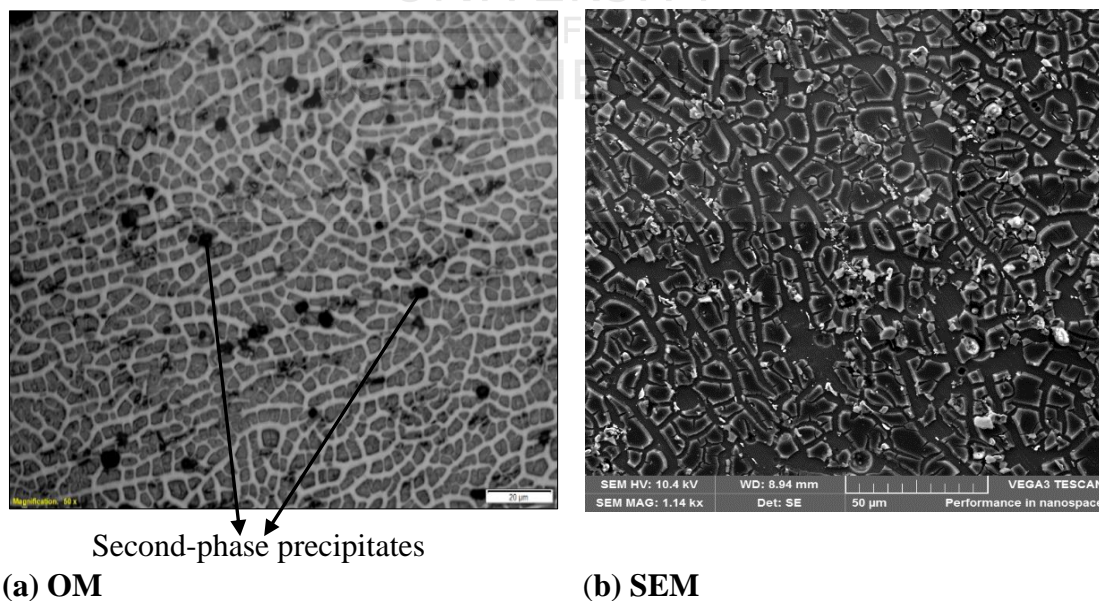
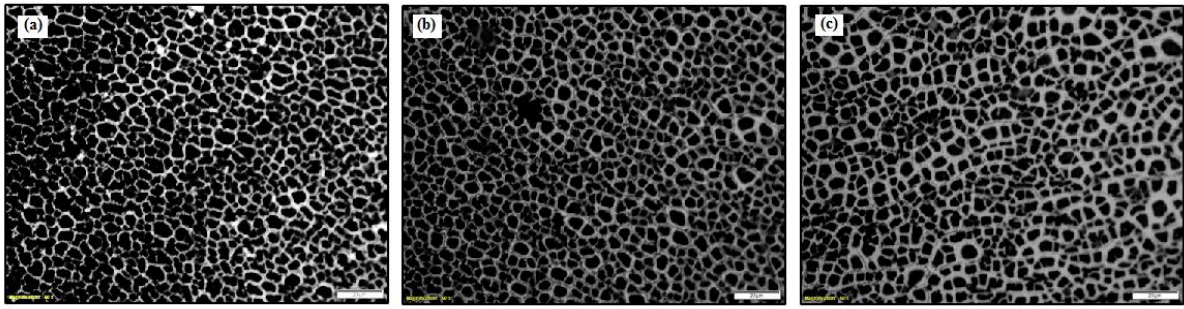
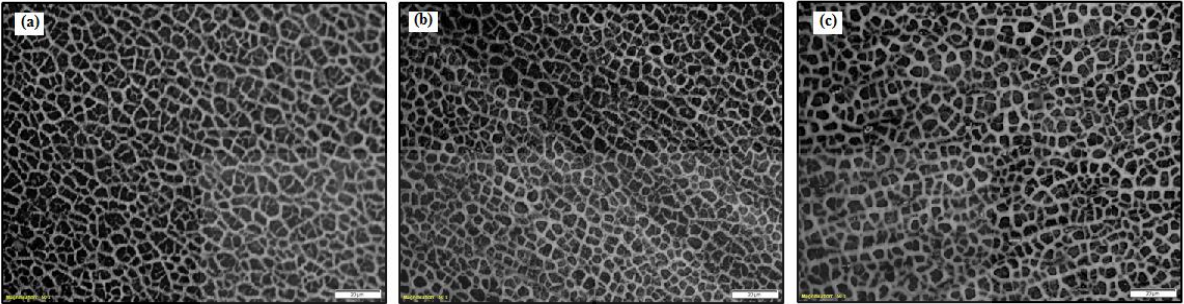


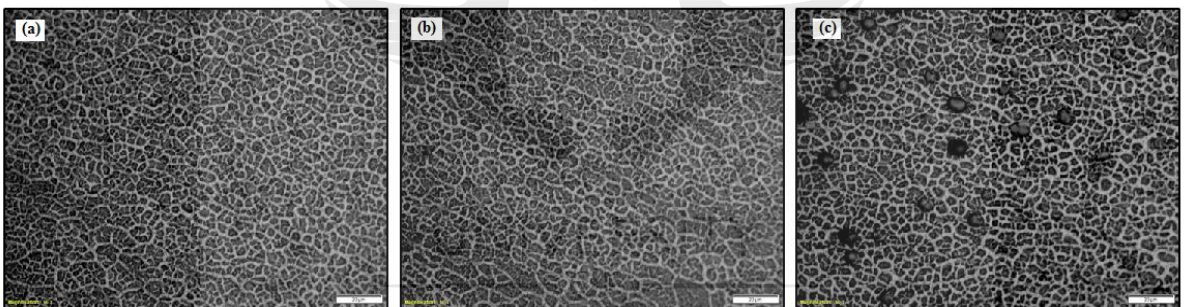
Figure 5.3: AA6061-T6 base material microstructure



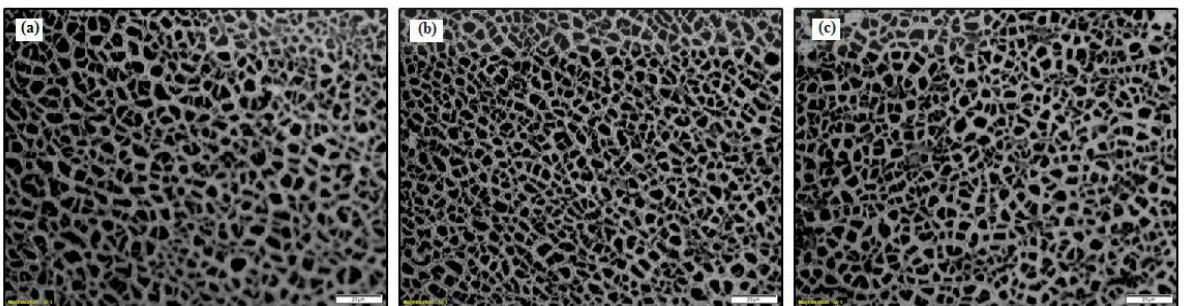
**Single-pass**



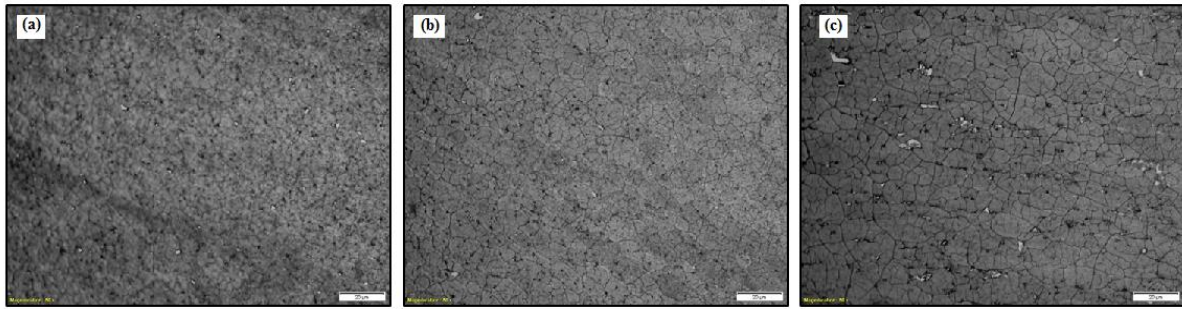
**Two-pass**



**Three-pass**



**Four-pass**



### Five-pass

**Figure 5.4: OM micrographs of FSPd samples (a) SZ (b) TMAZ (c) HAZ**

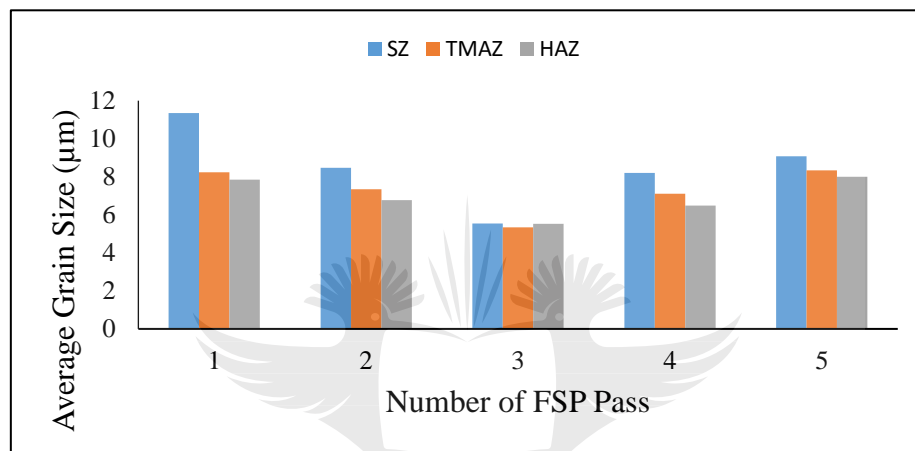
In the macrographs presented in section 5.3, the three distinct FSP zones (SZ, TMAZ, HAZ) as explained in section 2.11 are identified, and the microstructures of the various zones are illustrated in Figure 5.4 showing each zone in the various number of FSP passed samples. Microstructures in the different zones of the samples were carefully observed with OM to reveal the microstructural evolution after each successive FSP pass. It can be observed that the microstructure of the FSPd regions are different from that of the base material. The FSPd zones exhibited a much more distinct spherical grain morphology compared to the base material. The SZ of the single-pass sample consists of nearly equiaxed grains as a result of dynamic recrystallisation. Grain growth and a complete dissolution of the second-phase precipitate into the matrix is also clearly visible in the micrograph.

The complete dissolution of the second-phase precipitates could be attributed to the inability of the identified precipitates to withstand high temperatures. El-Rayes and El-Danaf [95] reported that the precipitates are not temperature resistant and rapidly dissolve when exposed to high temperatures resulting from FSP. Woo et al [148] in their study of the influence of the stirring pin and pressing tool shoulder on the microstructural development during FSP on Al6061 also reported that the frictional heating resulting from FSP had caused the dissolution of the precipitates. Chen et al [93] reported that during FSP, the SZ experiences intense plastic deformation and thermal exposure with peak temperatures almost up to the melting point of the alloy.

The size of the grains in the TMAZ and HAZ in the single-pass samples seems to appear similar to the grain size in the SZ. However, there are differences in grain size across the different zones. Details of the grain sizes in all the microstructural zones are presented in Table 5.1. with a graphic representation in Figure 5.5.

**Table 5.1: Average grain size in various region of FPZ**

Sample	SZ ( $\mu\text{m}$ )	TMAZ ( $\mu\text{m}$ )	HAZ ( $\mu\text{m}$ )
1 <sup>st</sup> PASS	11.35	8.23	7.85
2 <sup>nd</sup> PASS	8.47	7.34	6.77
3 <sup>rd</sup> PASS	5.55	5.34	5.52
4 <sup>th</sup> PASS	8.20	7.10	6.49
5 <sup>th</sup> PASS	9.07	8.33	8.00

**Figure 5.5: Graphic representation of various FPZ zones grain sizes**

The result obtained showed almost 70% increase in the SZ grain size after the first FSP pass, with 23% and 17% increases in the TMAZ and HAZ respectively. This shows that the TMAZ and HAZ of the base material have experienced lower strains and strain rates as well as lower peak temperatures compared to the SZ. It is noteworthy that the consequential grain growth in the SZ is defined by the factors impacting on the nucleation and growth of the dynamic recrystallisation. Mishra and Ma [14] reported that the FSP parameters, tool geometry, material chemistry, workpiece temperature, vertical pressure, and active cooling significantly impact on the size of the recrystallised grains in the SZ. Grain growth occurs when recovery and recrystallisation are complete [158].

The grain growth observed in this sample can be classified as abnormal grain growth (AGG), as the resulting microstructure is dominated by a few very large grains which usually results from a subset of grains growing at a high rate at the expense of their neighbours. AGG occurs when there is an inhibition in the normal growth of the matrix grains, and when the

temperature is high enough to allow a few special grains to overcome the inhibiting force and to grow disproportionately. The conditions commonly known for inhibiting grain growth are the presence of second-phase particles as observed in the base material matrix, a strong single-orientation texture, and a stabilised two-dimensional grain structure imposed by the material [158]. Rios et al [159] explained that in a region exempt of defects, recrystallisation proceeds by the growth of this "nucleus" over the yet non-recrystallised matrix. This can be observed in the various microstructural zones of the single-pass sample shown in Figures 5.4.

All two-pass sample microstructural zones show a refinement in grain size. This could be attributed to dynamic recrystallisation after the second pass. A grain refinement of 25%, 11%, and 14% decrease in grain size in the SZ, TMAZ, and HAZ respectively compared to the single-pass sample is recorded. This dynamic recrystallisation is usually attributed to the plastic deformation and the high temperatures from FSP [95]. It is noteworthy that in the micrograph of the two-pass sample SZ, it can be observed that there is competition between the dynamic recrystallisation and concurrent recovery. The rate of recrystallisation decreases towards completion as concurrent recovery of the matrix occurs, and as more of the new grains impinge on each other [160].

Dynamic recrystallisation also occurred in the three-pass sample resulting in further refinement in the grain sizes. The various microstructural zones show a 34%, 27%, and 18% reduction in size in the SZ, TMAZ, and HAZ respectively compared to the two-pass sample. Platelet-shaped re-precipitation of the second-phase precipitates is clearly visible in the HAZ of the sample. The precipitates were more relatively homogenous in the HAZ with an average size of 9.76  $\mu\text{m}$ , which is much larger than those found in the base material. This limited re-precipitation could be attributed to the thermal cycle as reported in similar studies [99,102]. A reduction in temperature as a result of reduced friction during the third pass FSP is assumed to have favoured the re-precipitation. It should be noted that the HAZ is the region which experiences fewer thermal cycles and no plastic deformation, resulting in lower temperatures when compared to other microstructural zones (SZ and TMAZ). It could thus be concluded that the lower temperature of the HAZ favoured the re-precipitation of the second-phase precipitates while the temperature of the SZ and TMAZ is assumed to be high enough to resist re-precipitation resulting in a limited non-homogenous precipitation across the FPZ. A similar two stage mechanism involving full dissolution of the precipitates followed by re-precipitation, was reported during FSW on 6056 aluminium alloy by Cabibbo et al [161].

The four-pass sample show grain growth in all the microstructural zones. There was a 47%, 32%, and 18% increase in grain sizes in the SZ, TMAZ, and HAZ respectively. There was a complete dissolution of the second-phase precipitates observed in the three-pass sample. The behaviour in the transition from the three-pass sample to the four-pass sample is similar to the transition of the base material to the single-pass sample with respect to second-phase precipitates dissolution and increase in grain size. The four-pass sample also exhibited nearly equiaxed distinct spherical grains in all the FPZ zones similar to the first sample. However, in this case, it is believed that normal grain growth (NGG) has occurred, as the grain growth seems to have occurred in a uniform manner.

A significant coarsening and growth of the grains is seen in all the five-pass sample FPZ zones; the SZ seems to be coarser than the TMAZ and HAZ. This coarsening could be attributed to the additional/accumulated thermal cycles which the plate has experienced. Sinhmar et al [102] stated a similar reason for grain coarsening after multiple FSP passes. Johannes and Mishra [162] also suggested that where multiple passes are to be used, there may be some grain coarsening due to the additional thermal cycles on the plate. It is apparent that the various mechanisms acting at different stages of the microstructure evolution after every successive multiple FSP pass are related to the strain, strain rate, and thermal cycle which the material undergoes at each stage. A summary of the mechanisms observed across the multiple-pass micrographs is given in Figure 5.6. Unfortunately, the thermal cycle experienced by the samples during each FSP pass was not quantitatively measured during this study; it would have been very interesting to study the relationship between the thermal cycles and the resulting microstructural evolutions. It is noteworthy that the resulting microstructural evolutions exercise significant influence on the mechanical properties of the FSPd samples. The tensile and hardness properties of the base material and the FSPd samples were studied and reported in sections 5.5 and 5.6 respectively.

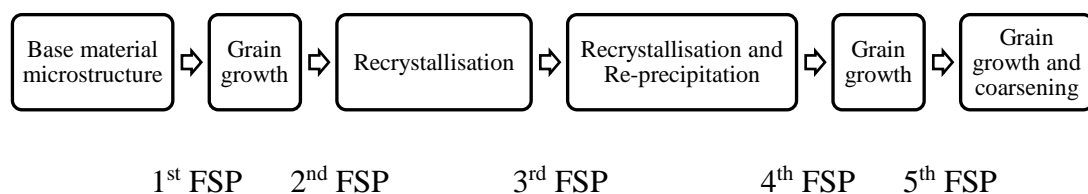


**Figure 5.6: Microstructural evolution of multi-pass FSP of AA6061-T6**

## 5.5 Tensile Properties

An Instron tensile testing machine (Figure 3.8) was used to evaluate the longitudinal tensile properties. The FSPd materials were evaluated by testing three specimens in each condition to measure tensile strength, and yield strength was taken by constructing a straight-line parallel to the initial linear portion of the stress-strain curve at 0.2% offset for each sample. The percentage of elongation of the FSPd samples were evaluated by measuring the final length of the failed specimens to determine the ductility of the samples. The elongation percentage is defined in equation 5.1.

$$\%El = \left[ \frac{L_f - L_o}{L_o} \right] \times 100 \quad \text{Eq. 5.1}$$

where  $L_o$  is the initial gage length, and  $L_f$  is the length of the gage section at fracture. Data showing a comparison of the base material and the FSPd samples in terms of tensile strength, yield strength, and the elongation percentage are presented in Appendix D. The first, second and third tensile samples are represented as T1, T2, and T3 respectively. The standard deviation was also evaluated to estimate the variation in the observed values across all three samples. A graphic representation of these properties is presented in Figure 5.7. Detailed tensile behaviour showing a stress vs strain diagram of the base materials and processed material of the all the multi-pass FSP across the three samples can also be seen in Appendix D.

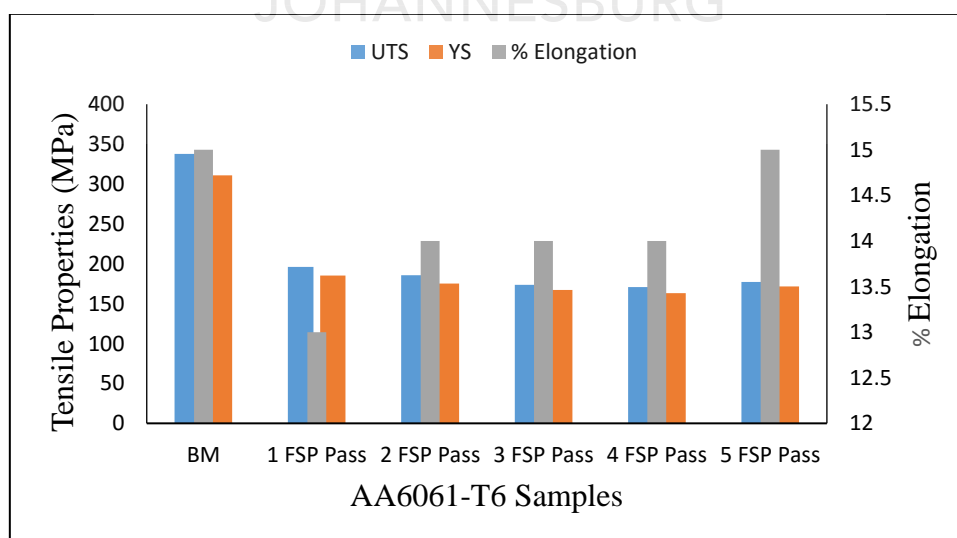


**Figure 5.7: Graphic representation of tensile properties of the AA6061-T6 base material and FSPd samples.**

From the results, it was observed that the standard deviations of the values in the ultimate tensile strength (UTS) and yield strength are in the range of 1-3 MPa because of the close values, which are very acceptable. The BM had a yield strength of ~311 MPa, a UTS of ~338 MPa and a ductility of 15%. It was clear that all the FSPd samples show a reduction in tensile and yield strength compared to BM samples. The samples tensile and yield strengths of all the FSPd samples are between the ranges of 170-200 MPa and 165-190 MPa respectively. However, there was no significant change in the elongation percentage in the processed samples compared to BM. There was a range of 1-2% reduction in the elongation percentage from the single-pass sample to the four-pass sample, while the five-pass sample exhibit the same elongation percentage as the BM. This shows that FSP does not have a significant effect on the ductility of the material using the processing parameters employed in this research.

The significant high strength in the base material could be attributed to the presence of the second-phase precipitates. Shankar et al [163] reported that precipitation treatable aluminum alloys such as Al6061-T6 which are peak aged (T6 temper) have an optimum distribution of precipitates that ensures the greatest strength of the material. A similar high strength is recorded in a study by Ravikumar et al [164] on the characterisation of the mechanical properties of Al6061-T6 after FSW. The study recorded a UTS and yield strength of ~354 MPa and 326 MPa respectively in the base material, while there were relatively low UTS and yield strength in the welded samples in the range of 200-240 MPa and 130-150 MPa respectively. It also reported a 17.6% elongation in the base material, and a drop in the elongation percentage across all welded samples similar to the one obtained in this research.

The yield strength is seen to decrease uniformly as the UTS decreases. A significant reduction in the tensile properties after the first FSP pass could be attributed to the dissolution of the precipitates resulting in softening as reported earlier to have occurred in the SZ, and a reduction in pre-existing dislocations [165]. Al-Fadhalah et al [166] reported that age-hardened aluminum alloys depend strongly on precipitate size and distributions rather than on grain size. This is displayed in the tensile values of the second and third passes, where there was a reduction in the grain size, and a reduction in the UTS and yield strength, against the expected increment in the values according to Hall-Petch relation [167]. It could be concluded that these reductions of UTS and yield strength are due to the overaging effect which the subsequent passes cause to the previous one, as suggested by El-Rayes and El-Danaf [95].

The re-precipitation seen in the three-pass sample is ~1.5 times bigger than the precipitates in the base material. It is noteworthy that the size of the precipitates has a significant influence on how the precipitates influence the mechanical properties of materials. The Mg<sub>2</sub>Si precipitates occur in several forms which can be divided into the β'' (beta double prime) Mg<sub>2</sub>Si, β' (beta prime) Mg<sub>2</sub>Si, and the β (beta) Mg<sub>2</sub>Si [168].

The β'' Mg<sub>2</sub>Si is the smallest rod-shaped type and contributes most to the mechanical properties when densely dispersed. This is the type which is exhibited in the AA6061-T6 base material. The precipitates observed in the three-pass sample is believed to be either a β' Mg<sub>2</sub>Si or β Mg<sub>2</sub>Si due to their large size, and their negligible effect on the material mechanical properties. The β' Mg<sub>2</sub>Si is a larger version of the rod-shaped precipitate that grows from the β'' category and makes a negligible contribution to mechanical properties, while the β Mg<sub>2</sub>Si is the largest Mg<sub>2</sub>Si precipitate that is mostly cube-like in shape and due to its size contributes nothing to the mechanical properties [168]. There was no significant change in the UTS and yield strength after the fourth FSP pass, but a sharp increase in these properties was observed after the fifth FSP pass. This could be attributed to the completely homogenous FPZ microstructure obtained after the pass. This shows that a complete homogenous FPZ in the AS and RS influences the mechanical properties of the processed material. The next section will look at how these microstructural evolutions affect the hardness of the processed material.

## 5.6 Hardness Properties

The effect of multi-pass FSP on the hardness of the samples has been studied. Figure 5.8 shows a graphic representation of the mean hardness values of all the samples. The reduction in the hardness of the FSPd samples compared to the BM can be attributed to the softening from the complete dissolution of the second-phase precipitates as recorded in previous studies [102, 169-171].

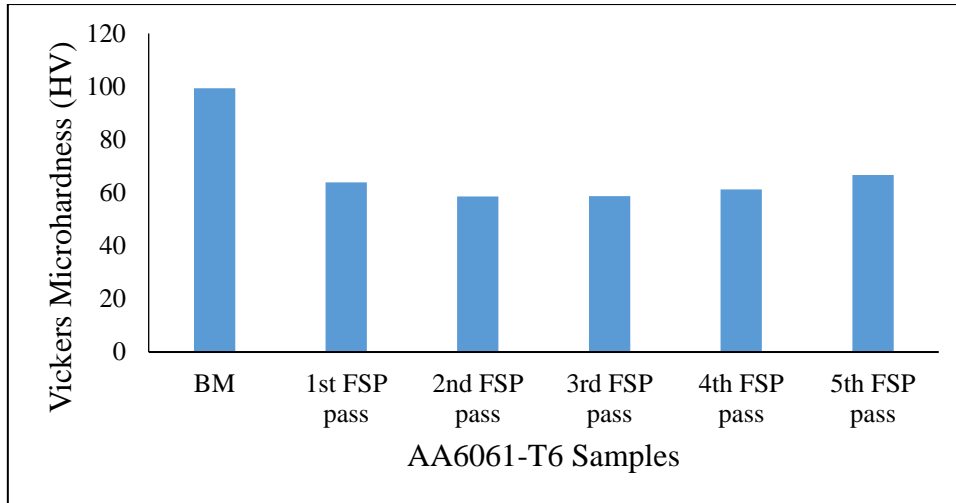


**Figure 5.8: Average hardness values of the BM and FSPd samples**

The hardness values obtained are presented in Appendix D. The highest hardness values were seen in the BM, similar to other reports [95,166,170]. All the FSPd samples exhibited a lower hardness compared to the BM. The microhardness profiles of the BM and the FSPd samples are presented in Figure 5.9 to fully understand the variation of the hardness values across the samples.

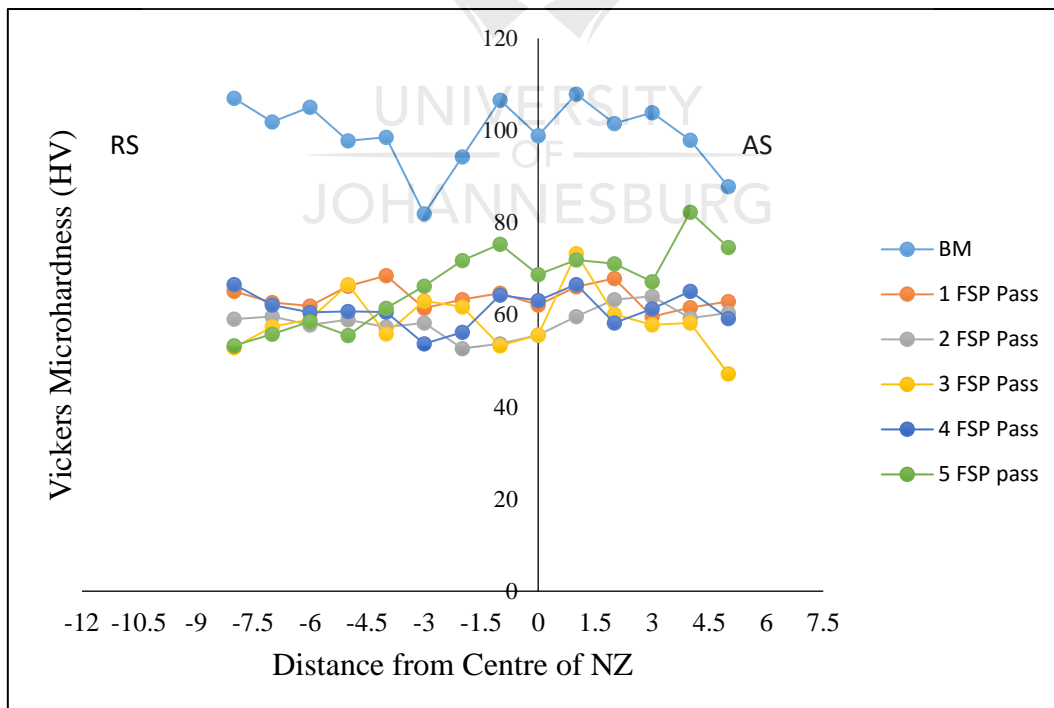


**Figure 5.9: Microhardness profile of BM and FSPd samples**

The BM has an average hardness of  $\sim 99 \pm 7.4$  HV reaching a peak hardness value of 107 HV. This is relatively high when compared to the 35% drop in hardness value to  $\sim 64 \pm 2.6$  HV after the first FSP pass. The single-pass sample shows a relatively uniform microhardness distribution with less scatter. An increase in the softening area in the sample after the second pass led to a reduction in the microhardness value to an average value of  $\sim 59 \pm 3.1$  HV. This increase in the area of the softened zone has been attributed to the increase in the heat input [169,172]. The two-pass sample show a distribution of hardness values lower in all regions when compared to the single-pass sample's hardness distribution. However, both samples' peak hardness values were observed to be on the AS. The fluctuation in the hardness values across the FPZ is a result of the difference in the metal flow between the tools AS and RS as reported earlier in this dissertation. Jiang and Kovacecis [173] also reported this behaviour as a result of the substantial fluctuation related to the heterogeneous constitution of the nugget. Yadav and Buari [79] claimed that hardness variations may result from different microstructural features at different locations in the FPZ. They explained that the flow of material from the RS to the AS during FSW/FSP gives rise to gradients in temperature, strain and strain rate in the stir zone.

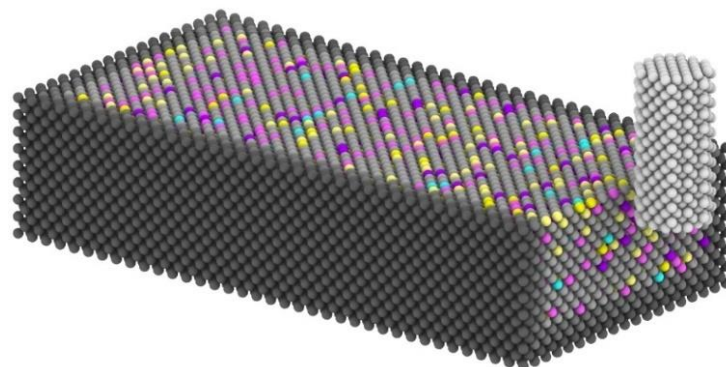
There was no significant change in the average hardness values of the three-pass sample compared with the two-pass sample. An average hardness value of  $\sim 59 \pm 6.3$  HV was recorded. However, a significant peak hardness up to 60 HV was observed towards the AS which could be attributed to the re-precipitation observed in the three-pass sample HAZ, even though the re-precipitation has a negligible effect on the tensile properties, this shows that it has an effect on the hardness properties of the material. From this observation, it could be said that the negligible effect of re-precipitation on the tensile properties of a material is not an indication that the precipitates will not influence the hardness properties of the material.

A significant observation in the behaviour of the microhardness values is its increase as the samples near a homogenous FPZ. A 4.4% increase in the average hardness value was observed in the four-pass sample, which further have an 8.8% increment in the five-pass sample. The four-pass and five-pass samples have an average hardness value of  $\sim 61 \pm 3.7$  HV and  $\sim 67 \pm 8.7$  HV respectively. The average hardness value, as well as the distribution of the hardness values in the fifth pass as shown in Figure 5.9, can be seen to be higher than all the values obtained from the preceding numbers of FSP passes. However, this is still far below the hardness values obtained from the BM. From the observations, it could be said that

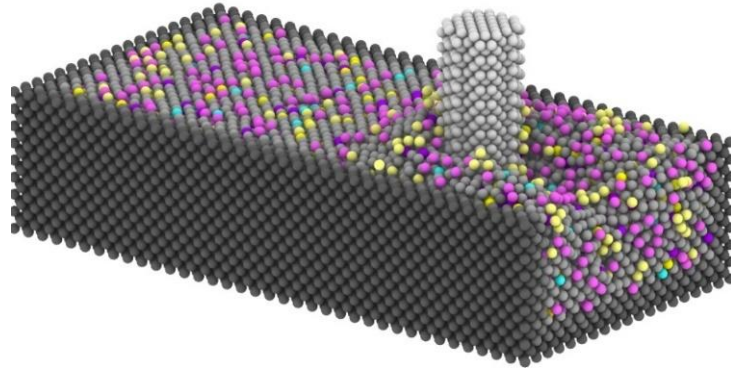
material flow and mixture have a strong effect on the hardness of the material making the microstructural homogeneity of the FPZ a very important factor in determining the hardness of a material. The increase in hardness after the fourth and fifth FSP passes could be attributed to the re-precipitation of the second-phase strengthening precipitates and the microstructural homogeneity. It is noteworthy that the peak hardness of all the FSP passes was not observed in the centre of the NZ. A similar microhardness profile indicating all the peak hardness away from the centre of the stir zone is been reported by Yutaka et al [174]. The results from the molecular dynamics simulation giving insights into the thermodynamic phenomenon not measured experimentally in the research, are presented and discussed in the next section.

### 5.7 Molecular Dynamics Simulation Results

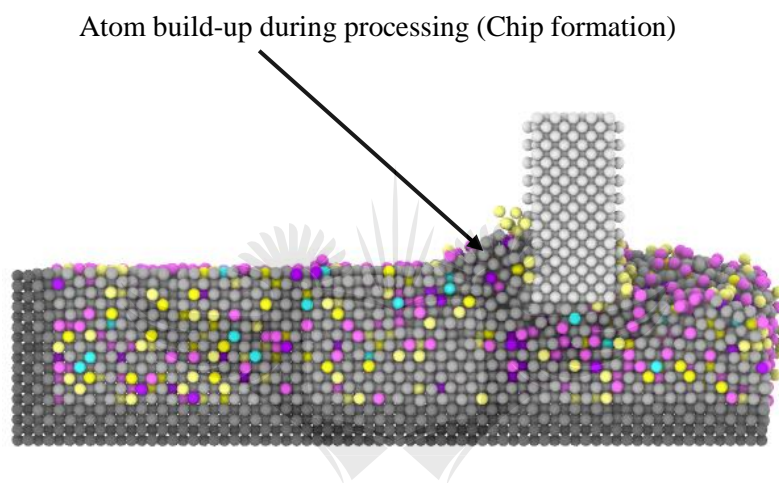
The FSP of AA6061-T6 was investigated with MD simulation using a rotational tool. The original workpiece was modelled in an atomic scale to produce nearly the same loading and processing conditions as experimentally performed. The MD simulation model is presented in Figure 4.7 with the different sets of atoms already identified. The dimensions of the model were made large enough to eradicate boundary effects. Full details of the modelling parameters are presented in Table 4.1 above, while the boundary conditions, interatomic potentials and thermodynamic ensemble used was discussed in section 4.9. The particles were equilibrated and the simulation performed after attaining equilibrium at 293 K at a time step of 2 fs. Figure 5.10 shows representative MD simulation snapshots during the FSP process as obtained from the OVITO software.



(a) Simulation starting configuration



**(b) Plastic deformation at beginning of the FSP process**



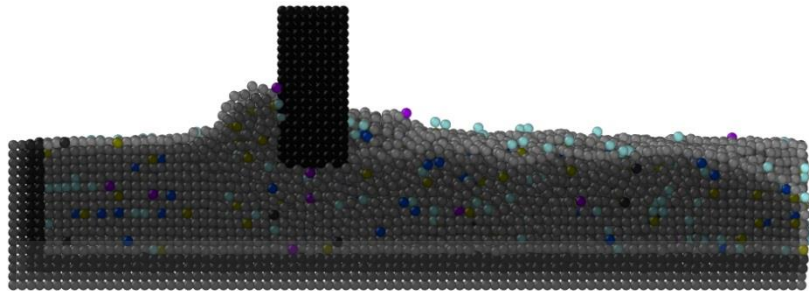
**(c) 2D representation of plastic deformation showing atom-build up**

**Figure 5.10: MD simulation snapshots of the FSP of AA6061-T6**

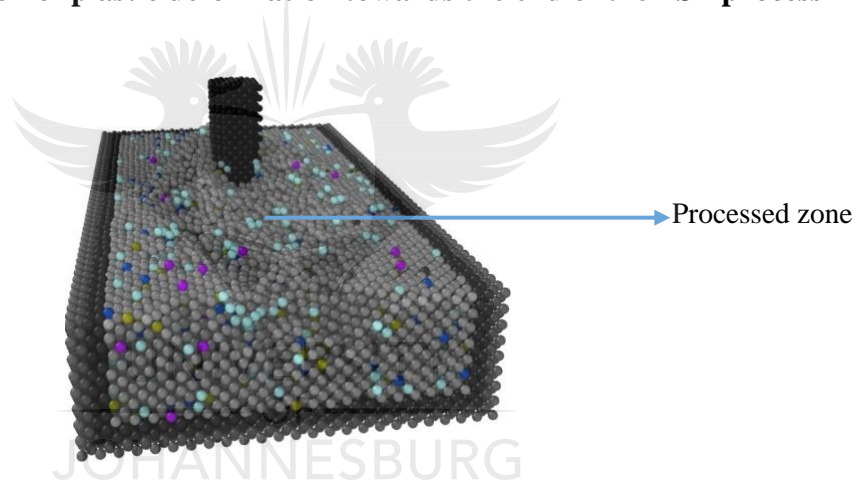
Figure 5.10b shows that there was plastic deformation during the processing of the material. The snapshot shows a breakup of the atoms in the lattice as the tool passes through, with chip formation represented by the build-up of atoms ahead of the tool. During the simulation, the plastic effect of the tightly bonded atoms could be clearly observed behind the tool as it passed through the workpiece. This is similar to what was observed in the FSP experiments during the mixing of the material and forming of the processed surface. The chip formation appears to occur mainly as a result of the large compression and shear strain experienced around the tool.

A multiple run of the simulations was conducted to ensure accuracy and repeatability of the results. No voids were observed after FSP, but the keyhole resulting from the withdrawal of the tool and flashes after the completion of the process were observed in both cases similar to

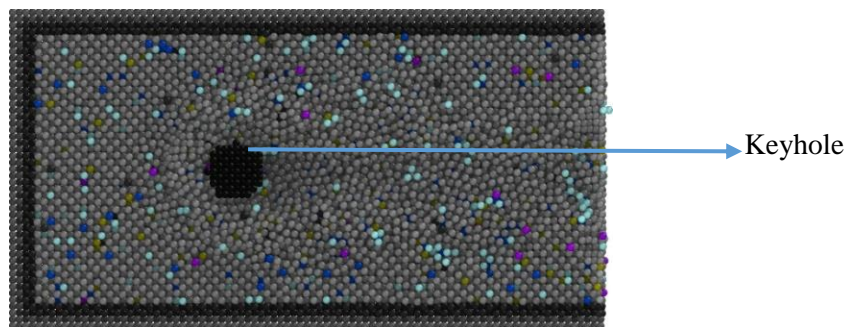
experimental observations. These can be seen in snapshot images of stages in the process obtained from the OVITO software in Figure 5.11. The images were obtained from the repeated MD simulations. The thermodynamic information obtained from the MD simulation is discussed in the subsections below. These discussions are based on the evaluation of the simulated results and observations of the animations of the process.



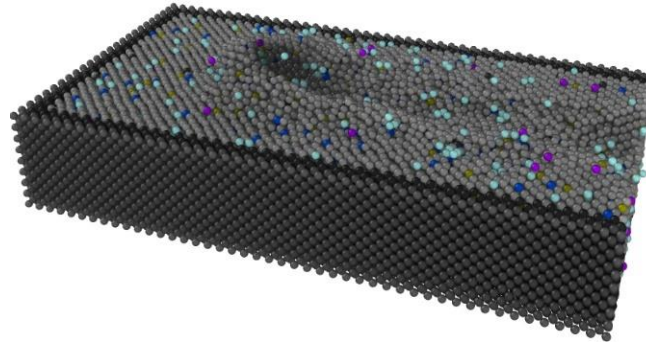
**(a) 2D representation of plastic deformation towards the end of the FSP process**



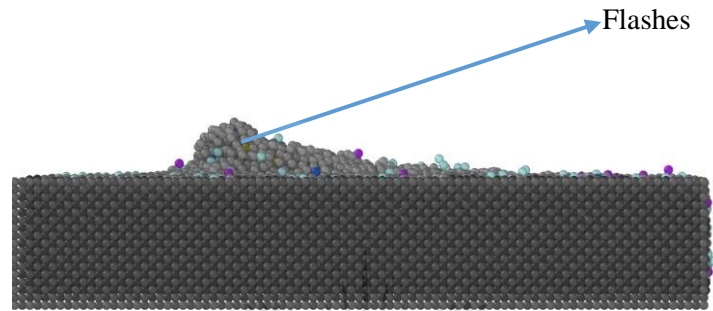
**(b) Completion of the FSP process**



**(c) Top view after removal of FSP tool**



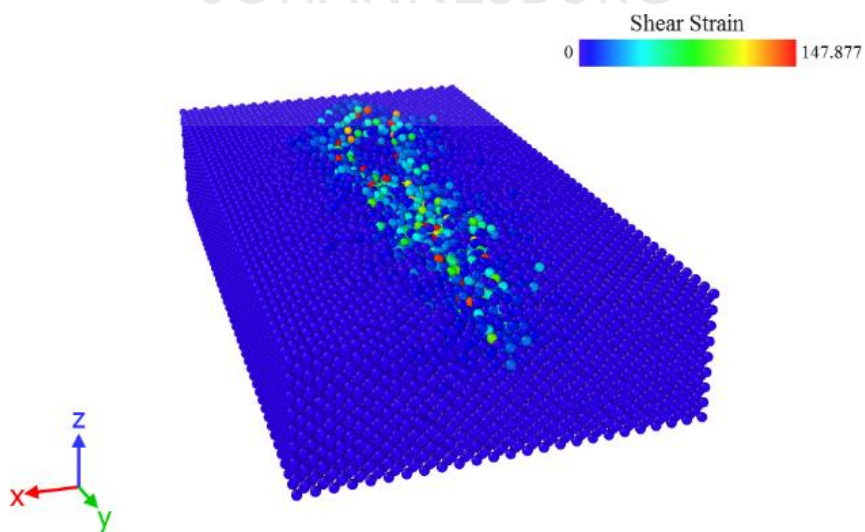
(d) Friction stir processed material



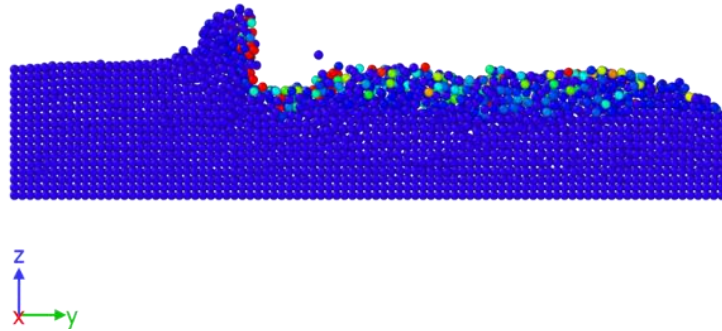
(e) 2D view of the FSPd material

Figure 5.11: Snapshots from repeated MD simulation

It can also be seen that the unprocessed material in the workpiece away from the tool experienced zero shear strain. A schematic of the shear strain distribution is given in Figure 5.12.



(a) 3D view



**(b) 2D view**

**Figure 5.12: Shear strain distribution in FSP of AA6061-T6**

### 5.7.1 Temperature Variation

MD simulation was used to study variations in temperature during the process. The average of the instantaneous kinetic temperatures over many molecular dynamics time steps are shown in Figure 5.13.

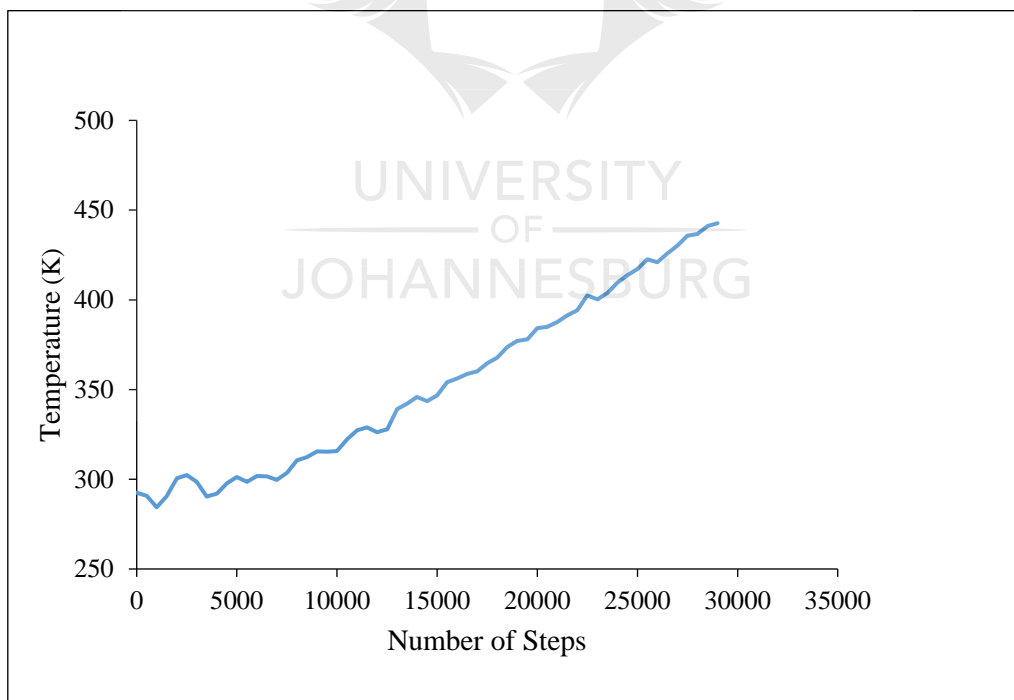


**Figure 5.13: Time step vs temperature plot of FSP of AA6061-T6**

The figure shows that the temperature at the start was at 293 K as a result of the equilibrium attained. The temperature is seen to increase almost linearly with increasing time steps, reaching a peak temperature of 442.68 K at 29000 steps. This proposes that the temperature during FSP increases with time which is in agreement with experimental reports from various studies as discussed earlier in this dissertation. However, it is noteworthy that the highest temperature attained during the processing is just a little above half of the melting point of AA6061-T6 which is reported to be 855.15 K [103]. A shortfall in this simulation is its inability to measure temperature distribution across each distinct FPZ zone (SZ, TMAZ and HAZ).

### 5.7.2 Pressure Variation and Force analysis

The variation in the force with respect to the cross-sectional area of the workpiece was also studied with the MD simulation. Figure 5.14 shows the pressure variation relative to the time steps.

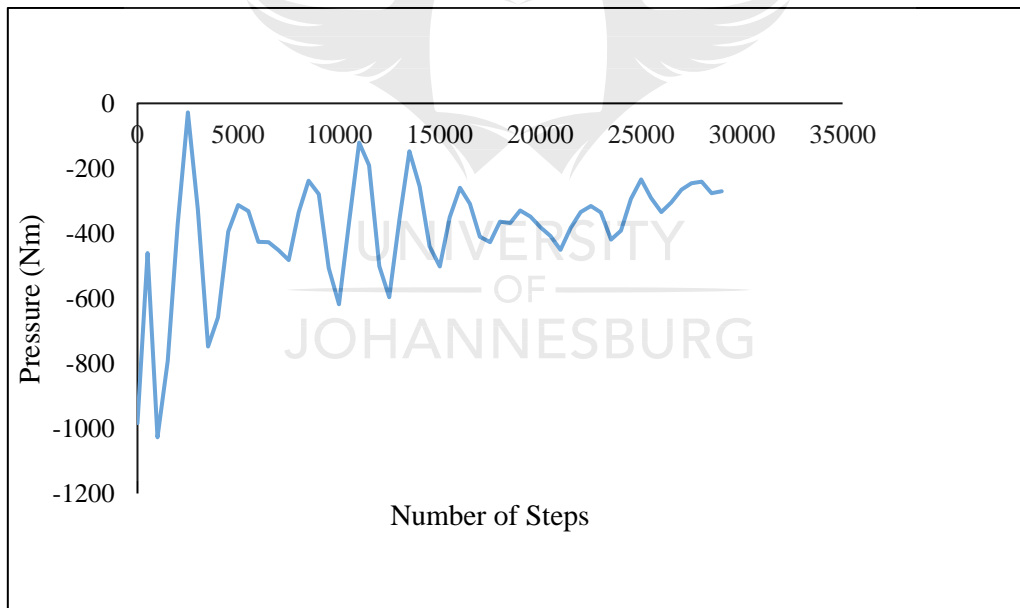


**Figure 5.14: Time step vs pressure plot of FSP of AA6061-T6**

As reported earlier, the shoulder applies pressure to the surface of the workpiece to constrain the deformed material around the pin, and produces heat through friction and plastic deformation. It is known that the decrease in both axial force and contact pressure is very likely to contribute to decreasing defects in the processed material. Figure 5.19 shows similar behaviour in the force feedback from FSP experiments reported in Appendix C. The pressure

was observed to be very high during penetration of the tool attaining its peak value, but tended to decrease and then stabilised throughout the process. The axial forces recorded in the simulation seems to exhibit different behaviour. A graphic representation of the axial forces relative to the time steps is shown in Figure 5.15.

While there was similar stability in the axial forces, the peak force was not recorded during the tool penetration stage as seen in the experimental results. This is a significant observation in the simulation, as it shows one of the shortcomings of the MD simulation in comparison to larger scale experimental FSP processes. The pressure and force distribution contours could also be attributed to differences in the behaviour of simulations measured over time steps and the duration of real-life experiments. A similar graph has been reported in molecular dynamics studies [133,139, and 141]. However, the stability of the pressure and axial forces can be proposed to have contributed immensely to the absence of any observable defect in the processed material. It could also be seen that the  $F_z$  is greater than the  $F_x$ , similar to the experimental results.

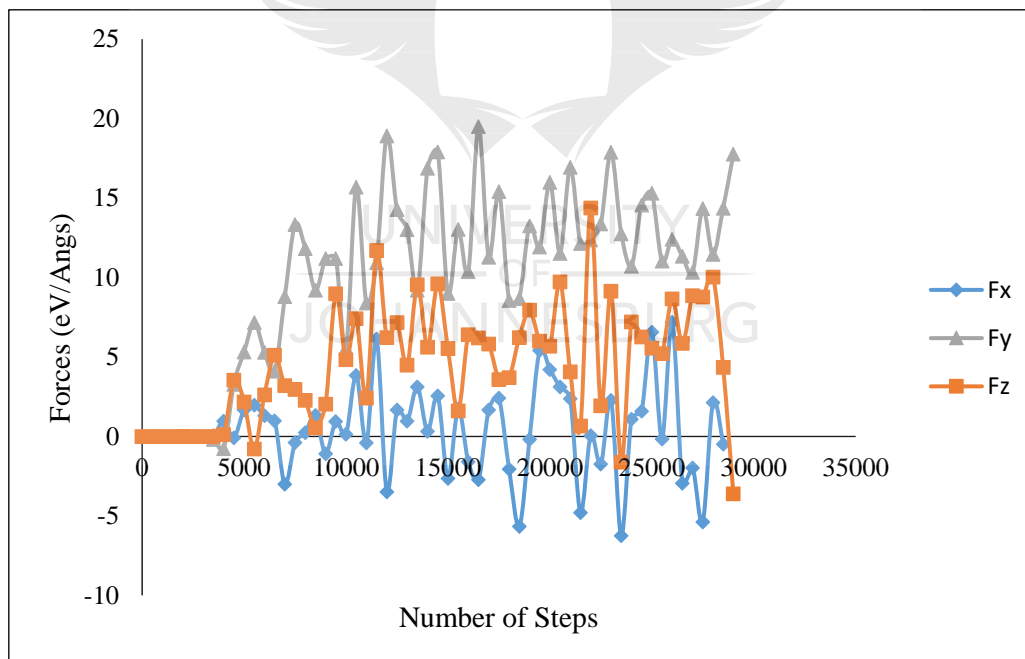


**Figure 5.15: Time step vs force plot of FSP of AA6061-T6**

### 5.7.3 Potential and Total Energy

The behaviour of the potential energy (PE) and total energy (TE) during the process is obtained and presented in Figure 5.16. The plot shows the distortion in the stability of the assembly as the tool penetrates it. The PE and TE can be seen to have increased significantly from -143848.88 eV to -142924.61 eV and -142712.84 eV to -141795.78 eV respectively. It is generally known that the lower the potential energy, the less able the structure is to change and the greater is its stability, and vice versa. The increase in the PE and TE causing a distortion in stability results from the initial atomic break in the lattice depicted by a clear scattering of atoms comparable to the plastic deformation that occurs in the experimental studies. Both the PE and TE reach a maximum of -142424.67 eV and -140705.95 eV respectively after 30000 time steps showing increases in instability as the tool passes across the material.

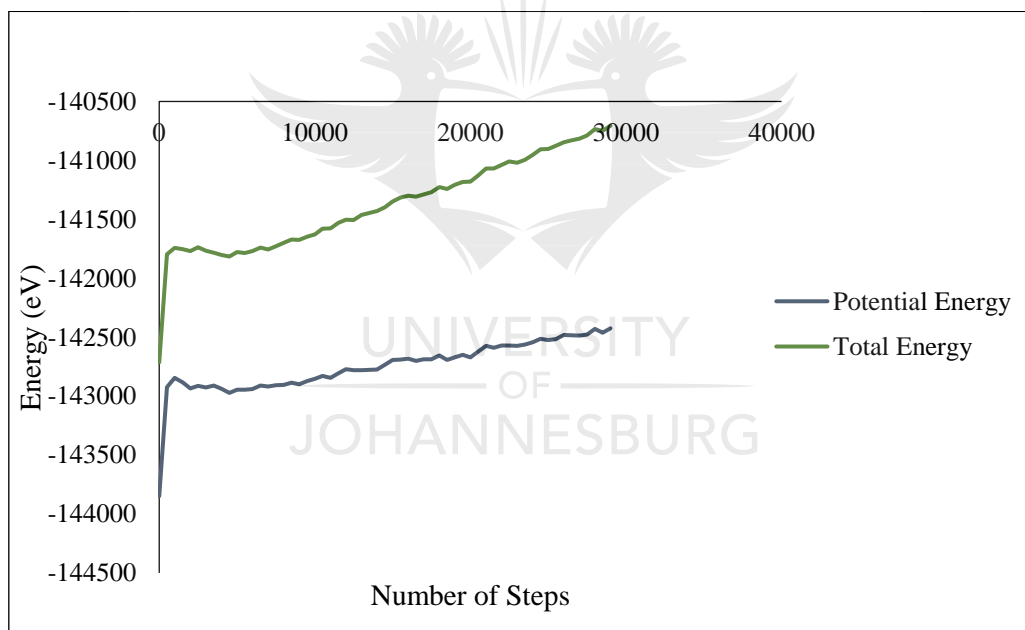


**Figure 5.16: Time step vs energy plot of FSP of AA6061-T6**

It is worthy to note the increase in TE relative to the PE showing that the kinetic energy is relatively constant throughout the process. This could be attributed to the fact that the kinetic energy is independent of the force field. However, the variation in the TE shows the interaction of the model with external force. The study of the PE and TE is very useful for comparing the stability of two systems; the system with the lower energy will have more stability than the other one.

## 5.8 Summary

The results obtained from the various characterisation techniques employed were presented and discussed in this chapter. The macro and microstructural evaluations revealed the material mixture, homogeneity, and effect of multi-pass FSP on the microstructure and mechanical properties of the material after every successive FSP pass. It is apparent that the phenomena acting at different stages of the microstructure evolution are related to strain, strain rate, and thermal cycles which the material undergoes at each stage. The complex thermomechanical mechanisms involved were seen to play a key role in determining the resulting microstructural evolution after multi-pass FSP on the aluminium alloy, making it very complex to predict. However, the phenomena after each FSP pass, and the results obtained have made it possible to holistically draw a conclusion on the correlation between the microstructural homogeneity and the mechanical properties of the material which is the aim of this research.

The molecular dynamics simulation results were also discussed. The simulation process was compared with real-life FSP experiments and found to be consistent. It is noteworthy that this study constitutes the first MD simulation of FSP on AA6061-T6. From a review of the literature, it is clear that there is yet no published work or research on this topic. The simulation has given insight into the sub-surface thermodynamic phenomena taking place during the process such as determination of the peak temperature, variations in pressure and cutting forces, and monitoring the stability of the system. The results obtained in this research are comparable to other published nanomachining research results [113, 123, 124, 127, 130, 132-134, 139, 141]. The general conclusions from the study and suggested future research are given in the next chapter.

## 6. Conclusions and Future Work

### 6.1 Introduction

This research work was conducted with the objective of studying the effect of multiple FSP passes on AA6061-T6 through metallurgical evaluation and mechanical testing, to correlate the microstructural homogeneity with the mechanical properties of the material. Pioneer research through using a molecular dynamics simulation to study and elucidate on the underlying thermodynamic phenomena in the FSP process, was also conducted.

A comprehensive literature review on FSP was presented in Chapter 2. The chapter discussed the FSP process in detail. The application of FSW and FSP, its basic parameters, the material flow, and previous microstructural studies on friction stir processed aluminium were also discussed. A review of the research reveals that random sets of parameters are used with a wide variety of results showcasing the dependency of the weld or processed material on the workpiece material and processing parameters. Some studies suggested that multi-pass FSP may improve the homogeneity of the FPZ of FSPd materials, it is possible that the microstructural inhomogeneity in the transition of the base material in the FPZ after single-pass FSP may be one of the major reasons for the degradation of mechanical properties. However, no published research seems to exist on the correlation between the FPZ microstructural homogeneity and the mechanical properties of processed materials. This is the knowledge gap which this research intends to fill. Details of the experimental procedures are presented in Chapter 3.

The history, advantages, limitations, applications, procedures, and basics of molecular dynamics simulation are discussed in Chapter 4. The chapter also described the simulation configuration and how it was conducted. The results and discussions of the multi-pass FSP, as well as the MD simulations results are presented in Chapter 5. The conclusion drawn from these results are discussed in the next section. It is important to state that the conclusions are solely based on the material and processing parameters used in this research.

## 6.2 Conclusions

The conclusions in this study, using an HDS tool with 6-7 mm tapered pin diameter and 25 mm concave shoulder diameter for conducting single and multiple FSP passes on AA6061-T6 at a constant rotational and transverse speed of 1600 rpm and 40 mm/min, and a plunge depth of 5.3 mm, at a 3° tilt angle with the main emphasis on the correlation of the microstructural evolution and FPZ homogeneity with the mechanical properties of the material, as well as the conclusions on the MD simulation, are highlighted below:

1. The microstructural evolution and resulting grain sizes are strongly dependent on the processing parameters, thermal cycle, and presence of second-phase precipitates and not only on microstructural homogeneity.
2. Single-pass FSP led to a non-homogenous FPZ, decreased strength, hardness and ductility, and abnormal grain growth.
3. Multi-pass FSP led to a completely homogenous FPZ after the fifth FSP pass, attributed to accumulative plastic strain. This indicates that the number of FSP passes have a significant effect on the homogeneity of FPZ in a material.
4. Completely homogenous FPZ led to improvements in previously reduced mechanical properties (hardness, and tensile strength, and ductility) of AA6061-T6.
5. The BM have more improved mechanical properties when compared to all FSPd samples, irrespective of the number of FSP passes. This is attributed to the presence of second-phase precipitates and T6 condition (heat-treated and artificially aged).
6. The increase in the number of FSP passes accumulated more heat which led to a complete dissolution of hardening second-phase precipitates. This dissolution impaired the mechanical properties.
7. In the case of multi-pass FSP where multiple thermal cycles are involved, the thermal cycle has more influence on the mechanical properties than the grain size.
8. The accumulated thermal cycle led to coarsening of the grains when the FPZ is completely homogenised.
9. Limited re-precipitating of second-phase precipitates occurred in the HAZ after third FSP pass, which improved hardness, but have no effect on the tensile properties. An increase in the grain sizes occurred after dissolution of the second-phase precipitates (as observed after the first and fourth FSP passes).

10. The MD simulation was in good qualitative agreement with the experimental studies. The results prove that it is possible to adequately represent an MD simulation of the FSP of an aluminium alloy. MD simulation will be a reliable test bed for better understanding of the various phenomena taking place during FSP on aluminium alloys without the need to conduct real-life experiments, thereby saving costs, energy and materials.

### **6.3 Future Works**

While tangible and significant work has been achieved in this research, further investigation could include:

1. More multi-pass FSP studies on other aluminium alloys, with results compared to the results obtained in this research to study the trend, and to draw a general conclusion on the effect of multi-pass FSP on microstructural homogeneity and its correlation with the mechanical properties of aluminium alloys.
2. Since the tool design, material and processing parameters play a crucial role in FSP, the optimal tool design and processing parameters for AA6061-T6 should be studied thoroughly against the use of AA6061 optimum processing parameters.
3. The study of temperature and heat input, and their effect on grain sizes of the material would be beneficial. Further investigations on subsequent heat treatment after each number of multiple passes should also be considered.
4. A multi-pass MD simulation should be conducted to study the thermodynamic phenomena after every successive FSP pass.
5. Experimental in-process monitoring techniques such as the use of thermocouples should be employed in the FSP of aluminium to adequately validate and certify the MD simulation results obtained.
6. Further research on eradicating the shortfalls observed in computational time step compared with real-life experiments should be conducted to make MD simulation results more adequate, efficient and reliable. More research should also be carried out on MD simulation to study each FPZ zone distinctly.
7. Researchers should also place more focus on exploring the full potential of the MD computational tool on FSP to obtain further tangible output that will contribute to knowledge on this process. This study has shown successful modelling of FSP of an aluminium alloy using MD simulation.

The suggestions listed above coupled with the work completed in this study would provide the basis for a comprehensive study on the effect of multi-pass FSP on aluminium, as well as serve as a basis for new knowledge on the use of molecular dynamics in studying underlying thermodynamic phenomena in FSP.



## References

- [1] Zalensa DL. Aluminium Casting Technology. 2<sup>nd</sup> ed., AFS Inc. Illinois. 1993: 77pp.
- [2] Zhang DL, Zheng L. The quench sensitivity of Cast Al-7 wt % Si-0.4 wt % Mg alloy. *Metallurgical and Materials Transactions A*. 1996; 27: 3983-3991
- [3] Din T, Campbell J. High-strength aerospace Aluminium casting alloys - A comparative study. *Materials Science and Technology*. 1996; 12: 644-650
- [4] Yu YB, Song PY, Kim SS, Lee JH. Possibility of improving tensile strength of semi-solid processed A356 alloy by a post heat treatment at an extremely high temperature. *Scripta Materials*. 1999; 41: 767-771
- [5] Ma ZY, Sharma SR, Mishra RS. Effects of friction stir processing on the microstructure of cast A356 aluminum. *Materials Science and Engineering*. 2006; A433: 269-278
- [6] Mishra RS, Mahoney MW, Mcfadden SX, Mara NA, Mukherjee AK. High strain rate superplasticity in a friction stir processed 7075 Al alloy. *Scripta Materials*. 2000; 42: 163-168
- [7] Ma ZY, Mishra RS, Mahoney MW. Superplastic deformation behavior of friction stir processed 7075Al alloy. *Acta materialia*. 2002; 50: 4419-4430
- [8] Johnson R, Kallee S. Friction stir welding technology. *Materials World*. 1999; 7: 751-753
- [9] Gan YX, Solomon D, Reinbolt M. Friction stir processing of particle reinforced composite materials. *Materials*. 2010; 3: 329-350
- [10] Thomas WM, Nicholas ED, Needham JC, Murch MG, Templesmith P, Dawes CB, G.B. *Patent Application No. 9125978.8*. 1991.
- [11] Dawes C, Thomas W. Friction stir joining of Aluminium alloys. *TWI Bulletin* 6. 1995: 124-127
- [12] Mishra RS, De PS, Kumar N. Friction stir welding and processing. *Science and Engineering, Springer International Publishing, Switzerland*. 2014: 347pp.

- [13] Akinlabi ET. Characterisation of dissimilar stir welds between 5754 aluminium alloy and C11000 copper. *Doctorate degree Thesis, Nelson Mandela Metropolitan University, South Africa*. 2011.
- [14] Mishra RS, Ma ZY. Friction stir welding and processing. *Materials Science and Engineering*. 2005; R50: 1-78
- [15] Amancio-Filho ST, Sheikhi S, dos Santos JF, Bolfarini C. Preliminary study on the microstructure and mechanical properties of dissimilar friction stir welds in aircraft aluminium alloys 2024T351 and 6056-T4. *Journal of Materials Processing Technology*. 2008; 206: 32–142
- [16] Akinlabi ET, Mahamood RM, Akinlabi SA, Ogunmuyiwa E. Processing parameters Influence on wear resistance behaviour of friction stir processed Al-TiC composites. *Advances in Materials Science and Engineering*. 2014: 12pp.
- [17] Jeganathan AV, Ranganath MS, Mishra RS. Effect of process parameters on friction stir processed copper and enhancement of mechanical properties of the composite material: a review on green process technology. *International Research Journal of Sustainable Science and Engineering, IRJSSE*. 2014; 2(4): 1-10
- [18] Jeganathan AV, Ranganath MS, Mishra RS. Experimental investigations on friction stir processed copper and enhancement of mechanical properties of the composite material. *International Journal of Advance Research and Innovation*. 2014; 2(3): 557-563
- [19] Liechty BC, Webb BW. Flow field characterisation of friction stir processing using a particle-grid method. *Journal of Materials Processing Technology*. 2008: 431–443
- [20] European Aluminium Association. Joining dissimilar materials. *The Aluminium Automotive Manual*. 2015: 1-31
- [21] Mathers G. The welding of aluminium and its alloys. *Woodhead Publishing Limited, Cambridge, UK*. 2002: 242pp.
- [22] Lohwasser D, Chen Z (Eds). Friction stir welding from basics to applications. *Woodhead Publishing Limited, Cambridge, UK*. 2010: 428pp.

- [23] ESAB. Friction stir welding-technical handbook. 2010: 27pp.
- [24] Amini A, Asadi P, Zolghadr P. Friction stir welding applications in industry. *Advances in Friction Stir Welding and Processing- Woodhead Publishing Series in Welding and Other Joining Technologies*. 2014: 671-722
- [25] Kumagai M, Tanaka S. Properties of aluminium wide panel by friction stir welding. In *Proceeding of the First International Symposium on Friction Stir Welding, Thousand Oaks, CA, USA*. June 14-16, 1999
- [26] Midling OT, Kvåle JS, Dahl O. Industrialisation of the friction stir welding technology in panels production for the maritime sector. In *Proceeding of the First International Symposium on Friction Stir Welding, Thousand Oaks, CA, USA*. June 14-16, 1999
- [27] Eriksson LG, Larsson R. Friction stir welding– New technology changing the rules of the game in Al construction. *Svetsaren*. 2001; 1: 3-6
- [28] Kallee S, Davenport J, Nicholas D. 2002. Railway manufacturers implement friction stir welding. *Welding Journal*. 2002: 47-50.
- [29] Smith CB, Mishra RS. Friction stir processing for enhanced low temperature formability. *Friction stir welding and processing book series. 1<sup>st</sup> ed., Butterworth-Heinemann, Waltham, USA*. 2014: 146pp.
- [30] Mishra RS, Mahoney MW. Friction stir welding and processing. *ASM International*. 2007: 1-333
- [31] Surekha K, Akinlabi ET. Surface engineering by friction stir processing and friction surfacing. *Surface Engineering Techniques and Applications: Research Advancements*. 2014: 44pp.
- [32] Nandan R, DebRoy T, Bhadeshia HKDH. Recent advances in friction stir welding-process, weldment structure and properties. *Progress in Material Science*. 2008; 53: 980-1023
- [33] Anonymous. Friction stir welding application. <http://www.fswelding.com/application-of-friction-stir-welding-in-aircraft-structures> Retrieved October 3, 2015.

- [34] Colegrove PA, Shercliff HR. Development of trivex friction stir welding tool. Part 1: Two-dimensional flow modelling and experimental validation. *Science and Technology of Welding and Joining*. 2004; 9: 345-351
- [35] Fratini L, Buffa G, Shivpuri R. In-process heat treatments to improve FS-welded butt joints. *International Journal of Advanced Manufacturing Technology*. 2009; 43: 664–670
- [36] Lohwasser D, Chen Z. Friction stir welding. *Woodhead Publishing Ltd, Cambridge, UK*. 2009: 1- 432
- [37] Shinoda T. Effect of tool angle on metal flow phenomenon in friction stir welds. *3<sup>rd</sup> International FSW Symposium, Kobe, Japan*. September 27-28, 2001. TWI (UK).
- [38] Arici A, Selale S. Effects of tool tilt angle on tensile strength and fracture locations of friction stir welding of polyethylene. *Science and Technology of Welding and Joining*. 2007; 12 (6): 536-539
- [39] Threadgill PL. Friction stir welding – the state of the art. *TWI Report*. 1999.
- [40] Kwon YJ, Shigematsu I, Saito N. Mechanical properties of fine-grained aluminum alloy produced by friction stir process. *Scripta Materialia*. 2003; 49(8): 785-789
- [41] Cavaliere P, Campanile G, Panella F, Squillace A. Effect of welding parameters on mechanical and microstructural properties of AA 6056 joints produced by friction stir welding. *Materials Processing Technology*. 2006; 180: 263-270
- [42] Tsai FY, Kao PW. Improvement of mechanical properties of a cast Al–Si base alloy by friction stir processing. *Materials Letters*. 2012; 80: 40-42
- [43] Sato YS, Urata M, Kokawa H. Parameters controlling microstructure and hardness during Friction-stir welding of precipitation hardenable aluminum alloy 6063. *Metallurgical and Materials Transactions*. 2002; 33: 625-635
- [44] Asadi P, Givi MKB, Abrinia K, Taherishargh M, Salek R. Effects of SiC particle size and process parameters on the microstructure and hardness of AZ91/SiC composite layer fabricated by FSP. *Journal of Materials Engineering and Performance (Impact Factor: 1)*. 2011; 20(9): 1554-1562

- [45] Mahmoud ERI, Ikeuchi K, Takahashi M. Fabrication of SiC particle reinforced composite on aluminium surface by friction stir processing. *Science and Technology of Welding and Joining*. 2008; 13: 607-618
- [46] Weglowski MSt, Dymek S. Friction stir processing of an AlSi6Cu4 cast aluminium alloy. *Archives of Foundry Engineering*. 2012; 11(2): 213-216
- [47] Peel M.J. The friction-stir welding of dissimilar aluminium alloys. *Doctorate degree Thesis, The University of Manchester*. 2005.
- [48] Wais AMH, Salman JM, Roubaïy AO. Effect of friction stir processing on mechanical properties and microstructure of the cast pure aluminium. *International Journal of Scientific and Technology Research*. 2013; 2(12): 154-163
- [49] Aruri D, Adepu K, Adepu K, Bazavada K. Wear and mechanical properties of 6061-T6 aluminum alloy surface hybrid composites [(SiC + Gr) and (SiC + Al)] fabricated by friction stir processing. *Journal of Material Research Technology*. 2013; 2(4): 362-369
- [50] Elangovan K, Balasubramanian V. Influences of pin profile and rotational speed of the tool on the formation of friction stir processing zone in AA2219 aluminium alloy. *Material Science Engineering*. 2007; A459: 7-18
- [51] Salman JM. Effect of friction stir processing on some mechanical properties and microstructure of cast (Al-Zn-Mg-Cu) alloy. *Journal of Babylon University Engineering Sciences*. 2014; 22(2): 10pp.
- [52] Anonymous. Friction stir welding. [http://en.wikipedia.org/wiki/Friction\\_stir\\_welding](http://en.wikipedia.org/wiki/Friction_stir_welding)  
Retrieved October 5, 2015.
- [53] Miranda RM, Gandra J and Vilaca P, Quintino L, Santos TG. Surface modification by friction based processes. *Woodhead Publishing Ltd, Cambridge, UK*. 2013: 210pp.
- [54] Seidel TU, Reynolds AP. Visualisation of the material flow in AA2195 friction-stir welds using a marker insert technique. *Metallurgical and Materials Transactions A: Physical Metallurgy and Materials Science*. 2001; 32A: 2879-2884

- [55] Fratini L, Buffa G, Palmeri D, Hua J, Shivpuri R. Material flow in FSW of AA7075-T6 butt joints: Numerical simulations and experimental verifications. *Science and Technology of Welding and Joining*. 2006; 11: 412-421
- [56] Ouyang JH, Kovacevic R. Material flow and microstructure in the friction stir butt welds of the same and dissimilar aluminum alloys. *Journal of Materials Engineering and Performance*. 2002; 11: 51-63
- [57] Kainer KU. *Metal Matrix Composites: Wiley-VCH, Weinheim, Germany*. 2006.
- [58] Morisada Y, Fujii H, Kawahito Y, Nakata K, Tanaka M. Three-dimensional visualisation of material flow during friction stir welding by two pairs of X-ray transmission systems. *Scripta Materialia*. 2011; 65: 1085-1088
- [59] Colegrove PA, Shercliff HR. Experimental and numerical analysis of aluminium alloy 7075-T7351 friction stir welds. *Science and Technology of Welding and Joining*. 2003; 8: 360-368
- [60] Bastier A, Maitournam MH, Dang Van K, Roger F. Steady state thermomechanical modelling of friction stir welding. *Science and Technology of Welding and Joining*. 2006; 11: 278-288
- [61] Nandan R, Roy GG, Debroy T. Numerical simulation of three-dimensional heat transfer and plastic flow during friction stir welding. *Metallurgical and Materials Transactions A: Physical Metallurgy and Materials Science*. 2006; 37: 1247-1259
- [62] Xu S, Deng X, Reynolds AP, Seidel TU. Finite element simulation of material flow in friction stir welding. *Science and Technology of Welding and Joining*. 2001; 6: 191-193
- [63] Colligan K. Material flow behaviour during friction stir welding of aluminium. *Welding Journal*. 1999; 78: 229-237
- [64] Reynolds AP. Visualisation of material flow in autogenous friction stir welds. *Science and Technology of Welding and Joining*. 2005; 5: 120-124

- [65] Trueba Jr. L, Heredia G, Rybicki D, Johannes LB. Effect of tool shoulder features on defects and tensile properties of friction stir welded aluminium 6061-T6. *Journal of Materials Processing Technology*. 2015; 219: 271-277
- [66] Givi MKB, Asadi P. General Introduction. *Advances in Friction Stir Welding and Processing- Woodhead Publishing Series in Welding and Other Joining Technologies*. 2014: 1-19
- [67] Bag S, Yaduwanshi D, Pal S. Heat transfer and material flow in friction stir welding. *Advances in Friction Stir Welding and Processing- Woodhead Publishing Series in Welding and Other Joining Technologies*. 2014: 21-63
- [68] Reynolds AP, Seidel TU, Simonsen M. In *Proceeding of the First International Symposium on Friction Stir Welding, Thousand Oaks, CA, USA*. June 14-16, 1999.
- [69] Seidel TU, Reynolds AP. Visualisation of the material flow in AA2195 friction-stir welds using a marker insert technique. *Metallurgical Materials Transactions A*. 2001; 32 (11): 2879-2884
- [70] Guerra M, Schmidt C, McClure JC, Murr LE, Nunes AC. Flow patterns during friction stir welding. *Materials Characterization*. 2003; 49: 95-101
- [71] Colligan K. In *Proceeding of the First International Symposium on Friction Stir Welding, Thousand Oaks, CA, USA*. June 14-16, 1999.
- [72] London B, Mahoney M, Bingel B, Calabrese M, Waldron D. In *Proceeding of the Third International Symposium on Friction Stir Welding, Kobe, Japan*. September 27-28, 2001.
- [73] Sanders Jr TH, Stake Jr. EA. In *Proceedings of the Fourth International conference on Aluminium Alloys, Vol. 1, Georgia Institute of Technology, School of Material Science and Engineering, Atlanta, GA, USA*. 1994.
- [74] Donatus U, Thompson GE, Zhou X, Wang J, Beamish K. Flow patterns in friction stir welds of AA5083 and AA6082 alloys. *Materials and Design*. 2015; 83: 203-213

- [75] Smith CB, Bendzsak GB, North TH, Hinrichs JF, Noruk JS, Heideman RJ. *Ninth International Conference on Computer Technology in Welding, Detroit, Michigan, USA*. September 28-30, 1999.
- [76] Bendzsak GJ, Smith CB. In *Proceedings of the Second International Symposium on Friction Stir Welding, Gothenburg, Sweden*. June 26-28, 2000.
- [77] Xu S, Deng X, Reynolds AP, Seidel TU. Finite element simulation of material flow in friction stir welding. *Science Technology of Welding and Joining*. 2001; 6(3): 191-193
- [78] Jata KV, Mahoney MW, Mishra RS, Semiatin SL, Filed DP. Friction stir welding and processing. *TMS, Warrendale, PA, USA*. 2001: 35pp.
- [79] Yadav D, Bauri R. Effect of friction stir processing on microstructure and mechanical properties of aluminium. *Materials Science and Engineering A*. 2012; 539: 85-92
- [80] Gan W, Zhou Z, Zhang H, Peng T. Evolution of microstructure and hardness of aluminium after friction stir processing. *Transactions of Nonferrous Metals Society of China*. 2014; 24: 975-981
- [81] Chainarong S, Muangjunburee P, Suthummanon S. Friction stir processing of SSM3356 aluminium alloy. *Procedia Engineering*. 2014; 97: 732-740
- [82] Kapoor R, Kandasamy K, Baumann JA, Grant G. Effect of friction stir processing on the tensile and fatigue behaviour of a cast A206 alloy. *Materials Science and Engineering A*. 2013; 561: 159-166
- [83] Mahoney MW, Lynch SP. Friction stir processing.  
[www.dtic.mil/cgi-bin/GetTRDoc?AD=ADA518811](http://www.dtic.mil/cgi-bin/GetTRDoc?AD=ADA518811) Retrieved June 30, 2016.
- [84] Sun N, Apelian D. Microstructural modification of A206 aluminum via friction stir processing. *Material Science Forum*. 2009; 618-619: 361-364
- [85] Hashim FA, Salim RK, Khudair BH. Effect of friction stir processing on (2024-T3) aluminium alloy. *International Journal of Innovative Research in Science, Engineering and Technology*. 2015; 4(4): 1822-1829

- [86] Karthikeyan L, Senthilkumar VS, Viswanathan D, Natarajan S. Effect of low feed rate FSP on microstructure and mechanical properties of extruded cast 2285 aluminium alloy. *Journal of Material Science and Technology*. 2007; 23(5): 614-618
- [87] Weglowski MSt. Microstructural characterisation of friction stir processed cast AlSi9Mg aluminium alloy. *Archives of Foundry Engineering*. 2014; 14(3): 75-78
- [88] Mandal PK. A new surface modification technique and their characterisation: friction stir processing of AL-ZN-MG alloy. *International Journal of Engineering Research and Applications*. 2015; 5(12): 191-195
- [89] Wais AMH, Salman JM, Roubaïy AO. Effect of friction stir processing on mechanical and microstructure of the sand casting eutectic Al-12wt%Si alloy. *International Journal of Science and Research*. 2013; 2(11): 380-384
- [90] Sampath P, Parangodath VK, Udupa KR, Kuruveri UB. Fabrication of friction stir processed Al-Ni particulate composite and its impression creep behaviour. *Journal of Composites*. 2015: 2015: 9pp
- [91] Salehi M, Saadatmand M, Mohandesi JA. Optimisation of process parameters for producing AA6061/SiC nanocomposites by friction stir processing. *Transactions of Nonferrous Metals Society of China*. 2012; 22: 1055-1063
- [92] Yang M, Xu C, Wu C, Lin K, Chao YJ, An L. Fabrication of AA6061/Al<sub>2</sub>O<sub>3</sub> nano ceramic particle reinforced composite coating by using friction stir processing. *Journal of Material Science*. 2010; 45(16): 4431-4438
- [93] Chen Y, Ding H, Li J, Cai Z, Zhao J, Yang W. Influence of multi-pass friction stir processing on the microstructure and mechanical properties of Al-5083 alloy. *Materials Science and Engineering A*. 2016; 650: 281-289
- [94] Nascimento F, Santos T, Vilaca P, Miranda RM, Quintino L. Microstructural modification and ductility enhancement of surfaces modified by FSP in aluminium alloys. *Materials Science and Engineering*. 2009; A506: 16–22

- [95] El-Rayes MM, El-Danaf EA. The influence of multi-pass friction stir processing on the microstructural and mechanical properties of Aluminum Alloy 6082. *Journal of Materials Processing Technology*. 2012; 212: 1157-1168
- [96] Rao AG, Rao BRK, Deshmukh VP, Shah AK, Kashyap BP. Microstructure; Refinement of a cast hypereutectic Al-30Si alloy by friction stir processing. *Materials Letters*. 2009; 63: 2628-2630
- [97] Shafiei-Zarghani A, Kashani-Bozorg SF, Zarei-Hanzaki, A. Microstructures and mechanical properties of Al/Al<sub>2</sub>O<sub>3</sub> surface nano-composite layer produced by friction stir processing. *Materials Science and Engineering*. 2009; A500: 84-91
- [98] Yang R, Zhang Z, Zhao Y, Chen G, Guo Y, Liyu M, Zhang J. Effect of multi-pass friction stir processing on microstructure and mechanical properties of Al<sub>3</sub>Ti/A356 composites. *Materials Characterization*. 2015; 106: 62-69
- [99] Krishna VVMG, Satyanarayana K. Microstructure and mechanical properties of multipass friction stir processed aluminum silicon carbide metal matrix. *International Journal of Scientific Engineering and Technology*. 2015; 4(2): 88-90
- [100] Ma ZY, Sharma SR, Mishra RS. Effect of multiple-pass friction stir processing on microstructure and tensile properties of a cast aluminum–silicon alloy. *Scripta Materialia*. 2006; 54: 1623–1626
- [101] Nakata K, Kim YG, Fujii H, Tsumura T, Komazaki T. Improvement of mechanical properties of aluminum die casting alloy by multi-pass friction stir processing. *Materials Science and Engineering*. 2006; A 437: 274–280
- [102] Sinhmar S, Dwivedi DK, Pancholi V. Friction stir processing of AA 7039 Alloy. *International Conference on Production and Mechanical Engineering (ICPME'2014)*, Bangkok, Thailand. December 30-31, 2014.
- [103] Howard EB, Timothy LG (Eds). Metals handbook. *American Society for Metals. Materials Park, OH*. 1985.

- [104] Struers application notes on metallographic preparation of aluminium and aluminium alloys. [www.struers.com](http://www.struers.com) Retrieved June 10, 2016.
- [105] Standard test methods for tension testing of metallic materials, E8M-13. *Copyright ©ASM International, USA. 2013.*
- [106] Standard test methods for determining average grain size, E112-12. *Copyright ©ASM International, USA. 2013.*
- [107] Standard test method for microindentation hardness of materials, E384-16 *Copyright ©ASM International, USA. 2016.*
- [108] Anonymous. Molecular Dynamics. [https://en.wikipedia.org/wiki/Molecular\\_dynamics](https://en.wikipedia.org/wiki/Molecular_dynamics) Retrieved July 2, 2016.
- [109] Thijsee B. Molecular dynamics in materials science. *IDEA Summer School Lecture Note. 2007.*
- [110] Alder BJ, Wainwright TE. Studies in molecular dynamics. I. General method. *Journal of Chemical Physics. 1959; 31(2): 459 – 466*
- [111] McCammon JA, Gelin BR, Karplus M. *Nature. 1977; 267: 585–590*
- [112] Raymond K, Giovanni C. Molecular dynamics: an account of its evolution. *Theory and Applications of Computational Chemistry. 2005; 425-441*
- [113] Promyoo R. Molecular dynamics simulation of nanometric machining under realistic nanometric machining under realistic cutting conditions using LAMMPS. *Thesis Presentation, Department of Mechanical Engineering, Purdue School of Engineering and Technology, IUPUI. February 18, 2008.*
- [114] Meuner M. Industrial applications of molecular simulations. *CRC Press, Taylor and Francis Group, Boca Raton, FL, USA. 2012; 412pp.*
- [115] Ansari R, Ajori S, Rouhi S. Characterisation of the mechanical properties of polyphenylene polymer using molecular dynamics simulations. *Physica B. 2016; 481: 80-85*

- [116] Kurban M, Erkoc S. Mechanical properties of CdZnTe nanowires under uniaxial stretching and compression: A molecular dynamics simulation study. *Computational Materials Science*. 2016; 122: 295-300
- [117] Tavakoli D, Tarighat A. Molecular dynamics study on the mechanical properties of Portland cement clinker phases. *Computational Materials Science*. 2016; 119: 65-73
- [118] Bhasin A, Bommavaram R, Greenfield ML, Little DN. Use of molecular dynamics to investigate self-healing mechanisms in asphalt binders. *Journal of Materials in Civil Engineering*. 2011; 23(4): 485-492
- [119] Xu J, Xiaoxia L, Chaofeng H, Limin W, Guangzheng Z, Wei G, Jinghai L. Engineering molecular dynamics simulation in chemical engineering. *Chemical Engineering Science*. 2015; 121: 200-216
- [120] Ungerer P, Lachet V, Tavitian B. Applications of molecular simulation in oil and gas production and processing. *Oil and Gas Science and Technology – Rev. IFP*. 2006; 61(3): 387-403
- [121] Nyden MR, Stoliarov SI, Westmoreland PR, Guo ZX, Jee C. Applications of reactive molecular dynamics to the study of the thermal decomposition of polymers and nanoscale structures. *Materials Science and Engineering*. 2004; A365: 114–121
- [122] Jabbarzadeh A, Tanner RI. Molecular dynamics simulation and its application to nanorheology. *Rheology Reviews*. 2006; 165 - 216.
- [123] Yan YD, Sun T, Dong S, Luo XC, Liang YC. Molecular dynamics simulation of processing using AFM pin tool. *Applied Surface Science*. 2006; 252: 7523–7531
- [124] Zhu P, Hu Y, Ma T, Wang H. Study of AFM-based nanometric cutting process using molecular dynamics. *Applied Surface Science*. 2010; 256: 7160–7165
- [125] Taniguchi N. Current status in, and future trends of, ultraprecision machining and ultrafine materials processing. *CIRP Annals-manufacturing Technology*. 1983; 32 (2): 573-582

- [126] Belak J, Stowers IF. A molecular dynamics model of the orthogonal cutting process. In *Proceedings of the American Society of Precision Engineering*. 1990; 76-79.
- [127] Goel S, Luo X, Agrawal A. Diamond machining of silicon: A review of advances in molecular dynamics simulation. *International Journal of Machine Tools and Manufacture*. 2015; 88: 131-164
- [128] Olufayo OA, Abou-El-Hossein K. Molecular dynamics modeling of nanoscale machining of silicon. *Procedia CIRP*. 2013; 8: 504 – 509
- [129] De Chiffre L, Kunzmann H, Peggs G, Lucca D. Surfaces in precision engineering, microengineering and nanotechnology. *CIRP Annals-Manufacturing Technology*. 2003; 52(2): 561-577.
- [130] Cai MB, Li XP, Rahman M. Study of the mechanism of nanoscale ductile mode cutting of silicon using molecular dynamics simulation. *International Journal of Machine Tools and Manufacture*. 2007; 47(1): 75-80.
- [131] Aly MF, Eugene N, Veldhuis SC. Cutting force prediction using molecular dynamics assisted finite element simulation model. *19th Annual meeting of American Society for precision Engineers (ASPE), Orlando, Florida*. October 24-29, 2004.
- [132] Oluwajobi AO, Chen X. The effect of depth of cut on the Molecular Dynamics (MD) simulation of multi-pass nanometric machining. *17<sup>th</sup> International Conference on Automation and Computing (ICAC), University of Huddersfield, UK*. September 10, 2011.
- [133] Oluwajobi AO, Chen X. The effect of interatomic potentials on the molecular dynamics simulation of nanometric machining. *International Journal of Automation and Computing*. 2011; 8(3): 326-332
- [134] Yanhua H, Zong W. Molecular dynamic simulation for nanometric cutting of single-crystal face-centered cubic metals. *Nanoscale Research Letters*. 2014; 9: 9pp
- [135] Dandekar CR, Shin Y. Modeling of machining of composite materials: a review. *International Journal of Machine Tools and Manufacture*. 2012; 57: 102-121

- [136] Han XS, Lin B, Yu SY, Wang SX. Investigation of tool geometry in nanometric cutting by molecular dynamics simulation. *Journal of Materials Processing Technology*. 2002; 129: 105-108
- [137] Dmitriev AI, Kolubaev EA, Nikonov AY, Rubtsov VE, Psakhie SG. Study patterns of microstructure formation during friction stir welding. In *Proceedings of XLII International Summer School–Conference ‘Advanced Problems in Mechanics’*, St. Petersburg, Russia. June 30 - July 5, 2014.
- [138] Konovalenko I, Konovalenko IS, Dmitriev A, Psakhie S, Kolubaev E. Mass Transfer at Atomic Scale in MD Simulation of Friction Stir Welding. *Key Engineering Materials*. 2016; 683: 626-631
- [139] Oluwajobi A. Molecular dynamics simulation of nanoscale machining. *Molecular Dynamics - Studies of Synthetic and Biological Macromolecules, InTech*. 2012; 389-418
- [140] Michael PA. Introduction to molecular dynamics simulation. *Computational Soft Matter: From Synthetic Polymers to Proteins. John von Neumann Institute for Computing NIC Series*. 2004; 23:1-28
- [141] Spreiter Q, Walter M. Classical molecular dynamics simulation with the velocity verlet algorithm at strong external magnetic field. *Journal of Computational Physics*. 1999; 152: 102-119
- [142] Narayan K, Behdinan K, Fawaz Z. An engineering-oriented embedded-atom-method potential fitting procedure for pure FCC and BCC metals. *Journal of Materials Processing Technology*. 2006; 182: 387–397
- [143] Bekker H. Molecular Dynamics Simulation Methods. *Doctorate degree Thesis, University of Groningen, Netherlands*. 2006.
- [144] Lu J. Computer Modelling of Intergranular Fracture in textured materials. *Doctorate degree thesis, McGill University, Canada*. 1995.

- [145] Shahl P, Bahmouz M. Force and torque in friction stir welding. *Advances in Friction Stir Welding and Processing- Woodhead Publishing Series in Welding and Other Joining Technologies*. 2014: 459-497
- [146] Perumalla JR, Ganesh RN, Satish VK, Jayachandra R. Internal defect and process parameter analysis during friction stir welding of Al 6061 sheets. *International Journal of Advanced Manufacturing Technology*. 2012; 65: 9-12
- [147] Krishna GG, Reddy PR, Hussain MM. Effect of Tool Tilt Angle on Aluminum 2014 Friction Stir Welds. *Global Journal of Researches in Engineering: (J)*. 2014; 14(7): 61-70
- [148] Woo W, Choo H, Brown DW, Feng Z. Influence of the tool pin and shoulder on microstructure and natural aging kinetics in a friction-stir-processed 6061-T6 aluminum alloy. *Metallurgical and Materials Transactions A*. 2007; 38A: 69–76
- [149] Prantik M. Alloy designation, processing, and use of aa6xxx series aluminium alloys. *ISRN Metallurgy*. 2012: 15pp
- [150] Dutta I, Allen SM. A calorimetric study of precipitation in commercial aluminium alloy 6061. *Journal of Materials Science Letters*. 1991; 10: 323-326
- [151] Anthony M, Pavithran BT, Thamban I. Friction stir processing of AA6061-A study. *International Journal of Emerging Technology and Advanced Engineering*. 2013; 3(1): 589-595
- [152] Osten J, Milkereit B, Schick C, Kessler O. Dissolution and precipitation behaviour during continuous heating of Al–Mg–Si alloys in a wide range of heating rates. *Materials*. 2015; 8: 2830-2848
- [153] Lee WB, Yeon YM, Jung SB. the mechanical properties related to the dominant microstructure in the weld zone of dissimilar formed Al alloy joints by friction stir welding. *Journal of Material Science*. 2003; 38: 4183–4191
- [154] Lee WB, Yeon YM, Jung SB. Mechanical properties related to microstructural variation of 6061 al alloy joints by friction stir welding. *Materials Transactions*. 2004; 45(5): 1700-1705

- [155] Couper MJ, Parson NC. Automotive applications: Precipitation strengthening and alloy design for 6061 Al-Mg-Si alloys. *Aluminium Alloys: Their Physical and Mechanical Properties*, Weinheim: Wiley-VCH. 2008; 1: 96-104
- [156] Wang HQ, Sun WL, Xing YQ. Microstructure analysis on 6061 aluminum alloy after casting and diffuses annealing process. *Physics Procedia*. 2013; 50: 68-75
- [157] Olea CAW, Roldo L, Strohaecker TR, Dos Santos JF. Friction stir welding of precipitate hardenable aluminium alloys: A review. *Welding in the World*. 2006; 50: 78-87
- [158] Anonymous. Grain growth. [https://en.wikipedia.org/wiki/Grain\\_growth](https://en.wikipedia.org/wiki/Grain_growth) Retrieved September 1, 2016.
- [159] Rios PR, Siciliano Jr F, Sandim HRZ, Plaut RL, Padilha AF. Nucleation and Growth During Recrystallisation. *Materials Research*. 2005; 8(3): 225-238
- [160] ASM Handbook. Metalworking: Bulk Forming. Volume 14A ©ASM International. 2005.
- [161] Cabibbo M, McQueen HJ, Evangelista E, Spigarelli S, Di Paola M, Falchero A. Microstructure and mechanical property studies of AA 6056 friction stir welded plate. *Materials Science and Engineering*. 2007; A 460–461:86.
- [162] Johannes LB, Mishra RS. Multiple passes of friction stir processing for the creation of superplastic 7075 aluminium. *Materials Science and Engineering*. 2007; A 464: 255–260
- [163] Shankar MR, Chandrasekar S, Compton WD, King AH. Characteristics of aluminum 6061-T6 deformed to large plastic strains by machining. *Materials Science and Engineering*. 2005; A 410–411: 364–368
- [164] Ravikumar E, Arunkumar N, Samhit SG. Characterisation of mechanical properties of aluminum (AA6061-T6) by friction welding. *3<sup>rd</sup> International Conference on Mechanical, Automotive and Materials Engineering (ICMAME'2013)*, Singapore. April 29-30, 2013
- [165] Murr LE, Liu G, McClure JC. Dynamic recrystallisation in friction-stir welding of aluminium alloy 1100. *Journal of Material Science Letters*. 1997; 16:1801–1803.

- [166] Al-Fadhalah AK, Almazrouee AI, Aloraier AS. Microstructure and mechanical properties of multi-pass friction stir processed aluminum alloy 6063. *Materials and Design*. 2014; 53: 550–560
- [167] Sato YS, Urata M, Kokawa H, Ikeda K. Hall-Petch relationship in friction stir welds of equal channel angular-pressed aluminium alloys. *Materials Science and Engineering*. 2003; A354: 298-305
- [168] VOSB. Basic metallurgy: 6000 series extrusion alloys.  
<http://www.vosbltd.com/site/wp-content/uploads/2015/10/extrusion-basic-metallurgy.pdf>  
Retrieved September 1, 2016.
- [169] Surekha K, Murty BS, Rao PK. Microstructural characterisation and corrosion behavior of multipass friction stir processed AA2219 aluminium alloy. *Surface and Coatings Technology*. 2008; 202: 4057–4068
- [170] Chen Y, Ding H, Li J, Cai Z, Zhao J, Yang W. Influence of multi-pass friction stir processing on the microstructure and mechanical properties of Al-5083 alloy. *Materials Science and Engineering*. 2016; A650: 281–289
- [171] Chen K, Gan W, Okamoto K, Chung K, Wagoner RH. The mechanism of grain coarsening in friction-stir-welded AA5083 after heat treatment. *Metallurgical and Materials Transactions A: Physical Metallurgy and Materials Science*. 2011; 42: 488-507
- [172] Tao W, Yong W, Xuemei L, Matsuda K. Special grain boundaries in the nugget zone of friction stir welded AA6061-T6 under various welding parameters. *Materials Science and Engineering A*. 2016; 671:7–16
- [173] Jiang WH, Kovacevic R. Feasibility study of friction stir welding of 6061-T6 aluminium alloy with AISI 1018 steel. In *Proceedings of the Institution of Mechanical Engineers, Part B: Journal of Engineering Manufacture*. 2004; 218: 1323-1331
- [174] Yutaka SS, Park SHC, Kokawa H. Microstructural Factors Governing Hardness in Friction-Stir-Welds of Solid-Solution-Hardened Al Alloys. *Metallurgical and Materials Transactions A*. 2001; 32A (12): 3033-3042



## Appendices

UNIVERSITY  
OF  
JOHANNESBURG

## Appendix A

### A1. Chemical Composition Analysis

2016/06/09 08:57:27 AM

### QMatrix Analysis Results

Sample Identification										
SampleNo	Si	Fe	Cu	Mn	Mg	Cr	Ni	Zn	Ti	Ag
	%	%	%	%	%	%	%	%	%	%
1.	0.678	0.549	0.221	0.085	0.802	0.058	0.0093	0.067	0.072	<0.0010
2.	0.681	0.470	0.206	0.082	0.858	0.055	0.0080	0.074	0.067	<0.0010
3.	0.692	0.462	0.208	0.084	0.861	0.054	0.0083	0.077	0.066	<0.0010
↑										
↑										
∅	0.684	0.494	0.212	0.084	0.840	0.056	0.0085	0.073	0.068	<0.0010
↓										
↓										
σ	0.0074	0.048	0.0082	0.0016	0.033	0.0021	0.00068	0.0051	0.0032	
∩	1.082	9.717	3.868	1.905	3.929	3.750	8.000	6.986	4.706	

	B	Ba	Be	Bi	Ca	Cd	Co	Ga	Li	Ni
	%	%	%	%	%	%	%	%	%	%
1.	0.0016	0.0024	<0.0020	0.0074	<0.0010	<0.0020	0.0023	0.018	0.0015	0.0012
2.	0.0013	0.0011	<0.0020	0.0051	<0.0010	<0.0020	<0.0020	0.015	<0.0010	0.0015
3.	0.0014	0.0011	<0.0020	0.0058	<0.0010	<0.0020	<0.0020	0.015	0.0011	<0.00050
↑										
↑										
∅	0.0014	0.0015	<0.0020	0.0061	<0.0010	<0.0020	0.0021	0.016	0.0012	0.0014
↓										
↓										
σ	0.00016	0.00075		0.0012			0.00017	0.0017	0.00026	0.0014
∩	11.43	50.00		19.67			8.095	10.63	21.67	54.05

	P	Pb	Sa	Sr	V	Zr	Al
	%	%	%	%	%	%	%
1.	<0.0010	0.021	0.010	<0.0010	0.019	0.0024	97.36
2.	<0.0010	0.016	0.0079	<0.0010	0.016	0.0015	97.42
3.	<0.0010	0.018	0.0080	<0.0010	0.016	0.0017	97.41
↑							
↑							
∅	<0.0010	0.018	0.0086	<0.0010	0.017	0.0019	97.40
↓							
↓							
σ		0.0025	0.0012		0.0017	0.00047	0.032
∩		13.89	13.95		10.00	24.74	0.033

Figure A1: AA6061-T6 chemical composition

## Appendix B

### B1. Metallographic Procedure Employed in Grinding and Polishing of AA6061-T6 Samples

**Table B1-1: Grinding procedure**

Step	Plane grinding	Final grinding		
		1	2	3
Surface	SiC- Paper (#320)	SiC- Paper (#800)	SiC- Paper (#1200)	SiC- Paper (#4000)
Suspension	Water	Water	Water	Water
Rpm	300	300	300	300
Force (N)	25	25	25	25
Time (min)	Until plane	0.5	0.5	0.5

**Table B1-2: Polishing procedure**

Step	Diamond Polishing	Final Polishing
Surface	MD-Mol	OP-Chem
Suspension	DiaPro Mol R	OP-S
Rpm	150	150
Force (N)	25	15
Time (min)	4	5

**Table B1-3: Etchant procedure**

Etchant	Composition	Immersion time (secs)
	3ml HCl, 5ml HNO <sub>3</sub> , 2ml HF, 190ml	
Keller's Reagent	Distilled H <sub>2</sub> O	10 - 30
Weck's Reagent	4g KMnO <sub>4</sub> , 1g NaOH, 100ml Distilled H <sub>2</sub> O	120 - 180

## Appendix C

### C1. Force Feedback for Multi-Pass FSP on AA6061-T6

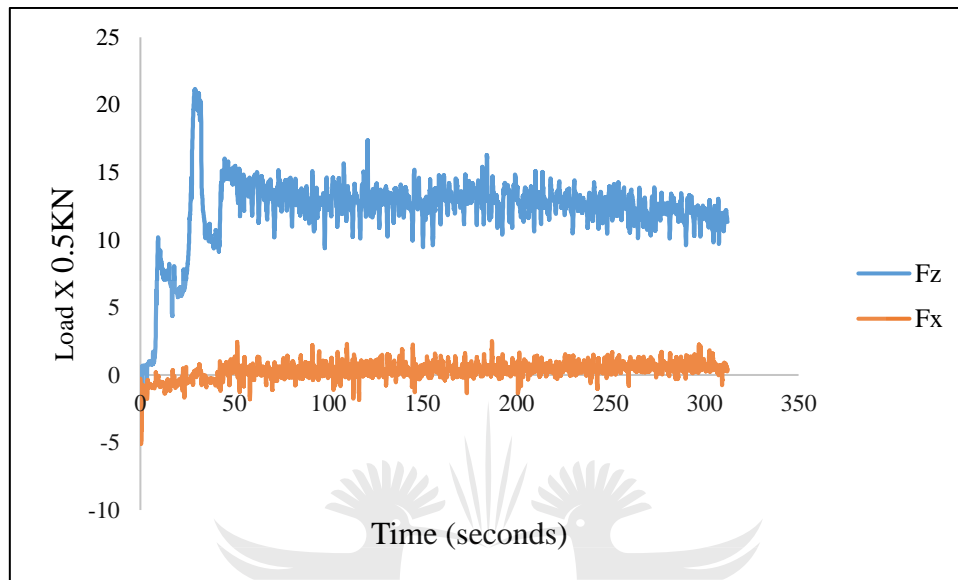


Figure C1-1: 1<sup>st</sup> FSP pass force feedback

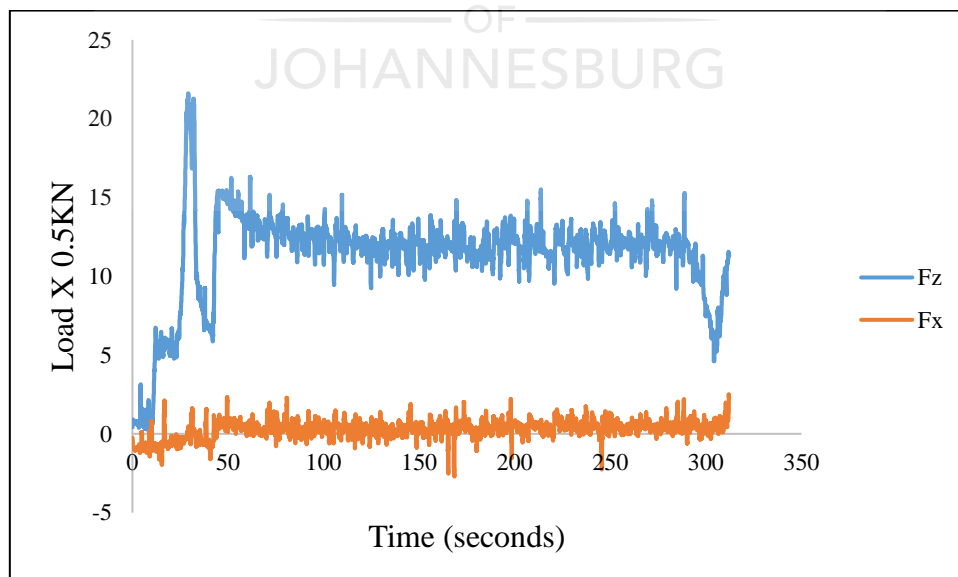
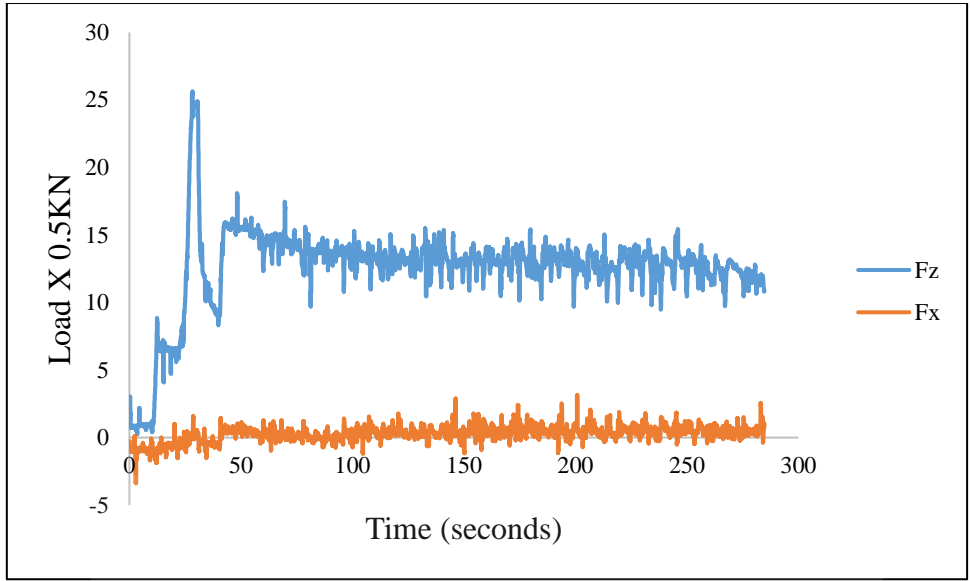
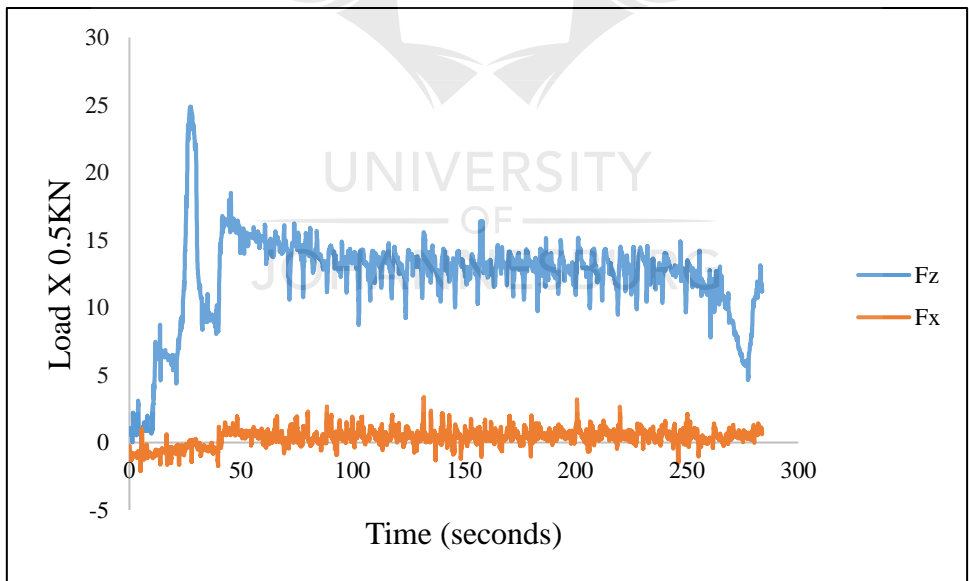


Figure C1-2: 2<sup>nd</sup> FSP pass force feedback



**Figure C1-3: 3<sup>rd</sup> FSP pass force feedback**



**Figure C1-4: 4<sup>th</sup> FSP pass force feedback**

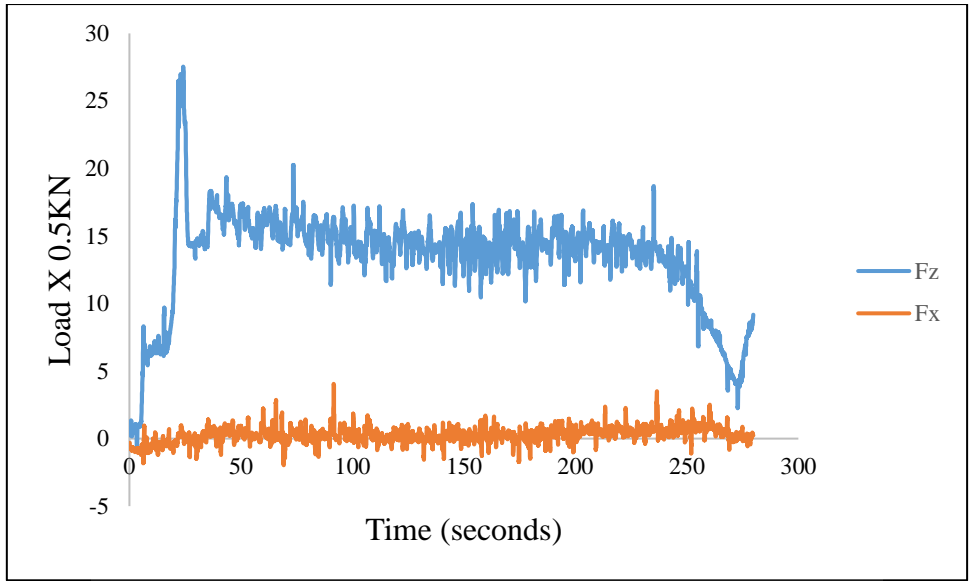


**Figure C1-5: 5<sup>th</sup> FSP pass force feedback**



## Appendix D

### D1. Tensile Properties of Multi-Pass FSPd AA6061-T6

**Table D1-1: Ultimate tensile strength of the base material and processed samples**

Sample	T1 (MPa)	T2 (MPa)	T3 (MPa)	Mean UTS (MPa)	s (MPa)
BM	337.49	336.79	338.83	337.70	1.04
Single-pass	196.01	195.76	196.31	196.02	0.28
Two-pass	186.22	186.31	184.23	185.59	1.18
Three-pass	172.87	173.84	173.65	173.45	0.51
Four-pass	171.11	169.84	171.98	170.98	1.08
Five-pass	177.37	176.95	176.96	177.09	0.24

**Table D1-2: Yield strength of the base material and processed samples**

Sample	T1 (MPa)	T2 (MPa)	T3 (MPa)	Mean YS (MPa)	s (MPa)
BM	309	313	310	310.67	2.08
Single-pass	186	186	184	185.33	1.16
Two-pass	178	175	173	175.33	2.52
Three-pass	168	166	167	167.00	1.00
Four-pass	162	164	164	163.33	1.16
Five-pass	172	170	173	171.67	1.53

**Table D1-3: Elongation percentage of the base material and processed samples**

Sample	Approximate % Elongation
BM	15
Single-pass	13
Two-pass	14
Three-pass	14
Four-pass	14
Five-pass	15

**D2. Graphic Representation of Tensile Behaviour**

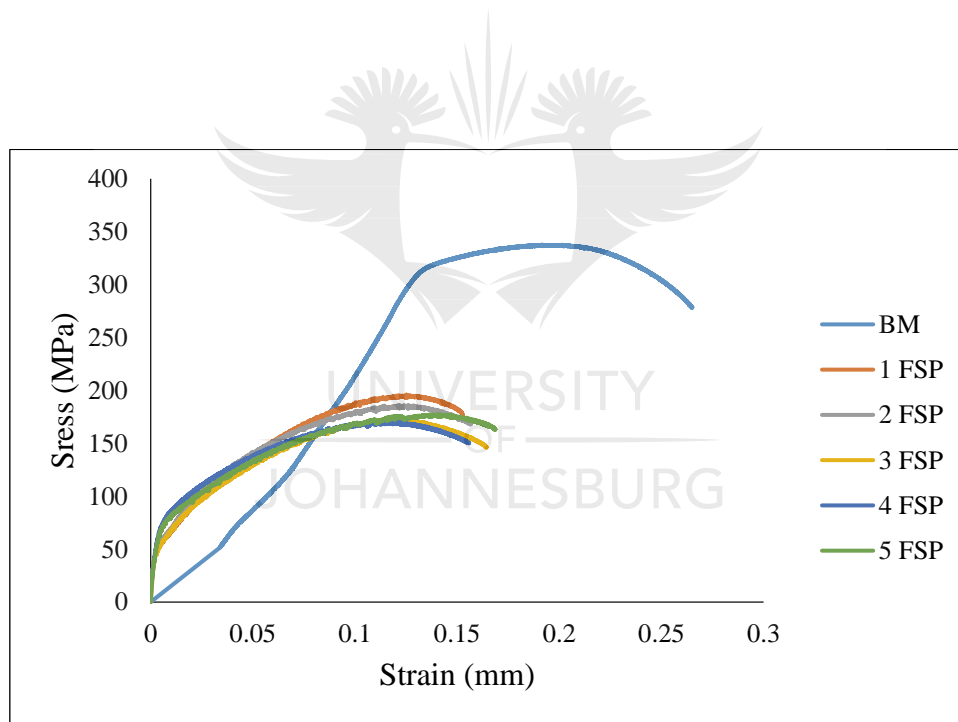


**Figure D2-1: Tensile behaviour – 1<sup>st</sup> samples (T1)**

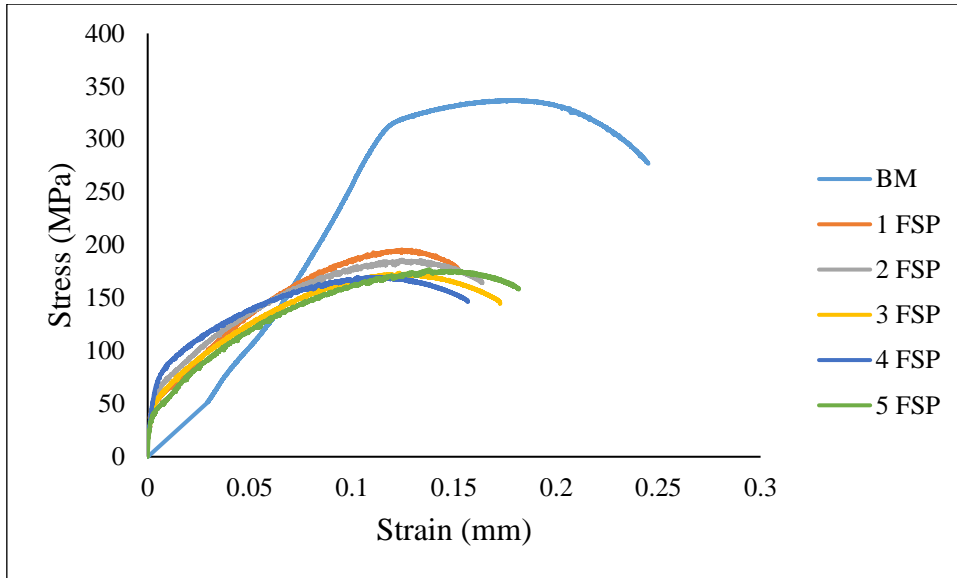


**Figure D2-2: Tensile behaviour – 2<sup>nd</sup> samples (T2)**

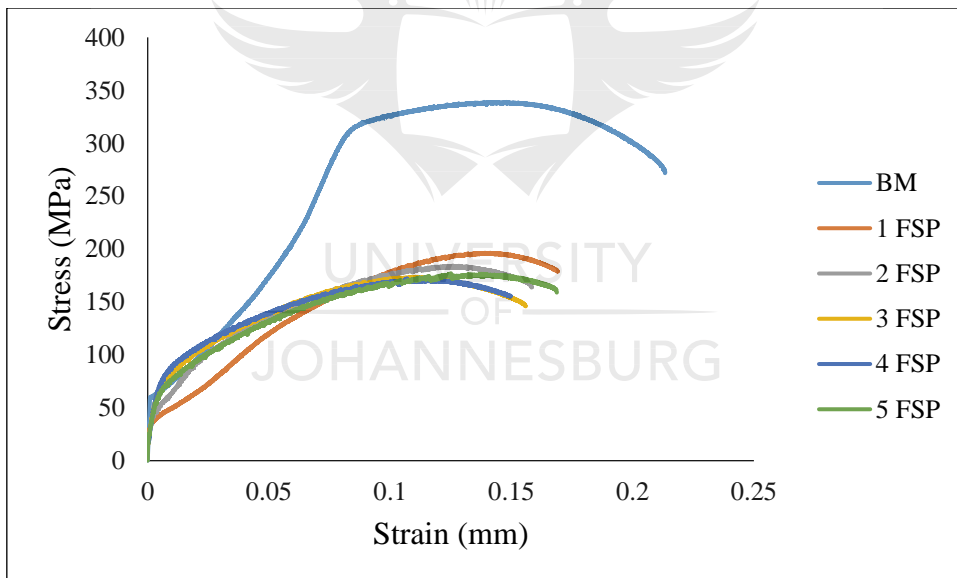


**Figure D2-3: Tensile behaviour – 3<sup>rd</sup> samples (T3)**

**D3. Hardness Values of Multi-Pass FSPd AA6061-T6**

**Table D3-1a: Hardness values; BM, single-pass, and two-pass**

Base Metal			Single-pass			Two-pass		
D1	D2	HV	D1	D2	HV	D1	D2	HV
71.75	72.43	107	92.66	92.23	65.1	97.52	97.52	59
74.26	73.51	101.9	93.46	95.05	62.7	96.19	97.01	59.6
71.47	71.47	105.1	93.53	96.14	61.9	101.32	94.7	57.8
75.78	75.08	97.8	90.81	92.5	66.2	97.68	96.67	58.9
75.02	75.28	98.5	90.37	89.91	68.5	95.93	101.1	57.3
77.5	77.5	81.9	96.06	96.06	61.4	95.76	99.73	58.2
76.46	77.15	94.3	94.67	92.88	63.3	104.42	101.02	52.7
72.91	71.56	106.6	92.21	93.24	64.7	103.94	99.62	53.7
75.72	74.27	98.9	94.56	94.72	62.1	99.23	100.82	55.6
70.26	73.38	107.9	92.69	90.75	66.1	96.59	96.59	59.6
72.51	75.59	101.5	89.36	91.67	67.9	93.57	93.87	63.3
72.39	73.93	103.9	98.34	94.82	59.6	92.47	94.04	64
74.97	75.8	97.9	94.45	95.57	61.6	97.32	96.43	59.3
82.33	76.87	87.8	93.63	94.47	62.9	96	96	60.4

UNIVERSITY OF JOHANNESBURG

**Table D3-1b: Hardness values; three-pass, four-pass and five-pass**

Three-pass			Four-pass			Five-pass		
D1	D2	HV	D1	D2	HV	D1	D2	HV
101.92	101.19	52.9	92.86	89.97	66.6	104.57	104.57	53.3
100.37	96.53	57.4	94.28	95.07	62.1	99.16	100.59	55.8
98.11	96.13	59	97.32	94.48	60.5	94.66	100.38	58.5
89.56	93.26	66.6	95.39	96	60.7	100.13	100.13	55.5
97.93	101.56	55.9	97.39	95.17	60.6	95.76	94.67	61.4
93.42	92.59	63	102.78	100.72	53.7	90.53	92.85	66.2
97.67	92.3	61.7	102.26	96.7	56.2	88.31	87.74	71.8
101.54	102.86	53.3	92.45	93.59	64.3	87.07	84.83	75.3
99.14	100.98	55.6	92.66	95.07	63.1	90.99	89.05	68.7
87.68	86.56	73.3	91.46	91.3	66.6	89.06	86.83	71.9
96.24	96.22	60.1	99	96.48	58.2	88.49	88.39	71.1
98.31	97.8	57.8	95.34	95.25	61.3	91.05	90.99	67.2
95.7	99.77	58.2	92.54	92.36	65.1	81.81	82.64	82.3
105.81	110.39	47.6	94.27	99.67	59.2	83.11	89.62	74.6